Title
The Study of Adipose Tissue Differentiation and Development

Author
Gulyaeva, Olga

Publication Date
2017

Peer reviewed|Thesis/dissertation

The Study of Adipose Tissue Differentiation and Development

By

Olga Gulyaeva

A dissertation submitted in partial satisfaction of the

requirements for the degree of

Doctor of Philosophy

in

Endocrinology

in the

Graduate Division

of the

University of California, Berkeley

Committee in charge:

Professor Hei Sook Sul, Chair

Professor Danica Chen

Professor James Olzmann

Professor Jen-Chywan Wang

Fall 2017

Abstract

The Study of Adipose Tissue Differentiation and Development

by

Olga Gulyaeva

Doctor of Philosophy in Endocrinology

University of California, Berkeley

Professor Hei Sook Sul, Chair

Two functionally different adipose tissues exist in mammals: white (WAT) and brown (BAT). WAT is the primary energy storage site and a critical organ for regulation of energy metabolism through secretion of various adipokines. In contrast, BAT is a key thermogenic organ, capable of burning chemical substrates for heat generation through unique protein UCP1. Interestingly, UCP1 is only expressed in brown or beige adipocytes found in WAT, however all the transcriptional activators of UCP1 promoter identified by far are not tissue-specific and, therefore, cannot solely explain BAT-specific expression of UCP1. BAT is believed to form early in embryogenesis from muscle-like progenitors, while WAT depending on the anatomical locations, develops in late embryogenesis or postnatally from non-muscle–like progenitors. Although embryogenic BAT precursors have been well characterized, the molecular identity of WAT precursors remains controversial. The aim of this dissertation work was to identify novel tissue-specific transcriptional regulator of UCP1 in BAT as well as to identify and characterize WAT precursors at various stages of adipogenic commitment and differentiation.

Chapter 1 reviews developmental origin of adipose tissue. Most of subcutaneous WAT depots develop perinatally, while visceral WAT develops postnatally from adipose precursors expressing markers such as Myf5, Pref-1, Wt1, and Prx1 depending on the anatomical location. BAT develops in early embryogenesis form Myf5^{+}, Pax7^{+} muscle-like precursors. Brown fat-like cells found in WAT upon cold exposure or β3-adrenergic stimulation may arise from transdifferentiation of white adipocytes or by *de-novo* differentiation of yet to be characterized precursors. Finally, transcriptional and epigenetic control of brown and beige adipocyte differentiation is discussed.

Chapter 2 demonstrates my efforts to characterize the hierarchy of adipose progenitors in WAT *in vivo*. By using Pref-1 promoter-mediated conditional ablation of Sox9, one of Pref-1 targets in inhibiting adipogenesis, coupled with fluorescent labeling, I identified and characterized a population of early adipose progenitors that express Pref-1, Sox9 and CD24. This early WAT precursor population is highly proliferative and does not yet express adipogenic markers and rather resembles stem cell-like population. Sox9 appeared to be critical for maintaining these early precursors in highly proliferative and undifferentiated state. Loss of Sox9 in Pref-1^{+} cells lead to a depletion of this precursor population and an increase in more committed PDGFRα^{+} preadipocytes that do not

proliferate and express early adipogenic markers. This switch in precursor populations from Pref-1^+ to PDGFRα^+ in the absence of Sox9 leads to enhanced adipogenesis and increased adiposity impairing insulin sensitivity *in vivo*.

Chapter 3 describes a role of novel BAT-enriched transcription factor, Zfp516 in regulating UCP1 transcription and BAT differentiation and development. I found that Zfp516 is induced upon cold exposure and directly binds and activates UCP1 and PGC1α promoters. I also showed that knockdown of Zfp516 in cultured cells impairs BAT-gene program and induces muscle-like gene signature. Thus, total body Zfp516 KO mice exhibit severe defect in BAT development, while transgenic mice overexpressing Zfp516 in all adipose tissues show increased browning of WAT. This leads to improved cold tolerance and reduces body weight accumulation upon high fat diet improving metabolic parameters.

Chapter 4 focuses on my efforts to identify Zfp516 interacting partners for activation BAT-gene program resulting in discovery of lysine-specific demethylase 1, Lsd1, as a direct binding partner of Zfp516. Lsd1 through interaction with Zfp516 is recruited to UCP1 and PGC1α promoters to demethylate H3K9 and therefore promoter transcription. Lsd1 is induced during BAT differentiation and its ablation using Myf5-Cre results in impaired embryonic BAT development. UCP1-Cre mediated ablation of Lsd1 impairs BAT gene program and results in formation of BAT that resembles WAT, therefore reducing thermogenic capacity and causing obesity in mice. Lastly, Zfp516-Lsd1 interaction is required for Lsd1 function for BAT gene program *in vitro*.

Supplement summarizes my effort to identify a novel gene critical for BAT function and characterizes one such gene, C11orf54. I found that C11orf54 is highly expressed in murine BAT, kidney and liver and is highly induced during BAT cell line differentiation. C11orf54 is localized to the nucleus and cytoplasm and appears to be important for BAT differentiation as CRISPR-mediated KO lines demonstrate dramatically impaired adipogenic differentiation. Overexpression of C11 in Cos7 cells results in increased formation of TAG through yet-to be identified mechanism.

Finally, chapter 5 summarizes my work describing importance of novel genes identified for BAT and WAT development, future directions and remaining questions.

Thus, these studies provide a better understanding of how BAT and WAT development and differentiation are regulated *in vivo*, as well as explain the hierarchy of adipose progenitors with various degree of commitment and differentiation in WAT.

To my family who has always been there for me. I would have never been able to get where I am today without their unconditional love, support and encouragement.

Table of contents

List of figures

List of tables

Acknowledgments

Graduate school has been a truly unforgettable and wonderful experience of my life. It not only shaped me into a person I am today, but also provided me opportunities to meet exceptional people.

I would like to express my deepest gratitude to my adviser Dr. Hei Sook Sul for taking me under her wing and admitting me to her laboratory. It is with the greatest appreciation and acute awareness of the opportunities this experience has given me that I took this chance to learn and invest myself. Thank you to Dr. Sul for this life-changing opportunity, her mentorship, guidance and unfailing enthusiasm. I would like to thank all members of my committee: Danica Chen, James Olzmann and Wally Wang for their support and guidance over the years.

My sincere appreciation to all my lab members and undergraduate researchers who either shared knowledge or extended their advice to me during the various stages of my projects. I would like to emphasize Carolyn Hudak and Jon Dempersmier who have been my indispensable partners and mentors throughout graduate school. A special acknowledgment to Hai Nguyen for his help and endless creative ideas.

Last, but not least, I would like to thank my friends and family for sharing such a special experience with me and being my biggest source of support and joy, always.

Chapter 1:

Genetic and Epigenetic Control of Adipose Development

Genetic and Epigenetic Control of Adipose Development

Abstract

White adipose tissue (WAT) is the primary energy storage organ and its excess contributes to obesity, while brown adipose tissue (BAT) and inducible thermogenic (beige/brite) adipocytes in WAT dissipate energy via Ucp1 to maintain body temperature. BAT and subcutaneous WAT develop perinatally while visceral WAT forms after birth from precursors expressing distinct markers, such as Myf5, Pref-1, Wt1, and Prx1, depending on the anatomical location. In addition to the embryonic adipose precursors, a pool of endothelial cells or mural cells expressing Pparγ, Pdgfrβ, Sma and Zfp423 may become adipocytes during WAT expansion in adults. Several markers, such as Cd29, Cd34, Sca-1, Cd24, Pdgfrα and Pref-1 are detected in adult WAT SVF cells that can be differentiated into adipocytes. However, potential heterogeneity and differences in developmental stage of these cells are not clear. Beige cells form in depot- and condition-specific manner by *de novo* differentiation of precursors or by transdifferentiation. Thermogenic gene activation in brown and beige adipocytes relies on common transcriptional machinery that includes Prdm16, Zfp516, Pgc1α and Ebf2. Moreover, through changing the chromatin landscape, histone methyltransferases, such as Mll3/4, as well as demethylases, such as Lsd1 and Ehmt1, play an important role for thermogenic gene program. With the presence of BAT and beige/brite cells in human adults, increasing thermogenic activity of BAT and BAT-like tissues may help promote energy expenditure to combat obesity.

Introduction

Adipose tissue plays crucial roles in mammalian metabolism. White adipose tissue (WAT) stores excess energy as triglycerides (TAGs) in a unilocular lipid droplet within adipocytes. WAT is also considered an endocrine organ that secretes adipokines to affect various processes including food intake and insulin sensitivity [1]. In contrast, brown adipose tissue (BAT) serves mostly as an oxidative tissue to regulate body temperature but also is beneficial to glucose and lipid homeostasis [2,3]. Brown adipocytes contain multilocular lipid droplets and abundant mitochondria with the unique protein Ucp1, which uncouples substrate oxidation from ATP synthesis to generate heat. In rodents, BAT is located primarily in the interscapular region, whereas WAT depots are found in various but specific regions in the body. More recently, "thermogenic" Ucp1 positive adipocytes, so called "beige" or "brite" cells, were found in mainly subcutaneous WAT, following cold exposure or stimulation by β3-adrenergic agonists, drawing much attention due to their potential benefit of weight-loss [4–6]. This review will focus on developmental origin of adipocytes, highlighting transcriptional and epigenetic control of brown and beige adipogenesis.

Developmental origin of WAT

Researchers have long puzzled over the origin of adipose tissue as well as the developmental process. WAT is categorized into subcutaneous and visceral WAT. Subcutaneous WAT is found in inguinal (posterior) and intrascapular (anterior) regions, whereas visceral WAT is found in perigonadal (often referred as epididymal WAT in males), perirenal, epicardial, retroperitoneal, mesenteric and omental regions (Shown in Figure 1A). Subcutaneous and visceral WAT are believed to have distinct response mechanisms as well as health consequence upon high-fat diet-induced expansion [7–10]. In addition, subcutaneous as opposed to visceral WAT, is considered to be the major site of "browning" during cold exposure (will be discussed in detail in a later section). Moreover, although both subcutaneous and visceral WAT are believed to be of mesodermal origin, it has been unclear whether these WAT depots have the same origin or developmental process.

To address temporal and developmental origin of adipose tissue, Hudak et al. utilized lineage tracing with an inducible Preadipocyte factor 1 (Pref-1 or Dlk1) promoter coupled with two fluorescent reporters- H2BGFP for transient labeling and Rosa26-flox-stop-flox-tdTomato for permanent labeling in mice [11]. Pref-1 represents a useful tool for studying adipose tissue development since its expression is detected only in preadipocytes and is absent from differentiated adipocytes [12]. From transient labeling studies, it became apparent that Pref-1^{+} cells first started appearing at E10.5 in mouse embryogenesis in the dorsal mesenteric region at the presumptive inguinal and dorsal subcutaneous depots. By E13.5 these cells formed a line at the dorsal stage of the embryo under the skin and these cells proliferated and did not yet contain lipids. At E17.5, these precursor cells differentiated into lipid-containing adipocytes forming subcutaneous WAT. By E19.5, the number of lipid-filled cells more than doubled in this region, indicating hyperplasia as a mechanism for WAT expansion during embryogenesis. This temporal aspect of adipogenesis that occurs prenatally was confirmed by using permanent labeling that showed that the lipid filled tdTomato positive cells in the subcutaneous region at E19.5 were descendants of Pref-1 cells. In contrast, no Pref-1 marked cells or lipid containing adipocytes were detected in the presumptive visceral WAT during embryogenesis in this study. It is not until P6 that Pref-1 cells were detected as lipid-laden adipocytes in the visceral WAT. This temporal difference in subcutaneous and visceral WAT development provided the first solid evidence that subcutaneous WAT starts its development perinatally, while visceral fat development takes place after birth. These findings are in agreement with the studies utilizing AdipoChaser model, an inducible system for permanent labeling with LacZ, relying on the adipocyte specific activity of AdipoQ promoter [13]. Regardless, in humans, since WAT is estimated to account for 16% of body weight of newborn, at least some of the adipose depots must develop prenatally [14]. Although genetic approaches cannot be used in humans, light microscopy examination showed the first traces of a fat organ between 14th and 16th weeks of prenatal life [15].

Given the temporal difference in formation of subcutaneous versus visceral WAT, it is unclear whether they arise from the same or distinct precursors. However, a study reported that formation of six different visceral WAT depots, but not subcutaneous WAT or BAT, occurred from cells expressing Wilms Tumor 1 (Wt1) in late gestation [16]. This work also suggested that WAT depots associated with visceral organs have a

mesothelial layer that serves as a source of adipocyte precursors, while, the subcutaneous depot was derived from cells marked by Prx1, a homeobox transcription factor expressed in embryonic limb and bud mesenchyme [17,18]. By lineage tracing using membrane fluorescent reporter, mT/mG, Myf5-Cre which was thought to be active in muscle and interscapular BAT as described below, also labeled most or all cells of anterior subcutaneous and renal WAT, but not inguinal or perigonadal WAT [19]. Moreover, by utilizing Sox10-Cre and R26-YFP to trace neural crest cells, Billon et al. found in adult mice that cephalic WAT around salivary glands, but not subcutaneous, gonadal, perirenal or interscapular WAT, was labelled by Sox10-YFP$^+$ cells that co-expressed Perilipin, indicating that the craniofacial adipocytes arise from neural crest cells [20]. These studies, overall, highlight that a simplistic division of WAT into visceral and subcutaneous may need to be reconsidered. It is probable that different WAT depots may have different origins and even cells within the same adipose tissue may be heterogeneous in origin.

Numerous studies also investigated the origin of white adipocytes during adipose expansion in adults. Mural cells (pericytes and vascular smooth muscle cells) are mainly derived from mesodermal lineages and, within WAT, were shown first to be a likely pool of adipose progenitors [21–24].The evidence came from Tang et al. who utilized Pparγ locus driving GFP or LacZ expression that detected Pparγ^+ cells within blood vessels in adult WAT but not in other tissues [24]. These Pparγ^+ cells also closely resembled mural cells based on the expression of Pdgfrβ, neural/glial antigen 2 (Ng2) and smooth muscle actin (Sma). In a later study, the same group reported that Pparγ marked both developmental and adult WAT progenitors that derived from distinct lineages, but only adult adipose progenitors came from Sma$^+$ mural lineage [22]. However, Pparγ is known to be expressed in macrophages and dendritic cells [25,26] in addition to being master a regulator of adipogenesis [27]. Therefore, Pparγ lineage tracing gives some information about adipocyte origin, but potential contribution from macrophages and dendritic cells cannot be completely ruled out. Another study that followed cells expressing Zfp423, zinc-finger transcription factor that regulates Pparγ expression, reported that adult adipose tissue was derived from not only mural cells but also from endothelial cells [28,29]. In the later study, Zfp423$^+$; Pdgfrβ^+ mural cells were shown to contribute to WAT hyperplasia in diet-induced obesity in a sex- and depot-dependent manner [30]. Additionally, two distinct pools of Perilipin$^+$ preadipocytes for both developmental and adult adipose expansion were identified but the majority of embryonic preadipocytes were not derived from Pdgfrβ^+ mural compartment [31], highlighting the importance of mural precursors for adult adipose tissue expansion. Recently, cells expressing Vstm2a, which is secreted from preadipocytes [32], were also associated closely with the vasculature, but interestingly, they did not express endothelial or mural markers. In addition, neural crest-derived adipose precursors were detected in subcutaneous WAT as well [33].

In addition to mural cells, other mesenchymal precursors have been shown to play role in adult WAT expansion. Ablation of Pref-1$^+$ cells using diphtheria toxin in early embryogenesis resulted in a severe lack of adipose tissue postnatally, further indicating the importance of Pref-1 expressing mesenchymal precursors in embryonic and postnatal adipogenesis. Upon high-fat diet feeding, Pref-1$^+$ cells proliferated and contributed to WAT expansion through hyperplasia. However, Pref-1$^+$adipose

precursors did not express hematopoietic markers (Cd45) and were not of endothelial ($Cd31^-$, Ve-$cadherin^-$) or pericyte origin (Sma^-, $Pdgfr\beta^-$ or $Cd146^-$) [11]. Permanent dual labeling with Tie2-GFP and Pref-1-tdTomato also showed that those cells labeled by Pref-1 were not co-stained with Tie2-GFP that labels vasculature, further excluding endothelial origin of Pref-1^+ cells. This study showed that Pref-1 labels population of early mesenchymal adipose precursors that do not coincide with precursor/preadipocyte populations associated with the vasculature. Similarly, $Pdgfr\alpha^+$ adipose precursor cells that give rise to all adult WAT depots and proliferate in visceral WAT upon high-fat diet [34,35], albeit close proximity to capillaries, were negative not only for Pparγ but also for Sma, Pdgfrβ, and endothelial marker, isolectin Ib4 [34]. These data indicate that the $Pdgfr\alpha^+$ progenitor cell population may reside outside of the mural compartment. These studies, overall, suggest that very early precursors expressing Pref-1 may migrate closer to the vasculature upon loss of Pref-1 and acquire mural or endothelial markers and then become Pdgfrα expressing cells. Alternatively, the mural cells or those cells at vasculature may represent a different progenitor pool from Pref-1 or Pdgfrα positive pools. However, the exact relationship between adipose cell populations traced by various markers and their relative contribution to each WAT depot in development and in adults in various conditions still need further investigation.

Isolation of adipose precursors in SVF of adult WAT

In adipose tissue, in addition to adipocytes, there are multiple other types of cells, such as preadipocytes or adipose precursors, stem cells, fibroblasts, endothelial cells, macrophages, leukocytes, often collectively called SVF based on the separation from lipid-containing adipocytes. Heterogeneity within SVF has long been an obstacle in isolating and characterizing pure precursor populations. Fluorescence activated cell sorting (FACS) using several stem cell markers allowed to enrich SVF for precursor/progenitor population and, thus, sorting for Lin^- ($Cd31^-$, $Cd45^-$, $Ter119^-$) eliminated the majority of endothelial, hematopoietic cells and erythrocytes [36]. However, it is not clear whether these markers may label cells at different stages of differentiation, such as stem cells, committed preadipocytes, or those cells at early stage of differentiation.

Rodeheffer et al. isolated Lin^-; $Cd29^+$; $Cd34^+$; $Sca1^+$; $Cd24^+$ population of proliferating adipose precursors that gave rise to $Cd24^-$ cells *in vivo* during adipogenesis [36]. In a later study, $Cd24^-$ cells of the precursor population were shown to represent preadipocytes that express Pparγ and C/ebpα, key adipogenic transcription factors [35]. Since $Pdgfr\alpha^+$ labeled both $Cd24^+$ and $Cd24^-$ precursor populations in WAT, isolation of Lin^-; $Pdgfr\alpha^+$ cells may represent a strategy to enrich for adipocyte precursors in adipose tissue [37,38]. In an attempt to characterize Pref-1^+ cells in the context of adipogenic lineage, Hudak et al. performed gene expression and immunostaining analysis of Pref-1^+ cells and showed their mesenchymal origin ($Sox9^+$, $Cd29^+$, $Sca1^+$, $Cd105^+$ and $Cd34^+$) [11]. The transiently labeled Pref-1^+ cells did not yet express adipogenic transcription factor Pparγ or adipose commitment factor Zfp423, but were proliferative precursors based on expression of Cd24 and Ki-67 and incorporation of BrdU. Some of the permanently labelled Pref-1 cells had lipid laden morphology and expressed Zfp423, PPARγ and C/EBPα indicating that Pref-1 cells indeed are adipose precursors. Additionally, when SVF from Pref-1-tdTomato mice was injected into SCID

mice, after 2 weeks these cells differentiated into adipocytes with characteristic gene expressing signature. These findings suggest that Pref-1 precursors represent very early stem cell-like population and highlight usefulness of Pref-1 as a marker for FACS or conditional ablation from adipose precursors at early stages of adipogenesis. Further research will shed light on when and under which physiological and molecular cues Pref-1 expression is lost in order for adipogenesis *in vivo* to proceed. Overall, these studies suggest that adipose SVF contains a hierarchy of progenitor populations with different degree of progression from adipose commitment to differentiation. Additionally, obese individuals show excessive fibrosis in WAT [39,40]. It has recently been reported that myofibroblasts arising from diet-induced obesity came from highly proliferative $Cd9^{high}$, $Pdgfr\alpha^{+}$ cells with high Pref-1 expression. In contract, $Cd9^{low}$, $Pdgfr\alpha^{+}$ population was enriched for Pparγ and C/ebpα, with low Pref-1 expression, having low proliferative capacity but high adipogenic potential [41]. Overall, the relationship between cell populations identified based on the expression of various markers needs further investigation. Identification and characterization of stage specific markers may help to isolate and define various precursor populations and their relationship during WAT development.

Developmental origin of BAT

Given the morphological and functional differences between brown and white adipocytes, these two types of adipocytes may have different developmental origin. Indeed, interscapular BAT (iBAT) formation in mice starts earlier than WAT during embryogenesis and BAT is fully thermogenically- competent at birth, providing defense mechanism against cold stress in newborns. As early as at E9.5, cells expressing engrailed 1 (En1), a homeobox domain containing gene that marks central dermomyotome, were shown to give rise to iBAT [42]. Moreover, cells that express En1 at E10.5-11.5 gave rise to iBAT as well as dermis and epaxial muscle, indicating a very early specification of cells to BAT and that BAT and muscle cells may share the same progenitors in early development. The next evidence came from study by Timmons et al. where, by microarray in primary preadipocytes, they found that brown fat preadipocytes had myogenic transcription signature (expressing transcription factors for muscle differentiation, such as MyoD and Myf5), differing from immortalized adipogenic cell lines [43]. Seale and colleagues then utilized mice harboring Myf5-Cre coupled with R26R3-YFP and found that Myf5 expressing cells gave rise to not only muscle but also iBAT and perirenal BAT (Seale et al., 2008). Later, a study with Myf5-Cre coupled with mT/mG, showed that $Myf5^{+}$ cells also gave rise to some WAT depots at anterior subcutaneous, interscapular subcutaneous and retroperitoneal regions. However, not all BAT depots may come from $Myf5^{+}$ cells, with only interscapular and subscapular BAT being fully labeled by Myf5-Cre, and only a population of cells in cervical BAT and none from periaortal or perirenal BAT [19]. Additionally, a study using $CreER^{T2}$ knock-in allele at the paired-homeodomain transcription factor- Pax7 locus combined with LacZ reporter, showed that somatic Pax7 expressing cells marked at E9.5 gave rise to dorsal dermis, BAT, trunk muscle and diaphragm muscle. After E12.5 these cells become restricted to muscle lineage [44]. Moreover, although Pref-1 is required for WAT development and expansion, only a few cells labeled by Pref-1 were detected in BAT, further indicating an early divergence of BAT precursors in development prior to Pref-1 expression [11].

Overall, it can be viewed that interscapular and subscapular BAT and muscle originate from common Myf5^{+}, Pax7^{+} progenitors, while brown adipocytes from periaortic and perirenal BAT as wells the most well studied WAT depots, such as inguinal and epididymal do not share the same developmental origin.

"Browning" of WAT

Typical adipocytes in WAT have unilocular lipid droplet morphology and a few mitochondria (Summarized in Figure 1B). Upon cold exposure or β-adrenergic stimulation, some cells in WAT acquire Ucp1 expression and have multilocular lipid droplets and abundant mitochondria. Thus, WAT may undergo "browning" with the appearance of thermogenic "beige" or "brite" adipocytes that share some similar features with brown adipocytes (Seale et al., 2008; Wang and Seale, 2016; Sanchez-Gurmaches et al., 2016). Historically, the first evidence of existence of these multilocular adipocytes in WAT came from the study in 1984, in which cold acclimation caused appearance of brown fat like cells in parametrial WAT depot of female BALB/c mice judged by morphology in EM and presence of Ucp1 [45]. Later in 1992, a report showed Ucp1 expression in various WAT depots of rats, that was induced by cold exposure [46]. Furthermore, mouse subcutaneous inguinal WAT depot is much more susceptible to "browning" even with mild stimulation compared to visceral epididymal WAT. Additionally, capacity to "brown" depends on the mouse strain: A/J strain showed a marked induction in Ucp1 in WAT depots following β3-adrenergic stimulation compared to C57BL/6J [47].

Study by Himms-Hagen et al. identified that multilocular brown adipocyte-like cells in retroperitoneal WAT following a 7-day treatment with β3-adrenergic agonist- CL-316,243, did not incorporate BrdU [48]. The authors concluded that these brown adipocyte-like cells did not derive from actively proliferating cells, and rather came from conversion of mature white adipocytes. Consistently, 95% of brown adipocyte-like multilocular cells with numerous mitochondria also did not incorporate BrdU in retroperitoneal WAT in rats following β3-adrenergic stimulation [49]. More recently, Rosenwald et al. showed appearance of Ucp1^{+} cells in ingWAT after one week cold exposure [50] by using two mouse models, Ucp1-GFP for transient labeling of Ucp1 expressing cells and Ucp1-CreER-ROSA-tdRFP for permanent labeling. They also reported that beige/brite adipocytes were not eliminated by apoptosis and reverted to white adipocyte unilocular morphology with characteristic gene expression after 5 weeks of warm adaptation. Furthermore, if subjected to a one-week cold exposure again, these cells could convert back to beige/brite cells. However, after restimulation, only half of the beige/brite adipocytes detected were from warm–adapted white, but previously beige adipocytes. These data suggested that in addition to transdifferentiation some of the beige adipocytes may have formed from *de novo* differentiation of precursor cells. In line with this evidence for transdifferentiation, another study showed that most if not all beige/brite adipocytes in ingWAT, but not abdominal WAT, following cold exposure did not arise from recruitment or proliferation precursors and rather came from unilocular adipocytes [51]. All together, these studies showed transdifferentiation as a mechanism for "browning" of WAT.

In contrast to the concept of transdifferentiation, various researchers have reported that, upon cold exposure or β3-adrenergic stimulation, a subset of SVF cells

isolated from WAT by using different markers, such as Pdgfrα and Ebf2, proliferate and become Ucp1$^+$ beige or brown-like cells [34,52]. The use of the AdipoChaser model also revealed that most of the "browning" in subcutaneous WAT following cold exposure or β3-adrenergic stimulation occurred from *de novo* adipogenesis [13]. Overall, these studies indicate a presence of precursors cells in WAT that upon cold or β3-adrenergic stimulation may undergo browning and acquire Ucp1 expression. Are beige precursors distinct from typical white or brown adipocyte precursors? Unlike brown adipocytes, the Ucp1$^+$ cells in WAT were originally believed to come from Myf5$^-$ lineage (Seale et al., 2008). However, a more recent study using Myf5-Cre coupled with fluorescent reporters (R26R3-YFP, R26R-LacZ or mT/mG) showed that beige/brite adipocytes can come from Myf5$^+$ or Myf5$^-$ lineages depending on the WAT depot and the type of stimulation (Sanchez-Gurmaches and Guertin, 2014). To understand the molecular identity of beige precursor cells, Wu et al. isolated clonal lines from ingWAT SVF to compare gene expression signature of adipogenic clones. This analysis revealed existence of a subset of cells in ingWAT that showed gene expression pattern more similar to *bona fide* brown fat cell lines than other ingWAT cell lines, suggesting presence of a distinct pool of progenitors that generate "beige" cells in ingWAT that are more similar to classical BAT progenitors. These "beige" progenitors in basal conditions had low expression of thermogenic genes. However, upon stimulation with cAMP, they responded by an increase in Ucp1 expression to the levels similar to brown fat cells, having enhanced respiration [53]. Additionally, Pdgfrα$^+$ cells from abdominal WAT, which represent white adipose precursors, can also become Ucp1$^+$ cells in response to β3-adrenergic stimulation but only in abdominal WAT [34]. Early B-cell factor 2 (Ebf2), a transcription factor critical for BAT development, was shown also to mark SVF cells in ingWAT capable of acquiring Ucp1 upon differentiation in culture [52]. The number of these Ebf2$^+$ cells in ingWAT increased upon cold-exposure contributing to *de novo* beige adipogenesis. In another study, beige/brite adipocytes were shown to share a molecular signature with smooth-muscle cells not observed in classical brown adipocytes [54]. Fate-mapping approach based on the myosin heavy chain 11 (Myh11) promoter active in smooth muscle or smooth muscle-like cells marked some of the beige adipocytes in ingWAT following 2-week cold exposure [54]. Gene expression analysis from Myh11$^+$ cells of WAT revealed that these cells were not enriched in pericyte, endothelial or hematopoietic markers, but they expressed some precursor/preadipocyte genes (Sca1, Pdgfrα, Zfp423). The authors concluded that the smooth muscle lineage may overlap with previously described preadipocyte populations. Another study showed that cells expressing mural marker Pdgfrβ which has been demonstrated to play a role in WAT adipogenesis were also recruited to become beige adipocytes after prolonged cold exposure [30]. Interestingly, after a short-term cold exposure (1 week), however, very few beige cells came from Pdgfrβ$^+$ cells, indicating that distinct "browning" mechanism may exist in short versus long term cold exposure. However, it remains unclear whether they represent a distinct pool or share precursors with classical WAT or BAT cells. Interestingly, it has also been reported that, following cold exposure, eWAT exhibited an increase in adipogenesis, however the newly formed adipocytes in this depot appeared to be Ucp1$^-$ further proving evidence that "browning" of WAT is depot- dependent [13]. Together these studies suggest the presence of a subpopulation within the WAT precursors that is capable of differentiating into Ucp1$^+$ adipocytes. Further investigation

is needed in order to establish markers that distinguish this cell population predisposed to "browning" to affect energy metabolism *in vivo.*

How can such a discrepancy in the origin of beige/brite adipocytes be explained? Potentially, different degrees of innervation that exist between subcutaneous and visceral WAT may play a role in different mechanisms governing "browning" between the two depots. Indeed, Granneman and coworkers reported that Pdgfrα^+ precursors from abdominal WAT proliferated to become Ucp1$^+$ cells, while brown-like adipocytes emerged in subcutaneous WAT (ingWAT) upon stimulation were from transdifferentiation of unilocular white adipocytes [34,51]. Regardless, results explaining either transdifferentiation or *de novo* adipogenesis for "browning" may partly arose due to technical limitations such as caveats associated with long lasting effect of tamoxifen when using Cre-ER or difficulty in substrate penetrance for β-galactosidase when using LacZ reporter mice [5,51]. Overall, all these studies point to the emerging complexity in the origin of brite or beige adipocytes. The mechanism of their formation may be highly dependent on the mouse strain and sex, the specific WAT depot analyzed, as well as the specific stimulation applied. Better studies using lineage- tracing and co-labeling with multiple precursor markers may help determine the relative contribution of each mechanism.

Is human BAT considered beige or classical brown? While BAT as an organ was originally described in 1551 [55], it was not ascribed to be present in all mammals until the 20th century. The presence in humans was discovered almost 40 years ago but was limited to outdoor workers, skid row alcoholics, and those with pro-brown adipogenic tumors [56,57]. Indeed, a breakthrough in 2009 showed that BAT in humans is either widespread or universal under cold stimulus and could be metabolically relevant [58–63]. In infancy, human BAT is localized to interscapular and perirenal depots, the molecular signature of which closely resembles classical rodent iBAT [60]. Recent studies suggest that in adult humans UCP1$^+$ adipocytes can be found in various depots around the body that are typically heterogeneous, also containing UCP1$^-$ adipocytes. Brown-like adipocytes have been detected in supraclavicular region, being the most enriched for UCP1$^+$ adipocytes, and also around aorta, carotid artery and subscapular region, as well as others [2,6]. Whether these UCP1$^+$ adipocytes in human adults represent beige or true brown adipocytes remains controversial. On the gene expression level, supraclavicular UCP1$^+$ adipocytes more closely resembled mouse beige adipocytes. Lee et al. showed that these adipocytes expressed some common BAT markers such as UCP1, PGC1α, PRDM16 and DIO2, but not MPZL2 which is thought to only be expressed in classical iBAT of rodents [64]. On the other hand, these cells expressed beige fat-specific genes such as Tmem26 and Hoxc9. Another study confirmed the "beige-like" molecular signature of human UCP1$^+$ adipocytes and discovered novel markers K3 (*KCNK3*) and mitochondrial tumor suppressor 1 (*MTUS1*) to be enriched in human beige cells versus white adipocytes [65]. However UCP1$^+$ adipocytes from other human depots such as cervical and perirenal regions, showed expression of classical BAT markers, ZIC1 and LHX8 [66,67]. All these studies point out heterogeneous composition of human BAT as well as an emerging need in novel markers that will allow to clearly distinguish classical BAT vs beige cells.

Transcriptional regulation of BAT development and "browning" of WAT

Since BAT mass is inversely correlated with BMI in humans, increasing BAT activity could be promising strategy for weight-loss and management of obesity-associated diseases [2,68]. With greatly higher mass of WAT in comparison to BAT, increasing WAT "browning" may improve insulin sensitivity and reduce weight gain under high fat diet as shown in mice [3,69–73]. This section summarizes the transcriptional regulation involved in BAT development and "browning" of WAT. The well-established transcriptional program for white adipocyte differentiation has extensively been reviewed elsewhere (Rosen and Spiegelman, 2014; Farmer, 2006).

Early work describing the transcriptional regulation of BAT centered on the norepinephrine-β3-adrenergic receptor-cAMP- cyclic AMP response element binding protein (Creb)/ p38 MAP kinase axis central to the response to cold. Thus, several target genes of this signaling pathway have been described such as Pparγ-coactivator 1α (Pgc1α), CCAAT-enhancer binding protein β (C/ebpβ), diodinase 2 (Dio2) as well as Ucp1 itself [74–76]. Further work showed that BAT gene regulation requires general adipogenic machinery including peroxisome proliferator-activated receptor gamma (Pparγ), Rxr, and the aforementioned C/ebpβ [77]. Importantly, by RT-qPCR analysis of WAT and BAT to identify transcription-related genes enriched in BAT, Seale et al. first identified Prdm16 as a BAT-enriched coregulator of the BAT gene program [78]. Prdm16 interacts with a wide variety of transcription factors and cofactors including C/ebpβ, C-terminal binding protein 1 and 2 (Ctbp1, Ctbp2), histone deacetylase 1 and 2 (Hdac1/2), mediator complex subunit 1 (Med1), Pgc1α, Pparγ, and Zfp516 as well as epigenetic regulators- euchromatic histone lysine methyltransferase 1 (Ehmt1) and lysine specific demethylase 1 (Lsd1) [71,78–84]. Interestingly, Harms et al. showed that while Prdm16 is required for maintenance of brown adipocyte identity, Prdm16 is not required for BAT development. While there may be some compensatory activity of Prdm3, prenatal development was not affected by Prdm3/Prdm16 double knockout [85]. Med1 that interacts with Prdm16 may mediate the active chromatin structure at BAT specific genes bringing distal enhancers to proximity to the transcription start site facilitating transcriptional activation [86]. However, markers of active transcription such as H3K27ac were only mildly affected by Prdm16 knockout. Interestingly, Prdm16 is not regulated by cold and must rely on interacting factors to facilitate Prdm16-mediated BAT gene induction. One such factor is Zfp516, which is induced upon cold exposure. Zfp516 binds and activates the Ucp1 promoter in response to cold to upregulate Ucp1[71]. In this regard, Zfp516 KO embryos show dramatically reduced BAT mass, while mice overexpressing Zfp516 in adipose tissue demonstrate enhanced "browning" of WAT even at room temperature. Although Zfp516 directly binds to Prdm16 and may be responsible for cold-inducible Prdm16-mediated activity, Dempersmier et al. showed that Zfp516 can induce Ucp1 expression in the absence of Prdm16. Perhaps in the absence of Prdm16, Zfp516 binding to a Prdm16 related protein, such as Prdm3, or a yet to be identified factor, may drive BAT gene expression.

Other factors involved in the cold-inducible regulation of Ucp1 include Pgc1α, a cofactor known to regulate mitochondrial biogenesis [87]. However, Pgc1α-deficient adipose tissue shows only a mild thermogenic defect [88]. Another cold inducible factor, Irf4 interacts with Pgc1α to drive expression of Ucp1 and Irf4-deficient mice have a greater thermogenic deficiency [89]. However, Irf4 has been shown to be important for

general adipogenesis and thus, the BAT specific role is unclear [90]. Recent work identified a critical role for histone deacetylase 3 (Hdac3) in basal and cold-inducible activation of thermogenic gene promoters including Ucp1. While normally working as a transcriptional repressor, Hdac3 was shown to deacetylate Pgc1α resulting in activation of thermogenic gene transcription even in the absence of thermogenic stimuli [91]. Another factor recently identified to play a role in regulation of thermogenic gene expression through inducing Pgc1α in response to acute cold exposure is the sirtuin, Sirt6. Yao et al. found that Sirt6 was induced by cold where it interacts with phosphorylated activating transcription factor 2 (Atf2) to drive Pgc1α promoter activity. Adipocyte specific Sirt6 knockout mice had significantly reduced Pgc1α levels as well as Pgc1α binding to the Ucp1 promoter. Interestingly, Sirt6 ablation did not result in decreased Pgc1α acetylation, which has been shown to be important for Pgc1α transcriptional coactivity, and the authors did not examine the role of Sirt6 deacetylase activity in regulating Pgc1α promoter activity [92].

While analyzing differential binding of Pparγ in WAT and BAT, Rajakumari et al. found that BAT-specific Pparγ response elements (PPRE) coincide commonly with early B-cell factor *cis*-elements and thus identified a critical role of Ebf2 recruiting Pparγ to the Prdm16 promoter for Prdm16 transcription [93]. Further work identified Dpf3 as a Ebf2-interacting histone reader, which identifies genes of the BAT program, leading to Ebf2-mediated recruitment of the chromatin remodeler, Brg1, resulting in opening of chromatin for transcription [94]. Thus, Ebf2 appears to be working as a pioneer factor during adipogenesis leading to activation of the BAT gene program.

While most of the transcriptional regulators mentioned above are common for brown and beige adipogenesis in order to induce thermogenic genes such as Ucp1, several genes were reported to be specifically important for induction or repression of "browning". For example, Myocardin-related transcription factor A (Mrtfa) was sown to inhibit beige adipocyte differentiation and Mrtfa KO mice show increased production of beige adipocytes in WAT and these mice were protected from diet induced obesity and insulin resistance [95]. Additionally, Smad3, a key mediator of Tgfβ signaling was shown to inhibit beige adipocyte differentiation [96,97]. Klf11 was also reported to activate selective beige gene expression by cooperation with Pparγ at superenhancers [98]. Interestingly, transcription factor Hes1, which is activated by Notch signaling, repressed Prdm16 and Pgc1α transcription during beige but not classical brown adipogenesis [99]. These studies describe common as well as distinct transcriptional mechanisms involved in BAT and beige adipogenesis. Given that not all brown and beige cells have the same origin, it is tempting to speculate that tissue-specific early developmental transcription factors may exist to establish brown versus beige cells differentiation and development.

Epigenetic control of BAT gene program

As in most biological processes, interaction between genes and the environment, such as temperature or diet [100,101], may influence BAT gene expression and thermogenesis, involving epigenetic events, i.e., heritable changes in traits without changes in DNA sequence. The broad umbrella of epigenetics research includes both DNA and histone modifications as well as microRNA and long noncoding RNA (lncRNA) either inhibiting or enhancing transcription. In this regard, DNA is wrapped around histone proteins- the building block of the nucleosome (the histone octamer core

contains 2 copies of H2A, H2B, H3 and H4) the structure of which is critical for regulation of transcription [102,103]. Histone modifications, such as methylation and acetylation, affect transcription by altering nucleosome compaction, changing the chromatin landscape, and thus DNA accessibility of transcription factors and co-regulators [104,105]. For example, H3K4me3 is a well-recognized hallmark of transcription activation, whereas H3K9me3 represents a repressive mark, all at the tail region of H3 [106,107]. The field of BAT epigenetics has been extensively reviewed of late [108–112] and this section focuses on writers and erasers of histone methylation marks, specifically, methyltransferases and demethylases, which are critical components of epigenetic regulation.

Lysine Methyltransferase 2C (KMT2C, Mll3/4), a H3K4 methyl transferase, has been shown to be involved in adipogenesis and mice with catalytic dead mutations show reduced adiposity. However, recent studies into the role of Mll3/4 in immortalized brown adipocytes found that Mll3/4 identifies critical super enhancers for BAT and general adipogenic genes and recruits Cbp/p300 to poised enhancers to drive transcription [113,114]. Interestingly, this study showed a broad spectrum of histone modifications in both brown preadipocytes and brown adipocytes, with differential patterning of H3K4me1/2, H3K9me2, H3K27me3, H3K27ac, and H3K36me3 implicating many, yet to be identified histone methyltransferases in this process.

Ehmt1, identified as a binding partner for Prdm16, catalyzes the demethylation of H3K9 di- or tri- methylation (H3K9me2/3). Loss of Ehmt1 resulted in loss of BAT gene expression and decreased BAT tissue mass [81]. However, the proposed mechanism of action was not due to the methylation activity, but due to stabilization of Prdm16 protein, a mechanism proposed for Pparγ agonist and “browning” agent, rosiglitazone [115]. Thus, the relative importance of Prdm16 stabilization versus the potential Ehmt1 demethylase activity in BAT gene program remains to be studied.

Another H3K9 demethylase, that has been shown to regulate the BAT gene program by histone modification, is lysine-specific demethylase 1 (Lsd1) which catalyzes the demethylation of mono- and dimethylated H3K9. Through direct interaction with Zfp516, Lsd1 is recruited to BAT gene promoters to promote transcription *in vivo* [82]. Indeed, BAT of Lsd1 KO mice using Ucp1-Cre showed reduced Ucp1 expression, which accompanied increased H3K9 mono and demethylation at the proximal Ucp1 promoter, a site where both Lsd1 and Zfp516 were bound. Therefore, BAT-specific Lsd1 ablation compromised BAT gene expression as well as development of BAT, resembling WAT with reduced thermogenic activity. Thus, Ucp1-driven Lsd1 ablation resulted in obesity with impaired glucose tolerance upon high fat feeding. Interestingly, later work by Zeng et al. identified an LSD1 complex containing Zfp516 and Prdm16 as well as Ctbp1/2, Hdac1/2 and others [84]. This complex was found to suppress WAT-specific genes by colocalizing in regions of H3K4me1 demethylation. Another group identified Lsd1 interaction with Nrf1 to drive mitochondriogenesis and thermogenic transcription in brown adipocytes maintaining their BAT identity [116].

Jumanji-C domain containing histone demethylase 2A (Jhdm2a, also known as Jmjd1a), a mono- and di-methyl H3K9 demethylase, was originally identified as a regulator of thermogenic gene expression when a global knockout, generated to identify the role of Jhdm2a in spermatogenesis, developed an obese phenotype. A closer examination of these mice showed that Jhdm2a was recruited to the Ucp1 promoter

during cold and isoproterenol treatment to remove H3K9 methylation resulting in promoter activation [117,118]. Interestingly, later work showed that the H3K9 demethylation activity of Jhdm2a may actually be a secondary activity and that Jhdm2a primarily functions as a PKA-mediated, phosphorylation-dependent scaffold protein that interacts with SWI/SNF complex members Arid1a, Brg1, and Baf60b as well as Pparγ in multiple locations of target promoters. Interestingly, non-phosphorylatable Jhdm2a mutants were unable to be recruited to target promoters resulting in decreased UCP1 expression and activity *in vitro* and *in vivo* [119]. The authors hypothesized that this may be facilitating long-range chromatin interaction, but further work using chromosome conformation capture (3C) needs to be done to validate these claims.

Several recent papers have identified the importance of the demethylation of trimethylated H3K27. Interestingly, two different enzymes have been attributed to be responsible for this activity, Jmjd3 and ubiquitously transcribed tetratricopeptide repeat on chromosome X (Utx). In cells, knockout of Jmjd3 and well as chemical inhibition of Jmjd3 enzymatic activity results in a decrease in Ucp1 mRNA and protein. However, *in vivo*, transgenic expression or chemical inhibition of Jmjd3 only affected Ucp1 expression in aged mice [120]. Similarly, Utx, which increases during brown adipogenesis and cold exposure, was found to decrease H3K27me3 at the Ucp1 enhancer and transcription start site (TSS). It is proposed that Utx then recruits Cbp to acetylate H3K27 thereby promoting BAT gene transcription [121]. This pro-thermogenic program of Utx is antagonized by the activity of Hdac1, which deacetylates H3K27 and recruits Ezh2 and Suz12 to facilitate H3K27 methylation while preventing Utx binding [122]. However, both studies into the function of Utx were performed *in vitro* so the relative contributions of Jmjd3 and Utx *in vivo* have yet to be discerned. Given the overlap in functionality, the lack of a strong phenotype in the Jmjd3 knockout mice could be due to compensatory activity of Utx. Further studies are needed to verify this hypothesis. These studies, overall, indicate a critical role for both transcriptional and epigenetic regulation of thermogenic gene expression. Further studies will provide molecular details of the chromatin modifications required for thermogenic gene program (See figure 2).

Future directions

Understanding WAT and BAT development and the underlying mechanism to promote “browning” of WAT may provide targets for combating and prevention of obesity and associated diseases. For some of the markers of adipose precursors recently identified, further investigation is needed to establish their contribution in embryogenic versus postnatal adipogenesis. Better FACS using multiple markers coupled with immunostaining and lineage tracing approaches will be needed. Moreover, single cell level genomic studies would allow the study of the possible mosaic developmental origin of WAT as well as potential mechanisms for “browning” of WAT. Additionally, many of the studies have focused on a specific depot or condition, e.g. adipose expansion during high fat diet or “browning” after cold exposure. Given that different WAT depots may have different developmental origin it would be beneficial to examine those markers in various depots and different conditions. In addition, as various “browning” mechanisms may exist depending on the type of stimulus applied, relative contribution of transdifferentiation versus *de novo* differentiation need to be

assessed under different conditions. Moreover, the relationship among transcription factors involved in transitioning from completely “closed” silent chromatin to open/poised chromatin in brown/beige adipocytes needs further investigation. With striking difference in histone modifications during brown/beige adipose development, the enzymes catalyzing these modifications and their contribution to thermogenic gene regulation remains to be elucidated.

Acknowledgements

The research programs of the author have been supported in part by NIDDK grant to H.S.S.

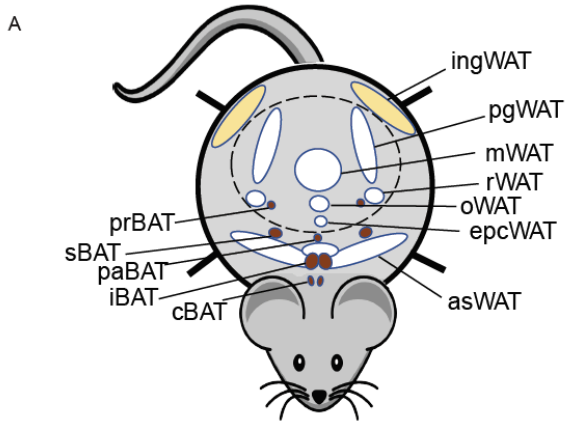

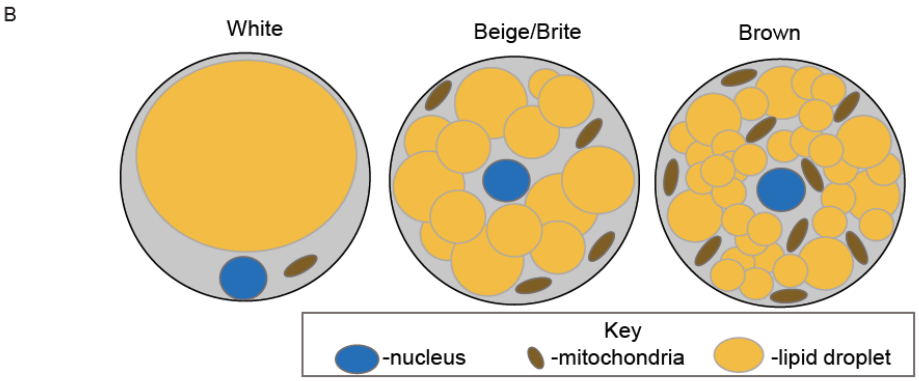

	Brown	Beige/Brite	White
UCP1 expression	-	+	+
Mitochondria Density	Low	High	High
Lipid droplet	One large	Multilocular	Multilocular
Function	Energy storage Endocrine (Leptin, AdipoQ, Resistin)	Thermogenic Endocrine?	Thermogenic Endocrine (Fgf21)

Figure 1. Anatomical location of murine adipose tissue and three types of adipocytes.
A. Anatomical location of mouse white adipose tissue (WAT) and brown adipose tissue (BAT). ingWAT-inguinal WAT also known as posterior subcutaneous, pgWAT-perigonadal WAT, rWAT-retroperitoneal WAT, mWAT-mesenteric WAT, oWAT-omental WAT, epcWAT- epicardial WAT, asWAT- anterior subcutaneous WAT. pgWAT, rWAT, mWAT, oWAT, epcWAT are collectively called visceral WAT, while ingWAT and asWAT are combined into subcutaneous WAT. prBAT- perirenal BAT, sBAT-subscapular BAT, paBAT-periaortal BAT, iBAT-interscapular BAT, cBAT-cervical BAT. The peritoneum is depicted as dotted line. B. Functional and morphological differences between 3 types of adipocyte: white, beige/brite and brown.

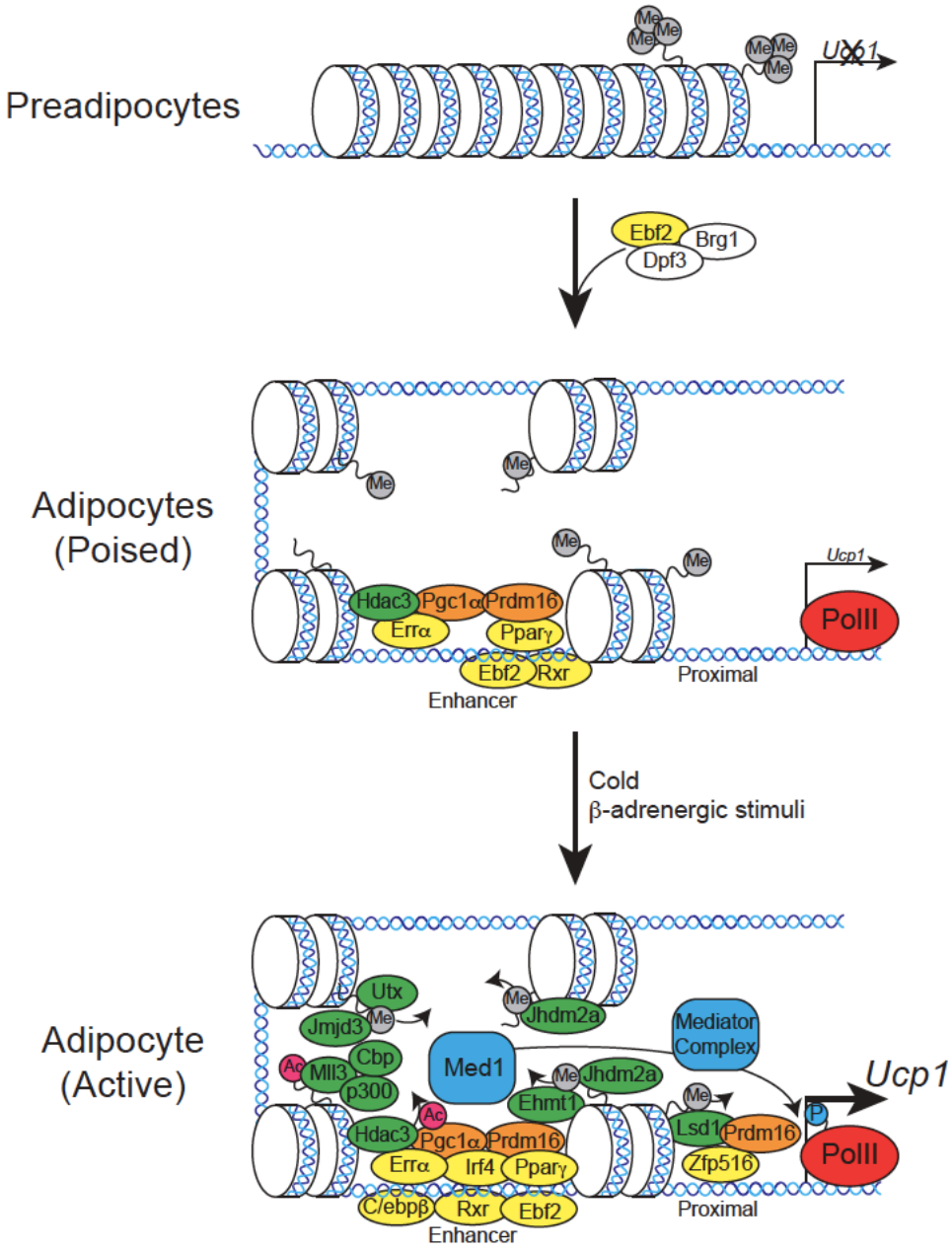

Figure 2. Graphical Representation of Transcriptional and Epigenetic Regulators binding to the UCP1 promoter in beige/brown adipocytes.

References

1. Rosen, E. D. & Spiegelman, B. M. What we talk about when we talk about fat. *Cell* **156,** 20–44 (2014).
2. Kajimura, S., Spiegelman, B. M. & Seale, P. Brown and Beige Fat: Physiological Roles beyond Heat Generation. *Cell Metab.* **22,** 546–559 (2015).
3. Seale, P. *et al.* Prdm16 determines the thermogenic program of subcutaneous white adipose tissue in mice. *J. Clin. Invest.* **121,** 96–105 (2011).
4. Seale, P. *et al.* PRDM16 controls a brown fat/skeletal muscle switch. *Nature* **454,** 961–967 (2008).
5. Wang, W. & Seale, P. Control of brown and beige fat development. *Nat Rev Mol Cell Biol* **17,** 691–702 (2016).
6. Sanchez-Gurmaches, J., Hung, C.-M. & Guertin, D. A. Emerging Complexities in Adipocyte Origins and Identity. *Trends in Cell Biology* **26,** 313–326 (2016).
7. Jeffery, E., Church, C. D., Holtrup, B., Colman, L. & Rodeheffer, M. S. Rapid depot-specific activation of adipocyte precursor cells at the onset of obesity. *Nat. Cell Biol.* **17,** 376–385 (2015).
8. Jeffery, E. *et al.* The Adipose Tissue Microenvironment Regulates Depot-Specific Adipogenesis in Obesity. *Cell Metab.* **24,** 142–150 (2016).
9. Kim, S. M. *et al.* Loss of White Adipose Hyperplastic Potential Is Associated with Enhanced Susceptibility to Insulin Resistance. *Cell Metabolism* **20,** 1049–1058 (2014).
10. Macotela, Y. *et al.* Intrinsic Differences in Adipocyte Precursor Cells From Different White Fat Depots. *Diabetes* **61,** 1691–1699 (2012).
11. Hudak, C. S. *et al.* Pref-1 Marks Very Early Mesenchymal Precursors Required for Adipose Tissue Development and Expansion. *Cell Rep* **8,** 678–687 (2014).
12. Smas, C. M. & Sul, H. S. Pref-1, a protein containing EGF-like repeats, inhibits adipocyte differentiation. *Cell* **73,** 725–734 (1993).
13. Wang, Q. A., Tao, C., Gupta, R. K. & Scherer, P. E. Tracking adipogenesis during white adipose tissue development, expansion and regeneration. *Nat. Med.* **19,** 1338–1344 (2013).
14. Poissonnet, C. M., Burdi, A. R. & Garn, S. M. The chronology of adipose tissue appearance and distribution in the human fetus. *Early Hum. Dev.* **10,** 1–11 (1984).
15. Ailhaud, G. & Hauner, H. Development of White Adipose Tissue. in *Handbook of obesity* 483
16. Chau, Y.-Y. *et al.* Visceral and subcutaneous fat have different origins and evidence supports a mesothelial source. *Nat Cell Biol* **16,** 367–375 (2014).
17. Krueger, K. C., Costa, M. J., Du, H. & Feldman, B. J. Characterization of Cre Recombinase Activity for In Vivo Targeting of Adipocyte Precursor Cells. *Stem Cell Reports* **3,** 1147–1158 (2014).
18. Sanchez-Gurmaches, J., Hsiao, W.-Y. & Guertin, D. A. Highly Selective In Vivo Labeling of Subcutaneous White Adipocyte Precursors with Prx1-Cre. *Stem Cell Reports* **4,** 541–550 (2015).
19. Sanchez-Gurmaches, J. & Guertin, D. A. Adipocytes arise from multiple lineages that are heterogeneously and dynamically distributed. *Nature Communications* **5,** 4099 (2014).

20. Billon, N. *et al.* The generation of adipocytes by the neural crest. *Development* **134,** 2283–2292 (2007).
21. Armulik, A., Genové, G. & Betsholtz, C. Pericytes: Developmental, Physiological, and Pathological Perspectives, Problems, and Promises. *Developmental Cell* **21,** 193–215 (2011).
22. Jiang, Y., Berry, D. C., Tang, W. & Graff, J. M. Independent Stem Cell Lineages Regulate Adipose Organogenesis and Adipose Homeostasis. *Cell Reports* **9,** 1007–1022 (2014).
23. Sinha, S., Iyer, D. & Granata, A. Embryonic origins of human vascular smooth muscle cells: implications for in vitro modeling and clinical application. *Cell Mol Life Sci* **71,** 2271–2288 (2014).
24. Tang, W. *et al.* White fat progenitor cells reside in the adipose vasculature. *Science* **322,** 583–586 (2008).
25. Nagy, L., Tontonoz, P., Alvarez, J. G., Chen, H. & Evans, R. M. Oxidized LDL regulates macrophage gene expression through ligand activation of PPARgamma. *Cell* **93,** 229–240 (1998).
26. Szatmari, I. *et al.* PPARgamma regulates the function of human dendritic cells primarily by altering lipid metabolism. *Blood* **110,** 3271–3280 (2007).
27. Tontonoz, P., Hu, E. & Spiegelman, B. M. Stimulation of adipogenesis in fibroblasts by PPARγ2, a lipid-activated transcription factor. *Cell* **79,** 1147–1156 (1994).
28. Gupta, R. K. *et al.* Transcriptional control of preadipocyte determination by Zfp423. *Nature* **464,** 619–623 (2010).
29. Gupta, R. K. *et al.* Zfp423 expression identifies committed preadipocytes and localizes to adipose endothelial and perivascular cells. *Cell Metab.* **15,** 230–239 (2012).
30. Vishvanath, L. *et al.* Pdgfrβ+ Mural Preadipocytes Contribute to Adipocyte Hyperplasia Induced by High-Fat-Diet Feeding and Prolonged Cold Exposure in Adult Mice. *Cell Metab.* **23,** 350–359 (2016).
31. Hong, K. Y. *et al.* Perilipin+ embryonic preadipocytes actively proliferate along growing vasculatures for adipose expansion. *Development* **142,** 2623–2632 (2015).
32. Secco, B. *et al.* Amplification of Adipogenic Commitment by VSTM2A. *Cell Reports* **18,** 93–106 (2017).
33. Sowa, Y. *et al.* Adipose Stromal Cells Contain Phenotypically Distinct Adipogenic Progenitors Derived from Neural Crest. *PLOS ONE* **8,** e84206 (2013).
34. Lee, Y.-H., Petkova, A. P., Mottillo, E. P. & Granneman, J. G. In Vivo Identification of Bipotential Adipocyte Progenitors Recruited by β3-Adrenoceptor Activation and High-Fat Feeding. *Cell Metabolism* **15,** 480–491 (2012).
35. Berry, R. & Rodeheffer, M. S. Characterization of the adipocyte cellular lineage in vivo. *Nat Cell Biol* **15,** 302–308 (2013).
36. Rodeheffer, M. S., Birsoy, K. & Friedman, J. M. Identification of white adipocyte progenitor cells in vivo. *Cell* **135,** 240–249 (2008).
37. Festa, E. *et al.* Adipocyte Lineage Cells Contribute to the Skin Stem Cell Niche to Drive Hair Cycling. *Cell* **146,** 761–771 (2011).
38. Uezumi, A., Fukada, S., Yamamoto, N., Takeda, S. 'ichi & Tsuchida, K. Mesenchymal progenitors distinct from satellite cells contribute to ectopic fat cell formation in skeletal muscle. *Nat Cell Biol* **12,** 143–152 (2010).

39. Iwayama, T. *et al.* PDGFRα signaling drives adipose tissue fibrosis by targeting progenitor cell plasticity. *Genes Dev.* **29,** 1106–1119 (2015).
40. Joe, A. W. B. *et al.* Muscle injury activates resident fibro/adipogenic progenitors that facilitate myogenesis. *Nat. Cell Biol.* **12,** 153–163 (2010).
41. Marcelin, G. *et al.* A PDGFRα-Mediated Switch toward CD9(high) Adipocyte Progenitors Controls Obesity-Induced Adipose Tissue Fibrosis. *Cell Metab.* **25,** 673–685 (2017).
42. Atit, R. *et al.* Beta-catenin activation is necessary and sufficient to specify the dorsal dermal fate in the mouse. *Dev. Biol.* **296,** 164–176 (2006).
43. Timmons, J. A. *et al.* Myogenic gene expression signature establishes that brown and white adipocytes originate from distinct cell lineages. *Proc Natl Acad Sci U S A* **104,** 4401–4406 (2007).
44. Lepper, C. & Fan, C.-M. Inducible lineage tracing of Pax7-descendant cells reveals embryonic origin of adult satellite cells. *Genesis* **48,** 424–436 (2010).
45. Young, P., Arch, J. r. s. & Ashwell, M. Brown adipose tissue in the parametrial fat pad of the mouse. *FEBS Letters* **167,** 10–14 (1984).
46. Cousin, B. *et al.* Occurrence of brown adipocytes in rat white adipose tissue: molecular and morphological characterization. *Journal of Cell Science* **103,** 931–942 (1992).
47. Collins, S., Daniel, K. W., Petro, A. E. & Surwit, R. S. Strain-specific response to beta 3-adrenergic receptor agonist treatment of diet-induced obesity in mice. *Endocrinology* **138,** 405–413 (1997).
48. Himms-Hagen, J. *et al.* Multilocular fat cells in WAT of CL-316243-treated rats derive directly from white adipocytes. *Am. J. Physiol., Cell Physiol.* **279,** C670-681 (2000).
49. Cinti, S. Adipocyte differentiation and transdifferentiation: Plasticity of the adipose organ. *J Endocrinol Invest* **25,** 823–835 (2002).
50. Rosenwald, M., Perdikari, A., Rülicke, T. & Wolfrum, C. Bi-directional interconversion of brite and white adipocytes. *Nat. Cell Biol.* **15,** 659–667 (2013).
51. Lee, Y.-H., Petkova, A. P., Konkar, A. A. & Granneman, J. G. Cellular origins of cold-induced brown adipocytes in adult mice. *FASEB J.* **29,** 286–299 (2015).
52. Wang, W. *et al.* Ebf2 is a selective marker of brown and beige adipogenic precursor cells. *Proc. Natl. Acad. Sci. U.S.A.* **111,** 14466–14471 (2014).
53. Wu, J. *et al.* Beige Adipocytes are a Distinct Type of Thermogenic Fat Cell in Mouse and Human. *Cell* **150,** 366–376 (2012).
54. Long, J. Z. *et al.* Ribosomal Profiling Provides Evidence for a Smooth Muscle-Like Origin of Beige Adipocytes. *Cell Metab* **19,** 810–820 (2014).
55. Gessner, C. *Conradi Gesneri medici Tigurini Historiæ animalium Lib. I. de quadrupedibus uiuiparis : opus philosophis, medicis, grammaticis, philologis, poëtis, & omnibus rerum linguarumq́; uariarum studiosis, utilissimum simul iucundissimumq́; futurum ...* (Apud Christ. Froschouerum, 1551).
56. Huttunen, P., Hirvonen, J. & Kinnula, V. The occurrence of brown adipose tissue in outdoor workers. *Eur J Appl Physiol Occup Physiol* **46,** 339–345 (1981).
57. Ricquier, D. & Mory, G. 4 - Factors affecting brown adipose tissue activity in animals and man. *Clinics in Endocrinology and Metabolism* **13,** 501–520 (1984).

58. Cypess, A. M. *et al.* Identification and importance of brown adipose tissue in adult humans. *N. Engl. J. Med.* **360,** 1509–1517 (2009).
59. Cypess, A. M. *et al.* Cold but not sympathomimetics activates human brown adipose tissue in vivo. *Proc. Natl. Acad. Sci. U.S.A.* **109,** 10001–10005 (2012).
60. Lidell, M. E. *et al.* Evidence for two types of brown adipose tissue in humans. *Nat Med* **19,** 631–634 (2013).
61. Nedergaard, J. & Cannon, B. The changed metabolic world with human brown adipose tissue: therapeutic visions. *Cell Metab.* **11,** 268–272 (2010).
62. van Marken Lichtenbelt, W. D. *et al.* Cold-activated brown adipose tissue in healthy men. *N. Engl. J. Med.* **360,** 1500–1508 (2009).
63. Virtanen, K. A. *et al.* Functional brown adipose tissue in healthy adults. *N. Engl. J. Med.* **360,** 1518–1525 (2009).
64. Lee, P., Werner, C. D., Kebebew, E. & Celi, F. S. Functional thermogenic beige adipogenesis is inducible in human neck fat. *International Journal of Obesity; London* **38,** 170–6 (2014).
65. Shinoda, K. *et al.* Genetic and functional characterization of clonally derived adult human brown adipocytes. *Nat Med* **21,** 389–394 (2015).
66. Cypess, A. M. *et al.* Anatomical localization, gene expression profiling and functional characterization of adult human neck brown fat. *Nat. Med.* **19,** 635–639 (2013).
67. Xue, R. *et al.* Clonal analyses and gene profiling identify genetic biomarkers of the thermogenic potential of human brown and white preadipocytes. *Nat. Med.* **21,** 760–768 (2015).
68. Kir, S. *et al.* Tumour-derived PTH-related protein triggers adipose tissue browning and cancer cachexia. *Nature* **513,** 100–104 (2014).
69. Brestoff, J. R. *et al.* Group 2 innate lymphoid cells promote beiging of white adipose tissue and limit obesity. *Nature* **519,** 242–246 (2015).
70. Dempersmier, J. & Sul, H. S. Shades of brown: a model for thermogenic fat. *Front Endocrinol (Lausanne)* **6,** 71 (2015).
71. Dempersmier, J. *et al.* Cold-inducible Zfp516 activates UCP1 transcription to promote browning of white fat and development of brown fat. *Mol. Cell* **57,** 235–246 (2015).
72. Rao, R. R. *et al.* Meteorin-like Is a Hormone that Regulates Immune-Adipose Interactions to Increase Beige Fat Thermogenesis. *Cell* **157,** 1279–1291 (2014).
73. Shao, M. *et al.* Zfp423 Maintains White Adipocyte Identity through Suppression of the Beige Cell Thermogenic Gene Program. *Cell Metab.* **23,** 1167–1184 (2016).
74. Cao, W., Medvedev, A. V., Daniel, K. W. & Collins, S. β-Adrenergic Activation of p38 MAP Kinase in Adipocytes cAMP induction of the uncoupling protein 1 (UCP1) gene requires p38 map kinase. *J. Biol. Chem.* **276,** 27077–27082 (2001).
75. Puigserver, P. *et al.* A Cold-Inducible Coactivator of Nuclear Receptors Linked to Adaptive Thermogenesis. *Cell* **92,** 829–839 (1998).
76. Xue, B., Coulter, A., Rim, J. S., Koza, R. A. & Kozak, L. P. Transcriptional Synergy and the Regulation of Ucp1 during Brown Adipocyte Induction in White Fat Depots. *Mol Cell Biol* **25,** 8311–8322 (2005).
77. Barak, Y. *et al.* PPARγ Is Required for Placental, Cardiac, and Adipose Tissue Development. *Molecular Cell* **4,** 585–595 (1999).

78. Seale, P. *et al.* Transcriptional control of brown fat determination by PRDM16. *Cell Metab.* **6,** 38–54 (2007).
79. Kajimura, S. *et al.* Regulation of the brown and white fat gene programs through a PRDM16/CtBP transcriptional complex. *Genes Dev.* **22,** 1397–1409 (2008).
80. Kajimura, S. *et al.* Initiation of myoblast to brown fat switch by a PRDM16-C/EBP-beta transcriptional complex. *Nature* **460,** 1154–1158 (2009).
81. Ohno, H., Shinoda, K., Ohyama, K., Sharp, L. Z. & Kajimura, S. EHMT1 controls brown adipose cell fate and thermogenesis through the PRDM16 complex. *Nature* **504,** 163–167 (2013).
82. Sambeat, A. *et al.* LSD1 interacts with Zfp516 to promote UCP1 Transcription and Brown Fat Program. *Cell Rep* **15,** 2536–2549 (2016).
83. Seale, P. *et al.* PRDM16 controls a brown fat/skeletal muscle switch. *Nature* **454,** 961–967 (2008).
84. Zeng, X. *et al.* Lysine-specific demethylase 1 promotes brown adipose tissue thermogenesis via repressing glucocorticoid activation. *Genes Dev.* **30,** 1822–1836 (2016).
85. Harms, M. J. *et al.* Prdm16 Is Required for the Maintenance of Brown Adipocyte Identity and Function in Adult Mice. *Cell Metabolism* **19,** 593–604 (2014).
86. Harms, M. J. *et al.* PRDM16 binds MED1 and controls chromatin architecture to determine a brown fat transcriptional program. *Genes Dev.* **29,** 298–307 (2015).
87. Arany, Z. *et al.* Transcriptional coactivator PGC-1α controls the energy state and contractile function of cardiac muscle. *Cell Metabolism* **1,** 259–271 (2005).
88. Kleiner, S. *et al.* Development of insulin resistance in mice lacking PGC-1α in adipose tissues. *PNAS* **109,** 9635–9640 (2012).
89. Kong, X. *et al.* IRF4 is a key thermogenic transcriptional partner of PGC-1α. *Cell* **158,** 69–83 (2014).
90. Eguchi, J. *et al.* Interferon-regulatory factors (IRFs) are transcriptional regulators of adipogenesis. *Cell Metab* **7,** 86–94 (2008).
91. Emmett, M. J. *et al.* Histone deacetylase 3 prepares brown adipose tissue for acute thermogenic challenge. *Nature* **546,** 544–548 (2017).
92. Yao, L. *et al.* Cold-Inducible SIRT6 Regulates Thermogenesis of Brown and Beige Fat. *Cell Reports* **20,** 641–654 (2017).
93. Rajakumari, S. *et al.* EBF2 Determines and Maintains Brown Adipocyte Identity. *Cell Metabolism* **17,** 562–574 (2013).
94. Shapira, S. N. *et al.* EBF2 transcriptionally regulates brown adipogenesis via the histone reader DPF3 and the BAF chromatin remodeling complex. *Genes Dev.* **31,** 660–673 (2017).
95. McDonald, M. E. *et al.* Myocardin-related transcription factor A regulates conversion of progenitors to beige adipocytes. *Cell* **160,** 105–118 (2015).
96. Koncarevic, A. *et al.* A novel therapeutic approach to treating obesity through modulation of TGFβ signaling. *Endocrinology* **153,** 3133–3146 (2012).
97. Yadav, H. *et al.* Protection from obesity and diabetes by blockade of TGF-β/Smad3 signaling. *Cell Metab.* **14,** 67–79 (2011).
98. Loft, A. *et al.* Browning of human adipocytes requires KLF11 and reprogramming of PPARγ superenhancers. *Genes Dev.* gad.250829.114 (2014). doi:10.1101/gad.250829.114

99. Bi, P. *et al.* Notch signaling regulates adipose browning and energy metabolism. *Nat Med* **20,** 911–918 (2014).
100. Mazzio, E. A. & Soliman, K. F. A. Epigenetics and nutritional environmental signals. *Integr. Comp. Biol.* **54,** 21–30 (2014).
101. Zhang, G., Sun, Q. & Liu, C. Influencing Factors of Thermogenic Adipose Tissue Activity. *Front Physiol* **7,** 29 (2016).
102. Patel, D. J. & Wang, Z. Readout of epigenetic modifications. *Annu. Rev. Biochem.* **82,** 81–118 (2013).
103. Petty, E. & Pillus, L. Balancing chromatin remodeling and histone modifications in transcription. *Trends Genet.* **29,** 621–629 (2013).
104. Kooistra, S. M. & Helin, K. Molecular mechanisms and potential functions of histone demethylases. *Nat. Rev. Mol. Cell Biol.* **13,** 297–311 (2012).
105. Venkatesh, S. & Workman, J. L. Histone exchange, chromatin structure and the regulation of transcription. *Nat. Rev. Mol. Cell Biol.* **16,** 178–189 (2015).
106. Kebede, A. F., Schneider, R. & Daujat, S. Novel types and sites of histone modifications emerge as players in the transcriptional regulation contest. *FEBS J.* **282,** 1658–1674 (2015).
107. Lawrence, M., Daujat, S. & Schneider, R. Lateral Thinking: How Histone Modifications Regulate Gene Expression. *Trends in Genetics* **32,** 42–56 (2016).
108. Inagaki, T., Sakai, J. & Kajimura, S. Transcriptional and epigenetic control of brown and beige adipose cell fate and function. *Nat Rev Mol Cell Biol* **17,** 480–495 (2016).
109. Sambeat, A., Gulyaeva, O., Dempersmier, J. & Sul, H. S. Epigenetic Regulation of the Thermogenic Adipose Program. *Trends in Endocrinology & Metabolism* **28,** 19–31 (2017).
110. Shamsi, F., Zhang, H. & Tseng, Y.-H. MicroRNA Regulation of Brown Adipogenesis and Thermogenic Energy Expenditure. *Front. Endocrinol.* **8,** (2017).
111. Trajkovski, M. & Lodish, H. MicroRNA networks regulate development of brown adipocytes. *Trends in Endocrinology & Metabolism* **24,** 442–450 (2013).
112. Xu, S., Chen, P. & Sun, L. Regulatory networks of non-coding RNAs in brown/beige adipogenesis. *Biosci Rep* **35,** (2015).
113. Lai, B. *et al.* MLL3/MLL4 are required for CBP/p300 binding on enhancers and super-enhancer formation in brown adipogenesis. *Nucleic Acids Res.* **45,** 6388–6403 (2017).
114. Visel, A. *et al.* ChIP-seq accurately predicts tissue-specific activity of enhancers. *Nature* **457,** 854–858 (2009).
115. Ohno, H., Shinoda, K., Spiegelman, B. M. & Kajimura, S. PPARγ agonists induce a white-to-brown fat conversion through stabilization of PRDM16 protein. *Cell Metab.* **15,** 395–404 (2012).
116. Duteil, D. *et al.* Lsd1 Ablation Triggers Metabolic Reprogramming of Brown Adipose Tissue. *Cell Rep* **17,** 1008–1021 (2016).
117. Inagaki, T. *et al.* Obesity and metabolic syndrome in histone demethylase JHDM2a-deficient mice. *Genes Cells* **14,** 991–1001 (2009).
118. Tateishi, K., Okada, Y., Kallin, E. M. & Zhang, Y. Role of Jhdm2a in regulating metabolic gene expression and obesity resistance. *Nature* **458,** 757–761 (2009).

119. Abe, Y. *et al.* JMJD1A is a signal-sensing scaffold that regulates acute chromatin dynamics via SWI/SNF association for thermogenesis. *Nat Commun* **6,** (2015).
120. Pan, D. *et al.* Jmjd3-Mediated H3K27me3 Dynamics Orchestrate Brown Fat Development and Regulate White Fat Plasticity. *Developmental Cell* **35,** 568–583 (2015).
121. Zha, L. *et al.* The Histone Demethylase UTX Promotes Brown Adipocyte Thermogenic Program Via Coordinated Regulation of H3K27 Demethylation and Acetylation. *J. Biol. Chem.* **290,** 25151–25163 (2015).
122. Li, F. *et al.* Histone Deacetylase 1 (HDAC1) Negatively Regulates Thermogenic Program in Brown Adipocytes via Coordinated Regulation of Histone H3 Lysine 27 (H3K27) Deacetylation and Methylation. *J. Biol. Chem.* **291,** 4523–4536 (2016).

Chapter 2:

Adipose Precursors Progress From Pref-1^{+} to PDGFRα^{+},

Requiring Sox9 Inactivation During Adipogenesis

Adipose precursors progress from Pref-1$^+$ to PDGFRα^+, requiring Sox9 inactivation during adipogenesis

Abstract

Adipocytes of white adipose tissue (WAT) arise from commitment and differentiation of adipose precursors. Various markers have been used in characterizing precursors from stromal vascular fraction of WAT but their relationship is not clear. Here, by inactivating Sox9, a target of Pref-1 which is secreted from adipose precursors to inhibit adipogenesis, we show for the first time that Pref-1$^+$: Sox9$^+$ cells precede PDGFRα^+ cells in the adipogenic pathway. We also show that Sox9 maintains the proliferative CD24$^+$ precursors in WAT and its inactivation is required for WAT development and expansion. Thus, Sox9 ablation promotes adipocyte differentiation and causes adiposity *in vivo*. Our study also demonstrates the effectiveness of the Pref-1 promoter for inducible gene ablation in very early adipose precursors

Introduction

White adipose tissue (WAT) represents a critical organ that serves as a major energy storage site in mammals. Adipocytes arise from differentiation of preadipocytes, which has been extensively studied *in vitro*, PPARγ and C/EBP family of transcription factors being the key drivers [1–3]. WAT contains not only lipid-filled adipocytes, but also so-called stromal vascular fraction (SVF) composed of multiple types of cells, including adipose precursors, endothelial cells, immune cells and fibroblasts. Various mesenchymal, stem and progenitor markers such as CD29, CD34, Sca-1, CD44, CD24, Pref-1 and PDGFRα have been used to isolate adipose precursors from SVF. However, whether cells labeled or sorted by these markers represent the same precursor population or cells at different stages of commitment and differentiation have not yet been established.

Preadipocyte factor-1 (Pref-1, also known as Dlk1/FA1), is one of the earliest genes described to be expressed in preadipocytes, but not in adipocytes, thus being used as a preadipocyte marker [4–7]. Pref-1 is a secreted factor that inhibits adipogenesis by activating MEK/ERK pathway. By lineage tracing, Pref-1 has been shown to mark WAT precursors, which are required for adipose development and expansion [8]. A subpopulation of adipose progenitors (Lin$^-$: CD29$^+$: CD34$^+$: Sca-1$^+$: CD24$^+$) has also been isolated using fluorescence activated cell sorting (FACS) [9] to give rise to more committed preadipocytes that are CD24$^-$, expressing early adipogenic transcription factors, PPARγ and C/EBPα [10]. In this study both CD24$^-$ and CD24$^+$ cells were reported to express PDGFRα. On the other hand, Lee et al, reported that PDGFRα^+ cells from WAT of high fat diet fed mice did not express PPARγ or CD24. Moreover, it is unclear whether CD24$^+$ or PDGFRα^+ cells represent the same population of precursors that express Pref-1. Since inhibition of proliferation in precursor cells is required for adipogenic differentiation, it remains unclear when the cells lose proliferative capacity and acquire early adipogenic gene signature during adipogenesis. The relationship among Pref-1, CD24 or PDGFRα^+ during adipogenic pathway also remains unclear.

Here, to understand the Sox9 function and to establish the order of these precursor populations in hierarchy of adipogenic progenitors, we used Pref-1 promoter to ablate Sox9, a target of Pref-1, in an inducible manner *in vivo*.

Sox9 belongs to a SoxE family of transcription factors that contain HMG domain- a highly conserved sequence specific DNA-binding motif. SoxE binds DNA as homo- or heterodimer with other members of SoxE family. Sox9 regulates transcription of genes involved in differentiation of multiple cell types [11–14] and is expressed in variety of cell types during embryogenesis as well as in various organs in mature mammals, including different cell types of intestinal epithelium [15], progenitor cells in the pancreas [16] and hair follicle stem cells (HF-SC) [17]. Due to perinatal lethality of Sox9 haploinsufficient mice [18], tissue-specific and developmental stage-specific ablation of Sox9 would allow to study relationship of adipose precursors and Sox9 function. In this regard, although Cre/LoxP technology has been widely used to knockout genes from adipose tissue, most of these studies utilized Cre driven by the promoters of genes that are expressed in differentiated adipocytes (such as AdipoQ or aP2/FABP4). Recently, PDGFRα has been used for gene ablation at the preadipocyte stage, although PDGFRα is also detected in various other tissues [19]. Since Pref-1 expression in adult tissues is restricted to precursor cells in WAT, the Pref-1 promoter may represent a powerful tool to inactivate Sox9 in adipose precursors.

Here, by using Pref-1-rtTA/TRE-Cre, we ablated Sox9 from WAT precursors in mice in an inducible manner (referred to as PreASKO mice). We demonstrate that ablating Sox9 in adipose precursors diminishes the pool of proliferating Pref-1$^+$ cells by progressing them to become PDGFRα$^+$ cells that do not proliferate but express early adipogenic genes. These results show the sequence of events in adipogenic pathway and for the first time demonstrate that Pref-1, Sox9$^+$ cells are earlier than PDGFRα$^+$ cells in hierarchy of adipose progenitors. Thus, the lack of Sox9 in PreASKO mice we generated in this study leads to enhanced adiposity with impaired insulin sensitivity, emphasizing the requirement of Sox9 inactivation for adipogenesis.

Results

Temporal ablation of Sox9 in Pref-1$^+$ cells *in vivo*

In order to characterize adipose precursors in the SVF of WAT and to understand the role of Sox9 in adipogenesis *in vivo*, we performed inducible Sox9 ablation by crossing Sox9 floxed mice with Pref-1-rtTA and TRE-Cre mice. In this system, rtTA induces transcription of Cre in the presence of doxycycline (Dox) to recombine LoxP sites for Sox9 inactivation in Pref-1 expressing cells (therein referred to as PreASKO) (Figure 3A). We first tested the presence of recombined Sox9 allele by PCR of genomic DNA from cultured primary cells of adipose SVF from PreASKO mice and control mice that were not exposed to Dox. Use of primers flanking the loxP sites in PCR predicts a 320 bp product (Sox9 Floxdel) upon Cre-mediated recombination of floxed allele, but not of wild type due to limited PCR extension time [11]. When these cells were exposed to Dox for 2 or 4 days, Sox9 Floxdel was detected in PreASKO SVF cells (Figure 3B left). Accordingly, with 2- and 8-fold increase in Cre expression at 2 and 4 days of Dox treatment, respectively, Sox9 mRNA levels were reduced by approximately 60% in PreASKO SVF cells (Figure 3B right). As expected, without Dox treatment, Sox9 allele

remained intact with no difference in Sox9 mRNA levels between control, floxed and PreASKO cells (data not shown). These data indicate that in this system, Sox9 can be ablated only in the presence of Dox, allowing inducible recombination of floxed allele at specific time points for examination of the role of Sox9, Pref-1+ cells in the adipogenic pathway *in vivo* and *in vitro*.

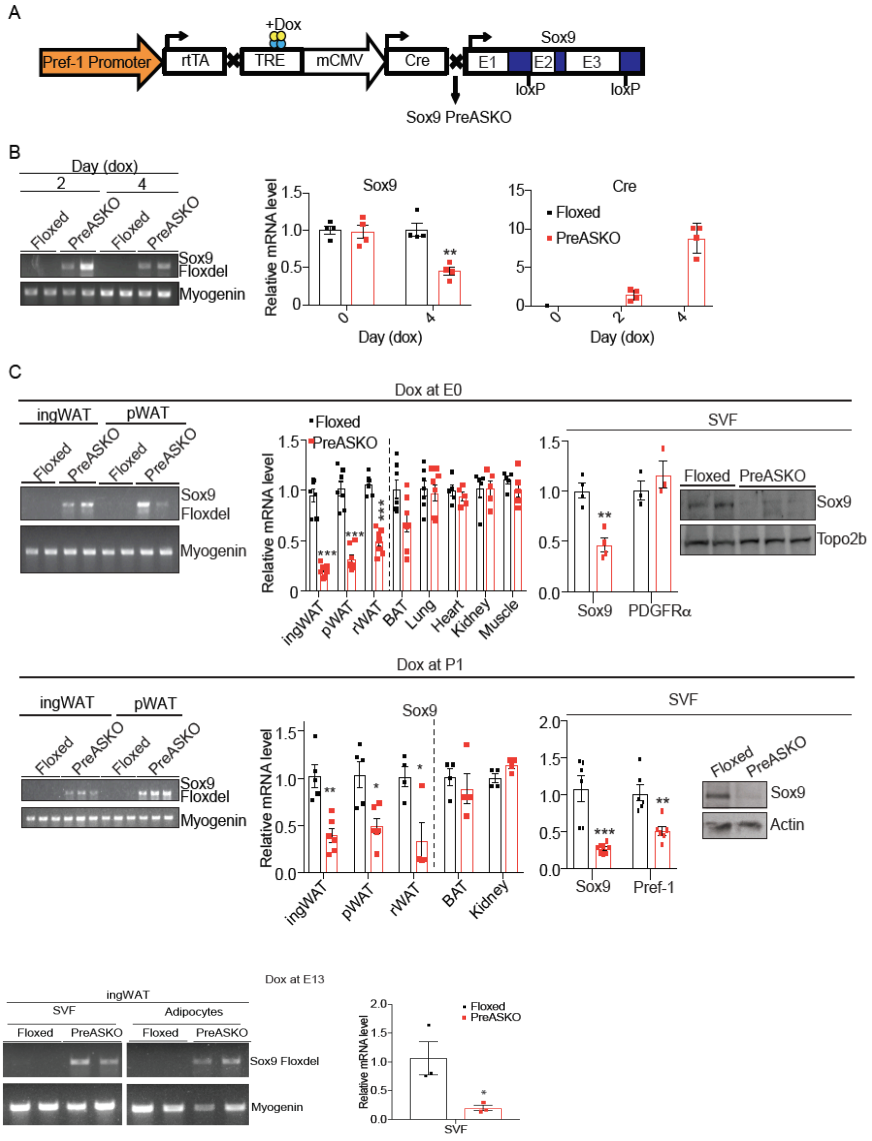

Figure 3. Temporal ablation of Sox9 in Pref-1^{+} cells *in vivo*.
(A) PreASKO mice generated by crossing mice with Pref-1-rtTA, TRE-Cre and Sox9 floxed mice. (B) Left: Sox9 Floxdel PCR with genomic DNA from primary ingWAT SVF cultured with Dox for 2 and 4 days. Right: Sox9 and Cre mRNA levels in the same cells. (C) Top left: Sox9 Floxdel PCR using gDNA from ingWAT and pWAT. Top center: RT-qPCR for Sox9 in various tissues of mice fed Dox since E0. Top right and far right: RT-qPCR and immunoblotting for Sox9 in WAT SVF of mice fed Dox at E0. Middle and bottom: Sox9 Floxdel PCR, RT-qPCR and immunoblotting for Sox9 in mice fed Dox at P1 or E13 respectively. * -p<0.05, ** -p<0.01.

We tested three different time points of Dox administration during mouse development to assess the effectiveness of Sox9 ablation. First, we started Dox at E0 to ablate Sox9 from Pref-1^{+} cells at the earliest stage during embryogenesis, and we observed the presence of Sox9 Floxdel product in ingWAT and pWAT of PreASKO mice as well as an effective diminution of Sox9 mRNA levels in WAT from PreASKO mice, approximately by 65%, 60%, and 50% in ingWAT, pWAT and rWAT, respectively (Figure 3C, top left and center).

There was no significant change in Sox9 expression in BAT, likely due to the low percentage of Pref-1 marked cells [8]. We have previously shown that Pref-1 and Sox9 are expressed only in SVF but not in adipocytes. Therefore, we measured Sox9 mRNA

level in SVF from ingWAT and observed an approximately 50% reduction in PreASKO mice, whereas expression of PDGFRα known to be enriched in SVF did not change (Figure 3C, top right). By immunoblotting, we verified that Sox9 protein was barely detectable in SVF of ingWAT when Dox was started at E0 (Figure 3C, top far right). Surprisingly, even with Dox administration started at E0, we did not detect any changes in Sox9 expression in tissues other than WAT, including lung, heart, kidney and muscle.

We next administered Dox starting at E13.5, an earliest time point when Pref-1 marked cells are detectable at the dorsal edge of the embryo [8]. This led to a presence of recombined Sox9 Floxdel PCR product in both SVF and adipocyte fraction of WAT from adult PreASKO mice (Figure 3, bottom left), the latter an indicative of adipocytes differentiated from Pref-1$^+$ precursors in which Sox9 was ablated. RT-qPCR of ingWAT SVF revealed a significant reduction in Sox9 mRNA level in PreASKO mice when Dox administration was started at E13.5 (Figure 3, bottom right). Overall, these results show that Pref-1-rtTA/TRE-Cre system can be successfully used for ablation of genes in precursor cells starting at E13.5.

Our previous work established that ingWAT starts to develop prenatally but expands mainly after birth, while pWAT develops postnatally [8].Therefore, we also assessed the effect of Dox starting at birth (P1) on recombination of Sox9 floxed allele. Using DNA from ingWAT and pWAT, we observed a presence of Sox9 Floxdel product in both ingWAT and pWAT from PreASKO mice, but not from control, floxed mice (Figure 3C, middle left). Sox9 mRNA levels were significantly lower by 50-60% in ingWAT, pWAT and rWAT, while remaining the same in other tissues, such as kidney (Figure 3C, middle center). We also documented a 70% reduction in Sox9 and a 50% in Pref-1 mRNA levels in SVF from ingWAT of PreASKO mice (Figure 3C middle right). Immunoblotting showed an almost undetectable Sox9 protein level in SVF of WAT from PreASKO mice (Figure 3C, middle far right). These results indicate that Pref-1-rtTA/TRE-Cre system can be used for ablation of Sox9 postnatally which circumvents potential effects during embryogenesis. These results, overall, show that Pref-1-rtTA/TRE-Cre system can be used for conditional and inducible ablation of genes specifically in precursor cells of WAT starting at E0, E13.5, or P1, allowing flexibility in the timing of ablation *in vivo*.

Sox9 ablation from Pref-1 cells depletes the pool of Pref-1$^+$ cells

In order to establish the hierarchy of adipocyte progenitor population(s) in WAT, we first traced the Pref-1$^+$ adipose precursors with Sox9 ablation, by crossing Pref-1-rtTA/TRE-Cre/Sox9 floxed mice with TRE-GFP mice. Thus, in the presence of Dox, cells with Sox9 ablation would also be labeled transiently by GFP fused to H2B (nGFP) (Figure 4A). Even with the low overall labeling efficiency due to the nuclear localization of nGFP, we still could detect by FACS, a 30% reduction in nGFP$^+$ cells in PreASKO mice, reflecting the proportion of Pref-1$^+$ cells (Figure 4B). Immunostaining of ingWAT with Pref-1 antibody revealed that, as expected, Pref-1 was colocalized with Na^+/K^+ channel in cells of ingWAT (Figure 4C), confirming its cell membrane localization. More importantly, we observed a decrease in Pref-1$^+$ cells in PreASKO mice, demonstrating that Sox9 ablation causes depletion of Pref-1$^+$ cells.

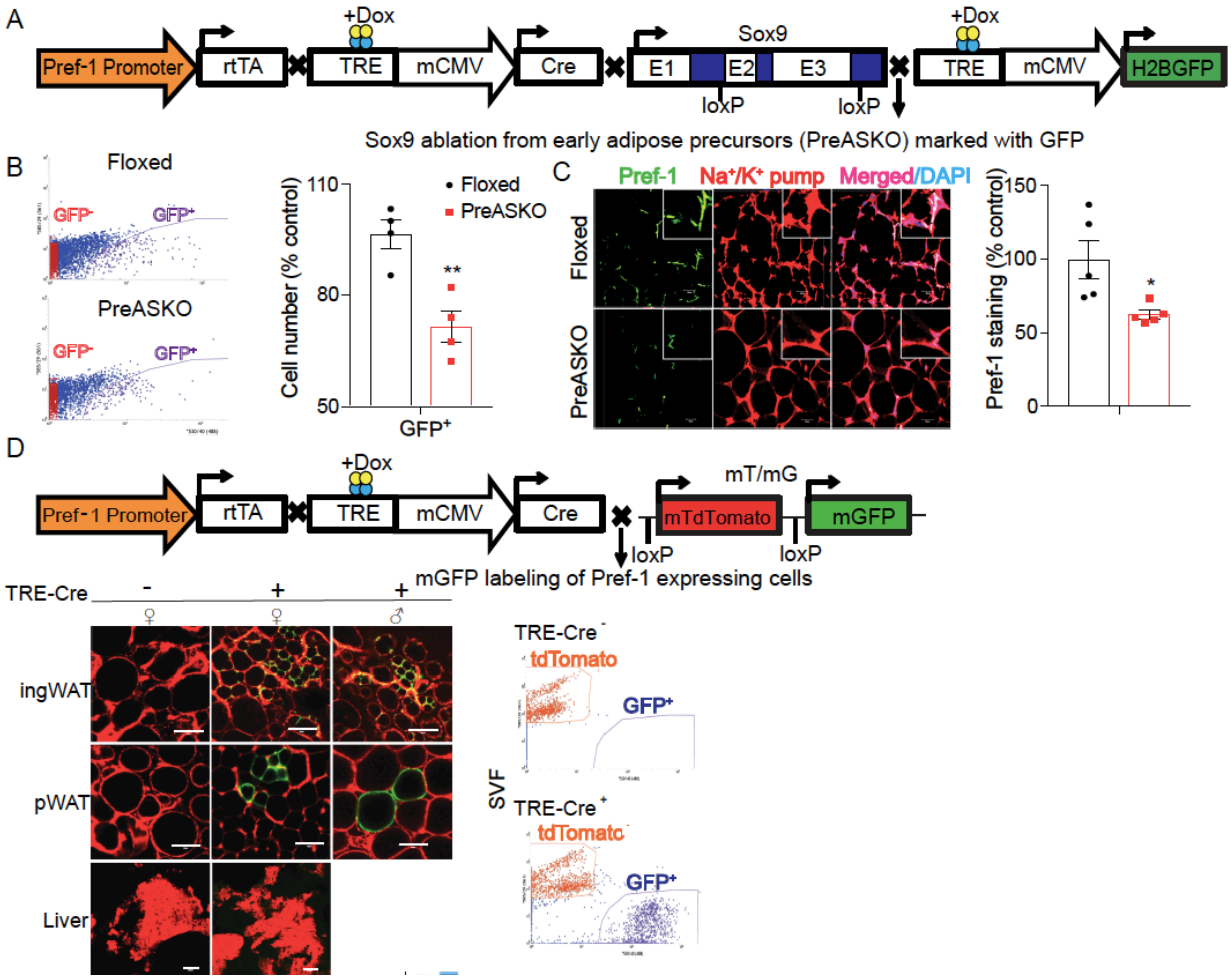

Figure 4. Sox9 ablation depletes the pool of Pref-1+ cells.
(A) PreASKO-GFP mice were generated by crossing PreASKO mice with TRE-GFP mice for fluorescent labeling of rtTA+ (therefore Pref-1+) cells with Sox9 ablation. (B) FACS plots (left) and quantification of average cell number of GFP+ cells in ingWAT SVF cells from 3 wk-old males fed Dox at P1. (C) Pref-1 immunostaining images and quantification in ingWAT (n=5), scale bar-20μm. (D) Top: Scheme of Pref-1-rtTA/TRE-Cre-mT/mG mice. Left: Representative confocal images with GFP and tdTomato fluorescence in various tissues of 3 wk-old Pref-1-rtTA positive female fed Dox at E0, 4 wk-old Pref-1-rtTA/Tre-Cre positive female and male fed Dox at E0, scale bar-50μm for WAT and 100μm for liver. Right: FACS plots for ingWAT SVF of 7 wk-old male mice fed Dox at E0. * -p<0.05, ** -p<0.01. ***-p<0.001.

In order to better characterize the specificity of TRE-Cre activated by rtTA driven by the Pref-1 promoter for conditional ablation and also to overcome the low signal of nuclear GFP, we next crossed Pref-1-rtTA/TRE-Cre positive mice with mT/mG mice to trace Pref-1$^+$ cells. All cells are expected to be labelled with membrane tdTomato, but Cre-expressing cells lose tdTomato and permanently acquire membrane GFP (mGFP), being more convenient for studying adipocytes and allowing for selection and tracing of Pref-1$^+$ cells (Figure 4D, top). Using this system, we observed that Pref-1-rtTA/TRE-Cre positive mice had approximately 30% of cells labeled with mGFP in ingWAT and approximately 10% in pWAT with only a handful of mGFP$^+$ cells in BAT due to low proportion of Pref-1$^+$ cells (data not shown) and no mGFP$^+$ cells in the liver, further

validating specificity for labeling of adipose tissue (Figure 4D, bottom left). Analysis of floating adipocytes by FACS was not feasible due to their large cell size and fragility [20]. However, we detected by FACS approximately 35% of SVF cells were mGFP positive and 44% were tdTomato positive in ingWAT of Pref-1-rtTA/TRE-Cre positive mice (Figure 4D bottom right). These observations indicate that Pref-1^{+} cells reside in ingWAT and pWAT but not in other tissues, and contribute to adipogenesis *in vivo*, further validating the use of our system for specific labeling of adipose precursors and gene ablation.

Given the reduction in Pref-1^{+} pool upon Sox9 ablation, we next tested gene expression changes in these Pref-1^{+} precursors at the global level. We performed RNA-Seq on nGFP^{+} cells from PreASKO-H2b-fused-GFP and control GFP mice. We found that 1220 and 891 genes were over 2-fold down- or up-regulated, respectively, in PreASKO mice, compared to control littermates (Figure 5A, left).

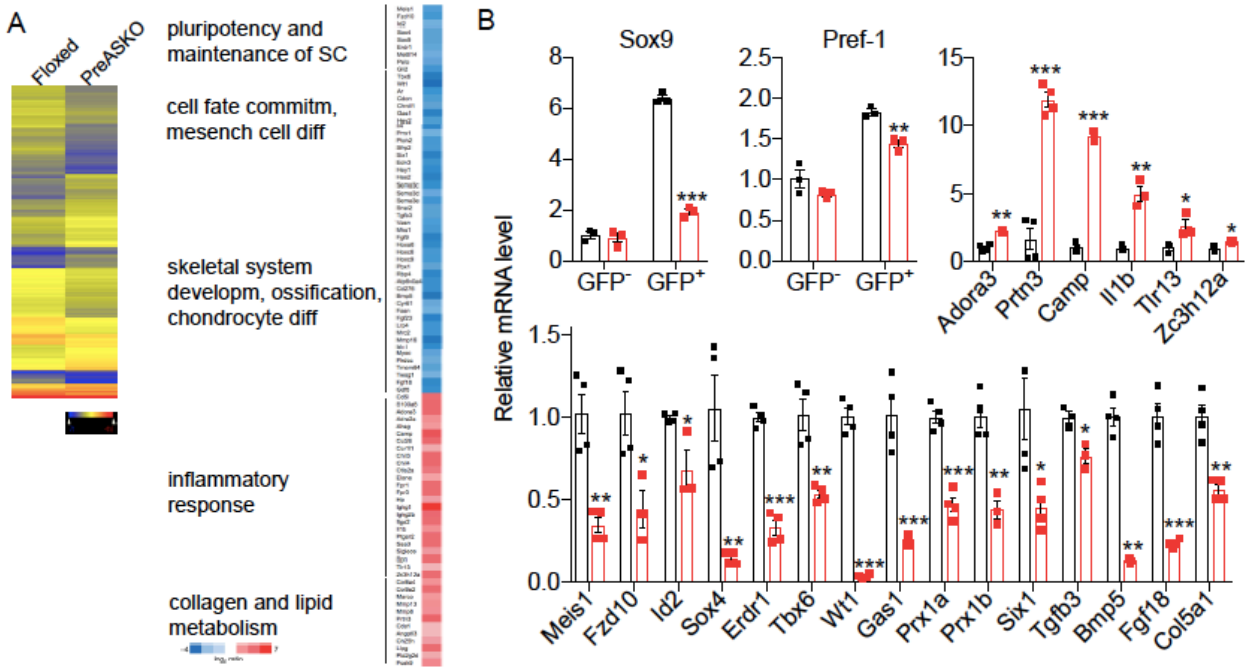

Figure 5. Sox9 ablation causes downregulation in stem cell and chondrocyte differentiation genes, inducing inflammatory and collagen metabolism genes.
(A) Left: RNA-sequencing heatmap of differentially expressed genes (more than 2-fold) between GFP^{+} floxed and PreASKO ingWAT SVF cells from 3 wk-old males fed Dox at P1 (n=6). (B) RT-qPCR verification of selected genes (n=4).* -p<0.05, ** -p<0.01. ***-p<0.001.

Down-regulated genes include those of signaling pathways that control pluripotency of stem cells (such as Meis1, Fzd10, Id2), stem cell population maintenance (e.g. Sox4, Erdr, Pelo), cell fate commitment (e.g. Tbx6, Prx1, Six1) and mesenchymal stem cell differentiation (e.g. Hey1, Hes2, Tgfb3), as well as embryonic skeletogenesis (e.g. Fgf9, Hoxa6), ossification and chondrocyte differentiation (e.g. Bmp5, Fgf18, Fgf23) (Figure 5A). Up-regulated genes include Inflammatory response genes (e.g. Adora3, Il1b, Tlr13), collagen metabolism genes (e.g. Col6a4, Col9a2, Marco, Mmp8, Mmp13) and of lipid metabolism (e.g. Angptl3, Lipg). RT-qPCR verified statistically significant changes in several representative genes that we examined

(Figure 5B). We also determined the expression levels of Sox9 and Pref-1 (Figure 5B) for verification of Sox9 ablation from Pref-1$^+$ cells.

We next measured proliferative capacity in sorted nGFP$^+$ cells from PreASKO mice. Indeed, we found an increase in proliferation in GFP$^+$ cells from PreASKO compared to control, floxed mice (Figure 6A).

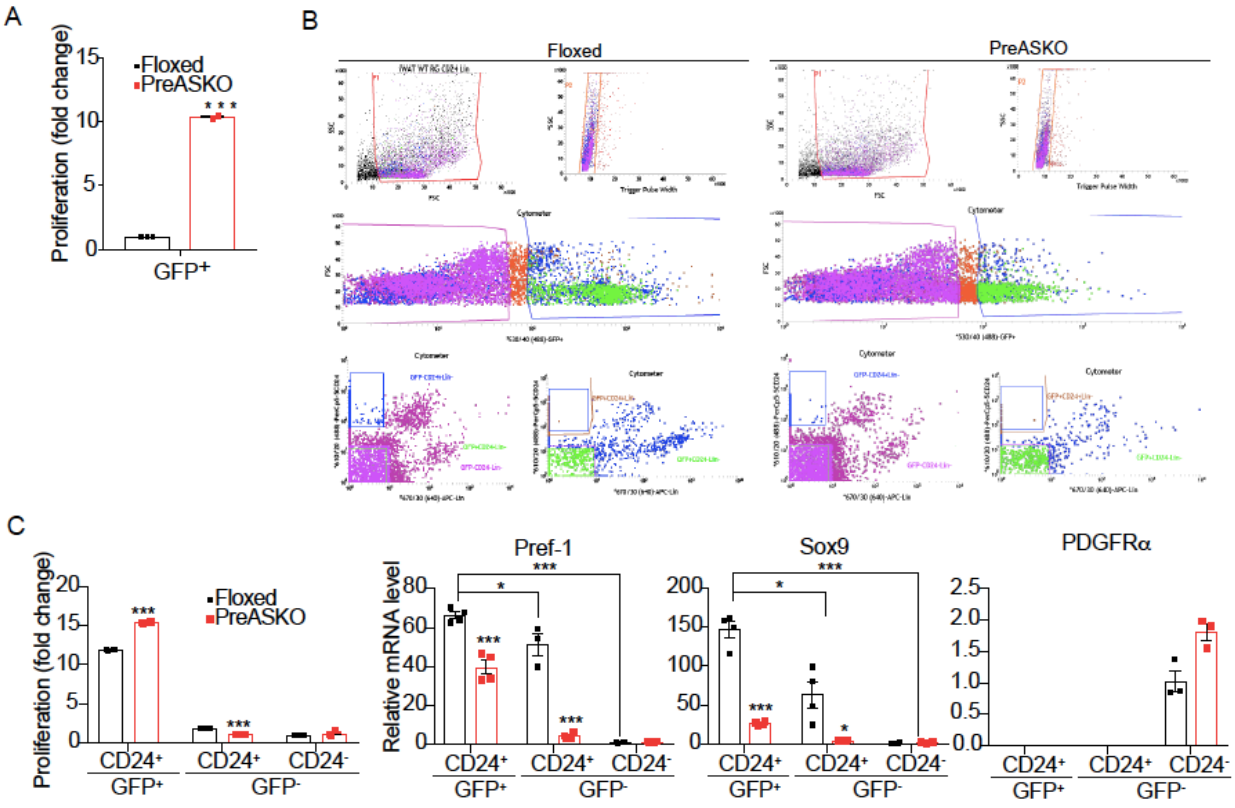

Figure 6. Sox9 inactivation causes incteased proliferation of Pref-1$^+$ cells.
(A) Proliferation capacity in floxed and PreASKO ingWAT SVF GFP$^+$ sorted cells, isolated from 7 wk-old mice given Dox at E0 (n=3). (B) FACS plots representing sorting strategy for GFP$^+$ and GFP$^-$ SVF cells first, out of which only Lin$^-$ cells were chosen and sorted for presence and absence of CD24. Cells were isolated form ingWAT of 5 wk-old mice given Dox at E0 (n=3). (C) Left: Proliferation capacity of various sorted populations in floxed and PreASKO mice, n=3. Right: RT-qPCR for Pref-1, Sox9 and PDGFRα in various sorted populations. * -p<0.05, ** -p<0.01. ***-p<0.001.

To characterize the specific population of precursor cells affected by Sox9 inactivation, we stained SVF cells from PreASKO-nGFP and floxed mice with CD24 for FACS analysis (Figure 6B). We found that floxed Lin$^-$: nGFP$^+$: CD24$^+$ population overall had the highest proliferation capacity compared to Lin$^-$: nGFP$^-$: CD24$^+$ or Lin$^-$: nGFP$^-$: CD24$^-$ population (Figure 6C left). Interestingly, Lin$^-$: nGFP$^+$: CD24$^+$ PreASKO cells exhibited higher proliferation rate than floxed cells, whereas Lin$^-$: nGFP$^-$: CD24$^+$ PreASKO cells showed reduced proliferation. RT-qPCR in various sorted populations revealed that Pref-1 and Sox9 were expressed at the highest level in Lin$^-$: nGFP$^+$: CD24$^+$ very early adipose precursors, and their expression gradually decreased as cells progressed in adipogenic development, being lower in Lin$^-$: nGFP$^-$: CD24$^+$ and being

lowest in Lin^-: $nGFP^-$: $CD24^-$ cells (Figure 6C right). Interestingly, PDGFRα expression was markedly higher in Lin^-: $nGFP^-$: $CD24^-$ cells (Figure 6C right), although we cannot rule out a low level of PDGFRα expression in $CD24^+$ cells that was not detected in our system. These data provided the first evidence that Pref-1 and Sox9 are expressed earlier than PDGFRα during adipose development and that Sox9 inactivation in Pref-1^+ cells directs the proliferative precursors into less proliferative preadipocytes at a later stage of adipogenic lineage. These results also demonstrate that Pref-1^+:$Sox9^+$ cells are very early adipose precursors with stem cell-like gene signature and Sox9 is required to maintain these very early adipose precursors in a state yet to undergo differentiation.

Sox9 ablation from Pref-1^+ cells increases PDGFRα$^+$ cells expressing adipogenic markers

Recently, PDGFRα has been used as a preadipocyte marker in FACS and thus, we next examined the relationship between Pref-1^+:$Sox9^+$ and PDGFRα$^+$ cells in the adipogenic pathway. By FACS we detected that approximately 10% of SVF cells from control ingWAT were positive for PDGFRα, whereas 16% of those from PreASKO mice were positive for PDGFRα (Figure 7A), representing a 60% increase in PDGFRα$^+$ cells as a result of Sox9 ablation. We also performed immunostaining of WAT sections using PDGFRα antibody to further quantify PDGFRα$^+$ population in ingWAT. We observed approximately 40% increase in PDGFRα$^+$ cells in ingWAT of PreASKO mice compared to control littermates (Figure 7B). These results point to the fact that lack of Sox9 drives very early adipose precursors to become PDGFRα$^+$ preadipose cells.

To further characterize and compare the Pref-1^+:$Sox9^+$ cells and PDGFRα$^+$ cells in the progression of adipogenesis, we analyzed gene expression in cells sorted with PDGFRα antibody by RT-qPCR. As expected, PDGFRα mRNA was almost undetectable in the PDGFRα$^-$ fraction indicating the efficiency of the FACS using the PDGFRα antibody (Figure 7C, right). More importantly, Sox9 mRNA level in PDGFRα$^+$ fraction of PreASKO showed approximately 60% reduction in Sox9 expression (Figure 7C, left). Interestingly, PDGFRα$^-$ population from PreASKO mice also showed a 50% lower Sox9 expression, indicating that Sox9 deletion using Pref-1-rtTA/TRE-Cre was detected in but not limited to PDGFRα$^+$ cells. This points to the concept that Pref-1 and PDGFRα do not mark the same population of cells.

Additionally, RNA-Seq revealed a minimal PDGFRα expression in floxed $nGFP^+$ (Pref-1^+) cells (data not shown), further proving that Pref-1 is expressed at an earlier stage of adipose precursors than PDGFRα. We, therefore, documented other changes in gene expression at the global level in these PDGFRα$^+$ cells that are further along in adipogenic pathway in the presence and absence of Sox9.

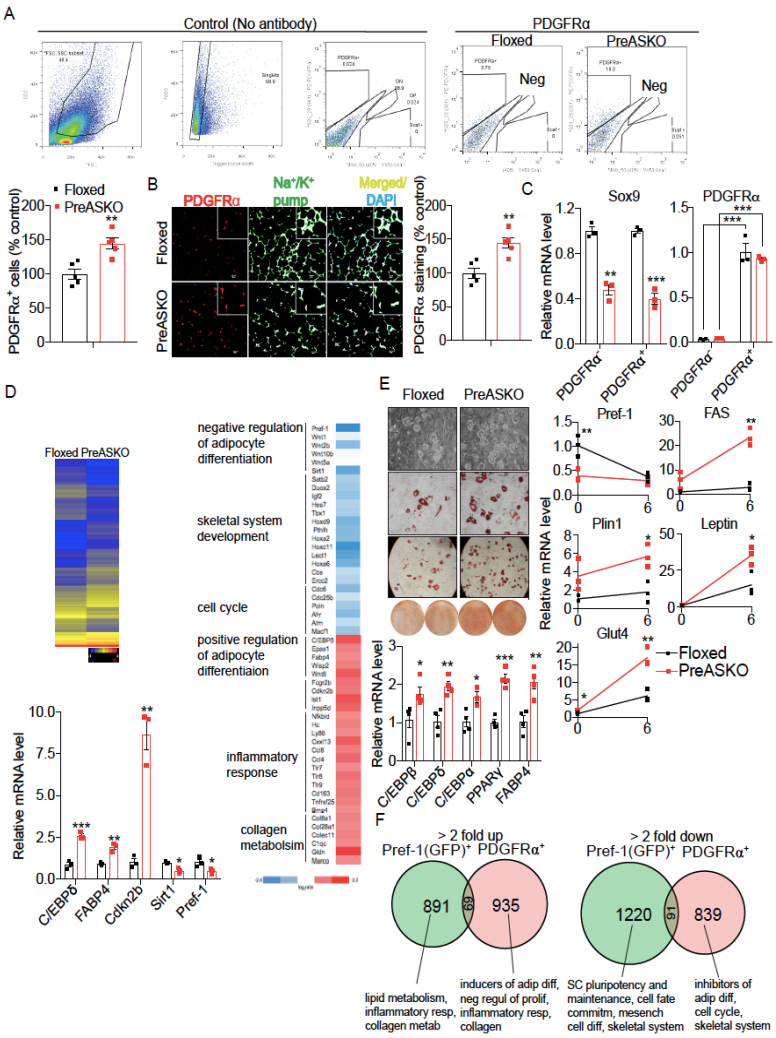

Figure 7. Sox9 ablation from Pref-1$^+$ cells increases PDGFRα$^+$ cells expressing adipogenic markers.
(A) Top: FACS plots for control or αPDGFRα antibody on ingWAT SVF cells from 6 wks old female mice (n=5). Bottom: average quantification of PDGFRα$^+$ cells in ingWAT. (B) Immunostaining and its quantification of ingWAT, scale bar-20μm. (C) RT-qPCR in sorted populations from ingWAT SVF of 3 wk-old males. (D) Top and right: RNA-Sequencing heatmap of differentially expressed genes (more than 2-fold) between PDGFRα$^+$ ingWAT SVF cells from floxed and PreASKO mice. Bottom: RT-qPCR verification of selected genes. (E) Top left: Brightfield and ORO pictures of sorted PDGFRα$^+$ cells at day 6 of differentiation. Right and bottom: RT-qPCR for during differentiation and at day 6, left (n=3). (F) Overlap of differentially expressed genes (> 2-fold) between RNA-Sequencing from GFP$^+$ and PDGFRα$^+$ cells. All mice in this Figure were fed Dox at P1. * - p<0.05, ** -p<0.01. ***-p<0.001.

We found that expression of 830 unique genes were more than 2-fold lower in PreASKO mice, while 639 were more than 2-fold higher (Figure 7D, top left). Pathway analysis indicated that genes involved in negative regulation of adipocyte differentiation such as Pref-1, Wnt1, Wnt2b, Wnt10b, Wnt5a and Sirt1, as well as genes responsible for skeletal system development and cell cycle were downregulated in PDGFRα$^+$ cells from PreASKO mice (Figure 7D, right). Conversely, markers of adipocyte differentiation, such as C/EBPδ, and FABP4, and those genes that negatively regulate proliferation, inflammatory response genes and genes involved in collagen metabolism were upregulated in PreASKO mice. RT-qPCR verified that expression of C/EBPδ and FABP4 was 2-2.5- fold higher, and Cdkn2b was 8-fold higher in PDGFRα$^+$ cells from PreASKO mice. In contrast, Pref-1 level was over 2-fold lower in PreASKO cells (Figure 7D, bottom left). Additional gene expression study by microarray analysis of PDGFRα$^+$ cells from ingWAT SVF showed downregulation of osteoblast/osteoclast differentiation genes and cell cycle genes and upregulation of inflammatory response genes in the absence of Sox9 (data not shown). Together, these data indicate that Pref-1$^+$ early precursors upon Sox9 ablation become PDGFRα$^+$ cells with elevated expression of

early adipogenic genes and inhibitors of proliferation and decreased expression of inhibitors of adipocyte differentiation and cell cycle genes.

To test whether these changes in gene expression indeed predispose cells to adipogenic differentiation, we subjected PDGFRα^+ sorted cells from floxed and PreASKO mice to adipogenic differentiation protocol. We found that, even prior to differentiation procedure, PreASKO cells had a markedly lower expression of Pref-1 and higher expression of adipocyte markers, such as Plin1 and Glut4 (Figure 7E, top right). Upon treatment with differentiation cocktail, albeit having lower than expected differentiation efficiency due to undergoing cell sorting procedure, PDGFRα^+ PreASKO cells differentiated at a higher degree than control cells, based on lipid accumulation by Oil Red O staining (Figure 7E, top left). As expected, the control floxed cells during differentiation showed a decrease in Pref-1 expression with an increase in expression of FAS, Plin1, Leptin, Glut4. More importantly, PreASKO cells showed an even higher increase in expression of those adipogenic markers, while Pref-1, which was low before differentiation, further decreased. These cells also showed increased expression of adipogenic transcription factors, C/EBPβ and C/EBPδ, as well as C/EBPα, PPARγ (Figure 7E, bottom). Based on these results, we conclude that Pref-1$^+$ cells upon Sox9 inactivation become PDGFRα^+ cells with high adipogenic potential.

To better establish the relationship between Pref-1$^+$:Sox9$^+$ cells and PDGFRα^+ cells, we compared RNA-Seq data from PDGFRα^+ and nGFP$^+$ cells and found only 69 upregulated genes and 91 down-regulated to be in common, representing less than 10% of total of approximately 800-1200 up-regulated or down-regulated genes (Figure 7F). Most of the common genes were those involved in general processes such as transcription or metabolism, and not directly related to cell commitment or differentiation. These data are in line with the concept that Sox9 maintains gene program of very early mesenchymal adipose precursors that do not yet express PDGFRα in adipogenic pathway**.**

Sox9 ablation from Pref-1 cells promotes *in vitro* adipocyte differentiation

Since we propose that Pref-1$^+$ precursors turn into PDGFRα^+ cells expressing adipogenic markers in the absence of Sox9 in WAT *in vivo*, we asked whether cells lacking Sox9 exhibit enhanced adipogenic differentiation in culture. By using primary culture of SVF from WAT subjected to adipocyte differentiation protocol *in vitro*, we observed that Sox9 mRNA and protein levels were 60% lower at day 0 remained low throughout differentiation procedure in PreASKO cells, while control, floxed cells exhibited a high level of Sox9, which was markedly reduced during adipocyte differentiation (Figure 8A, left and center). Immunostaining showed virtually no Sox9 staining in PreASKO cells, whereas most of the nuclei in control cells were positive for Sox9 (Figure 8A, right). Absence of Sox9 in PreASKO cells lead to enhanced adipocyte differentiation, characterized by higher percentage of cells accumulating lipids, as detected by Oil Red O staining (Figure 8B, left). Importantly, PreASKO cells showed an even greater induction of adipocyte markers at day 6 and day 8 of differentiation

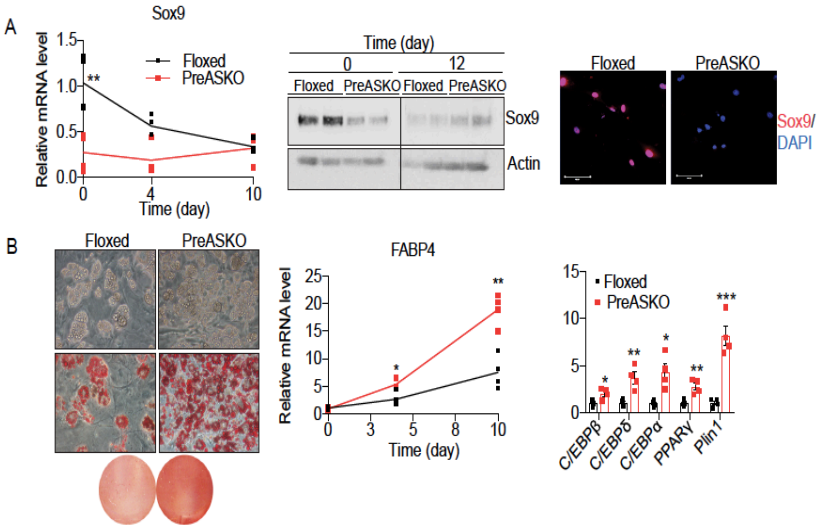

Figure 8. Sox9 ablation from Pref-1 cells promotes *in vitro* adipocyte differentiation. (A) RT-qPCR (left) and immunoblotting (center) during differentiation and immunostaining at day 0 (right) for Sox9 in cultured ingWAT SVF after 4 days of Dox treatment. (B) Brightfield and ORO pictures of cells from Figure 8A at day 7 of differentiation (top and middle left) and ORO picture of the whole dish at day 4 (bottom left). RT-qPCR for FABP4 during differentiation (center) and various adipogenic genes at day 8 (right). * - p<0.05, ** -p<0.01. ***-

compared to control cells. We also detected higher expression of adipogenic transcription factors, C/EBPα, PPARγ, as well as C/EBPβ and C/EBPδ that we previously reported to be suppressed by Sox9 [21] (Figure 8B, right). Overall, these results demonstrate that Pref-1-rtTA/TRE-Cre-mediated Sox9 inactivation in adipose precursors promotes adipocyte differentiation as judged by gene expression and lipid accumulation.

To further examine the role of Sox9 in adipocyte differentiation in cultured cells, we utilized CRISPR-Cas9 system using two different sgRNAs to create Sox9-KO 3T3-L1 cells. We performed FACS for Cas9/sgRNA expressing cells and expanded positive clones from a single cell. Sequencing of the genomic DNA from a single cell-derived clone showed mixed sequences in the region targeted by this sgRNA possibly due to hypertriploidy in 3T3-L1 cells [22] (data not shown). Regardless, this clonal line (KO-c) showed almost undetectable Sox9 protein by immunoblotting (Figure 8A). Upon adipogenic differentiation, compared to wild type (scr), KO-c cells showed a striking enhancement in lipid accumulation and a much higher induction in adipogenic genes at both mRNA and protein levels (Figure 8B,C). We also performed similar experiments using a pool of expanded cells sorted for expression of Cas9 with a different sgRNA, that showed very low Sox9 protein (data not shown). Pool of Sox9 KO cells upon differentiation showed a higher lipid accumulation with a significantly elevated expression of early and terminal adipogenic genes (data not shown).

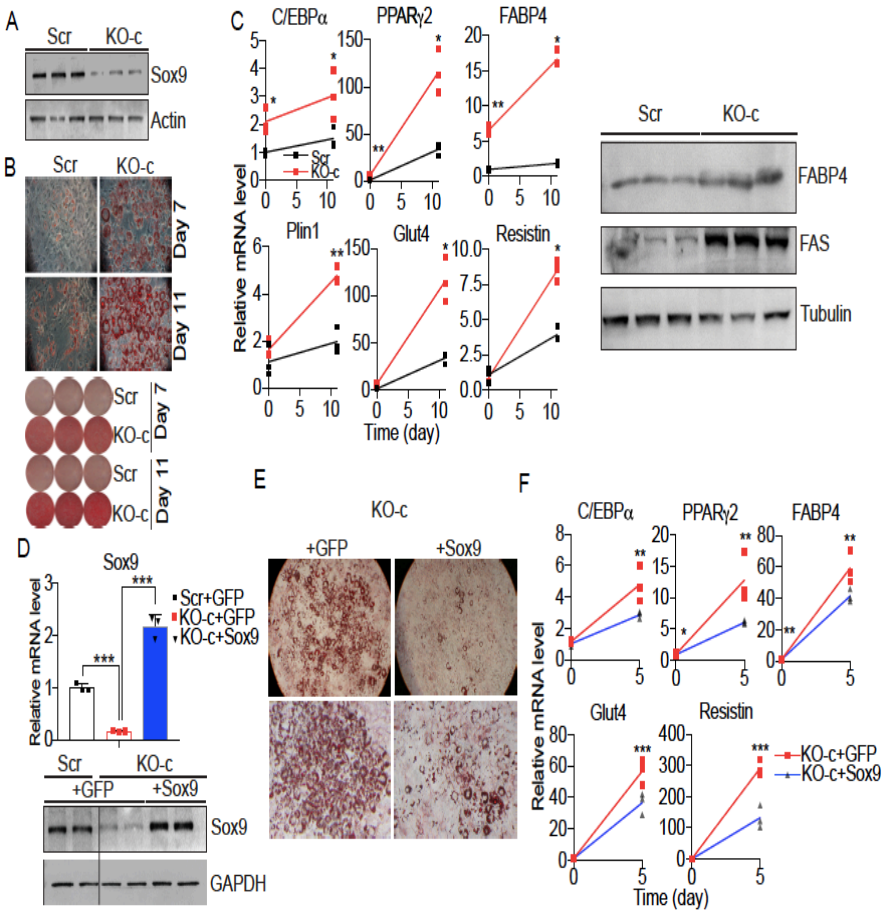

Figure 9. Sox9 ablation from 3T3-L1 cells promotes *in vitro* adipocyte differentiation. (A) Immunoblotting at day 0 for Sox9 in scr and KO-c (clonal) line that were grown from single cell. (B) ORO pictures of cells from Figure 4C at day 7 and 11 of differentiation with rosiglitazone. (C) RT-qPCR (left) (n=3) and immunoblotting (right) for adipogenic markers at day 11 of differentiation (cells were treated with rosiglitazone). (D) RT-qPCR (n=3) (top) and immunoblotting (bottom) for Sox9 at day 0 in scr and KO-c cells infected with Ad-GFP or Ad-Sox9. (E) ORO pictures of KO-c cells infected with Ad-GFP or Ad-Sox9. (H) RT-qPCR (n=3) for various markers during adipocyte differentiation in these cells. * -p<0.05, ** -p<0.01. ***-p<0.001.

To further verify that this enhancement of differentiation was indeed due to the loss of Sox9, we performed a rescue by introducing Sox9 adenovirus into KO-c cells. After viral transduction, Sox9 levels in the KO-c cells approached those of scr control cells (Figure 9D). Indeed, Sox9 addition was sufficient to dramatically slow down lipid accumulation and reduce adipogenic gene expression such as C/EBPα, PPARγ, FABP4, Glut4 and resistin during differentiation process (Figure 9E,F). Overall, these results clearly show that Sox9 ablation promotes adipocyte differentiation *in vitro* and that upon Sox9 rescue, these cells exhibit a dramatic slowdown in differentiation. Overall, these results further show the role of Sox9 to maintain Pref-1$^+$ cells as very early precursors and to prevent progression in adipocyte differentiation.

Sox9 ablation from Pref-1$^+$ cells in mice increases adiposity impairing insulin sensitivity

With the establishment of Pref-1$^+$: Sox9$^+$ cells as early precursors in adipogenic pathway and the role of Sox9 for maintenance of very early precursor preventing progression in adipocyte differentiation *in vitro*, we then examined the effect of Sox9 ablation on adipose tissue development *in vivo*. When Dox was administered starting at E0, PreASKO mice showed a higher body weight than floxed littermates starting at 7

and 5 wks of age for female and male mice, respectively (Figure 10A). There was no difference in body weight between the two genotypes when these mice were not exposed to Dox (Figure 11A). Moreover, echoMRI at 11 wks of age showed a 2-fold increase in fat mass of PreASKO mice compared to their floxed littermates with no significant difference in lean body mass (Figure 10B, top left). Dissection of ingWAT and pWAT of PreASKO mice showed 50% higher WAT weights, while other tissues, such as kidney, liver, heart and lung, had no detectable Sox9 ablation were grossly normal in size, weight and color (Figure 10B, top right, bottom). These data indicate that Pref-1^{+} very early adipose precursors without Sox9 prenatally, contribute to accumulation of WAT mass, demonstrating importance of Sox9 inactivation for embryonic adipogenesis. We next interrogated if increased WAT mass was accompanied by changes in adipocyte size. Histological analysis of ingWAT and pWAT sections after H&E staining revealed larger adipocyte size of PreASKO mice (Figure 10C, left). On average, PreASKO mice had a 2-fold larger cell size, having a higher number of larger cells and a lower number of smaller cells (Figure 10C, right). Gene expression analysis revealed that larger adipocyte size was accompanied by a 2-fold increase in mRNA levels for Sox9 targets, C/EBPβ and C/EBPδ, as well as a 2- to 6-fold increase in the expression levels of early and late adipocyte markers in ingWAT and, to a lesser degree in pWAT and rWAT, of PreASKO mice (Figure 10D, left and Figure 11C). Immunoblotting also revealed a substantial increase in C/EBPβ and C/EBPδ protein levels in ingWAT of PreASKO mice (Figure 10, right), indicating suppressive effect of Sox9 on adipogenesis.

When Dox administration was started at P1, PreASKO male mice on chow diet accumulated significantly higher body weight than floxed littermates starting at 8 wks of age, exactly 3 wks later when compared to mice given Dox at E0 (Figure 10E). Additionally, PreASKO mice showed higher WAT mass as measured by echoMRI than their floxed littermates with no significant difference in lean body mass (Figure 10F, left). Consistently, ingWAT and pWAT of PreASKO mice given Dox at P1 were markedly enlarged, while kidney, liver, heart and lung were not affected (Figure 10F, right). Computed tomography (CT-scan) for body composition analysis also revealed an expansion of ingWAT in PreASKO mice as shown in transverse sections, although no clear conclusion could be drawn in visceral WAT due to the presence of internal organs making the imaging analysis difficult (Figure 10G, left). Imaging of the whole mount adipose tissue stained with LipidTOX, also showed larger lipid-containing adipocytes in both ingWAT and pWAT of PreASKO mice (Figure 10G, right). Although Sox9 is known to be an important regulator of skeletal-osteoprogenitor cells, CT-scan images of transverse and mid-sagittal sections of mice given Dox at P1 did not show any notable differences in structure or size of the vertebrae or the whole skeletal system (Figure 11B).

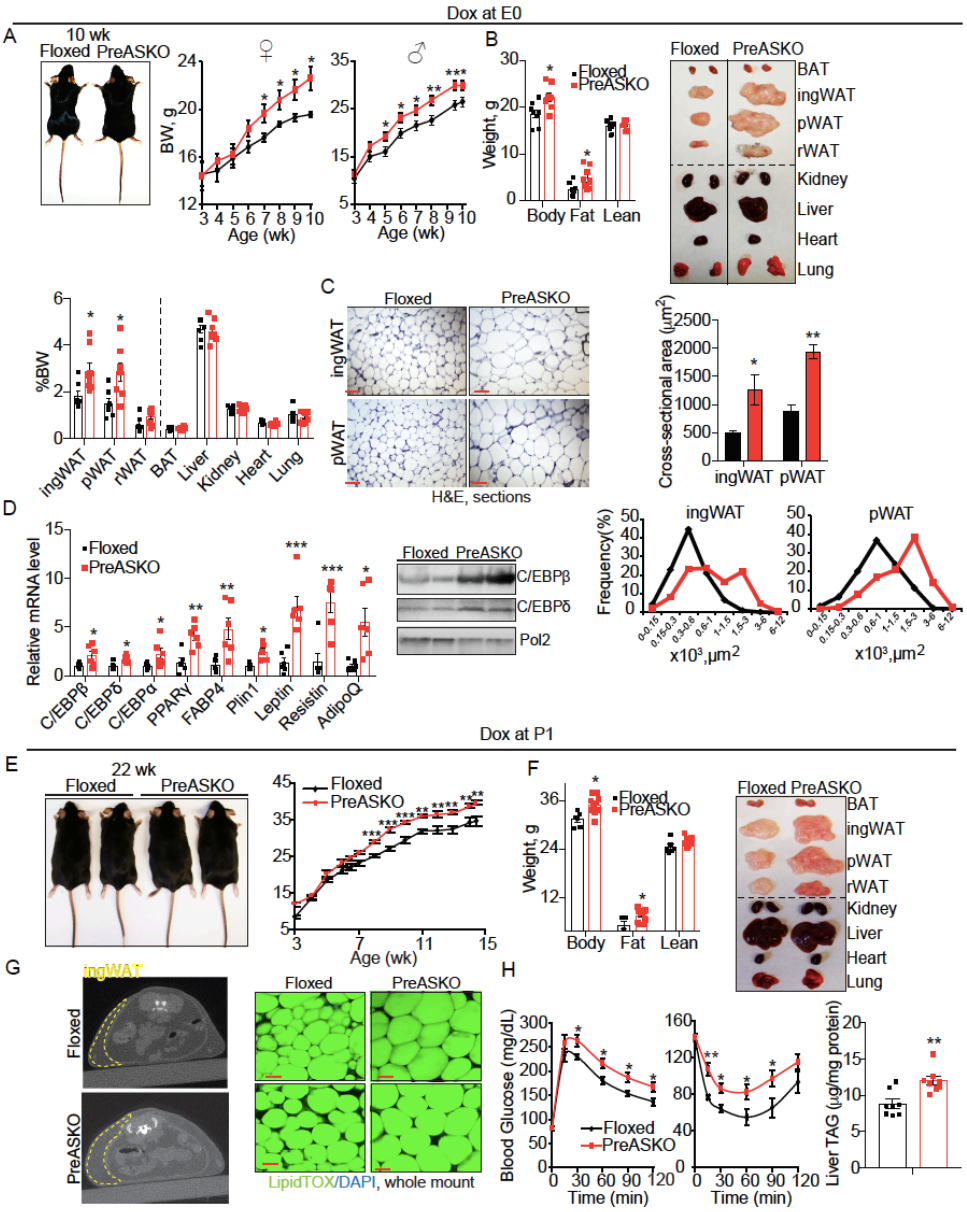

Figure 10. Sox9 ablation from Pref-1^{+} cells in mice increases adiposity impairing insulin sensitivity.

(A) Left: Representative image of 11 wk-old female mice. Center: Body weight in female (n=8) and male mice (n=8-7). (B) Weight determined by EchoMRI (top right), image of tissues and their weight, expressed as % of body weight (BW) (top right, bottom) (n=8). (C) Left: H&E staining of slides from ingWAT and pWAT, scale bar-100 μm. Right: Average cell size (n=90-230 cells analized). (D) RT-qPCR and immunoblotting in ingWAT (n=6). (E) Left: Image of 22 wk-old male mice. Right: Body weight of male mice (n=8-11). (F) Left: Weight determined by EchoMRI (n=6-10) in 22 wk-old male mice. Right: representative image of tissues. (G) Left: CT-scan image of transverse section. Right: whole mount images of ingWAT and pWAT, stained with LipidTOX Green and DAPI, from 22 wk-old male mice, scale bar- 50 μm. (H) GTT (left) on 14- wk old male mice and ITT (center) on 17 wk-old male mice (n=8-11) and TAG content in the liver (n=8). Dox administration at E0: Figure 10A-D, Dox administration at P1: Figure 10E-H. * -p<0.05, ** -p<0.01. ***-p<0.001.

Overall, using a temporally controlled Pref-1-rtTA/TRE-Cre system, we show that Sox9 ablation at E0 or at P1 leads to accumulation of WAT in mice, demonstrating inactivation of Sox9 in early Pref-1^{+} adipose precursors as an essential step for both embryonic and postnatal adipogenesis. These results also demonstrate the suitability of

our Pref-1-rtTA/TRE-Cre system for specific and inducible knockout in early adipose precursor cells.

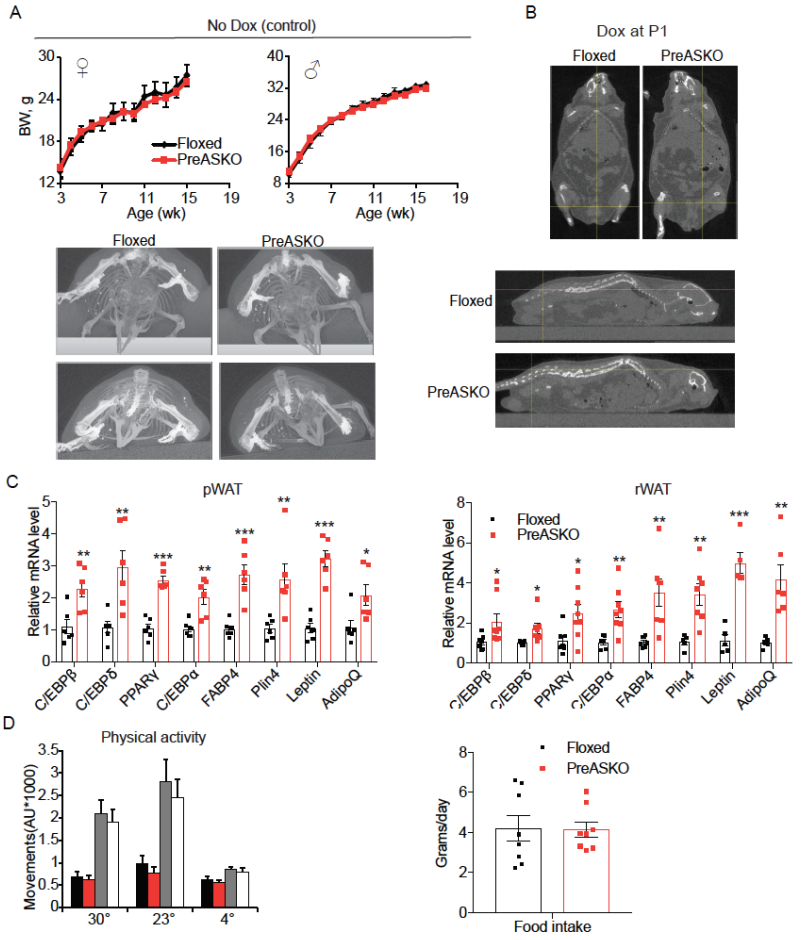

Figure 11. Sox9 ablation from Pref-1$^+$ cells in mice causes increased expression of adipogenic genes in WAT with no changes in skeletal system, physical activity or food intake.
(A) Body weight of female and male mice (n=12) that were never exposed to Dox. (B) CT-scan images of transverse and midsagittal sections of 22 wk-old male mice fed Dox at P1. (C) RT-qPCR for adipogenic markers in pWAT and rWAT from same mice as in Figure 10-A (n=6), left. (D) Physical activity and food intake of floxed and PreASKO mice.

We next examined glucose homeostasis in mice with Sox9 ablation in Pref-1$^+$ cells. PreASKO mice on chow diet revealed substantially higher blood glucose levels during glucose tolerance test (GTT) starting 30 min post glucose injection, indicating reduced glucose tolerance (Figure 10H, left). Additionally, during insulin tolerance test (ITT), while both genotypes responded to insulin with a reduction in blood glucose levels, PreASKO mice in comparison to control floxed mice had significantly higher glucose levels throughout ITT, showing reduced insulin sensitivity, which we detected to accompany a mild increase in TAG content in the liver (Figure 10H, middle and right). We did not observe any differences in food intake or physical activity in PreASKO mice, indicating the effect of Sox9 ablation on adipose tissue development which in turn affects insulin sensitivity (Figure 11D). Altogether, these data suggest that Sox9 inactivation in Pref-1$^+$ cells at E0 or at P1 induces adipogenic gene program in early adipose precursors causing increase in adipocyte size, thereby increasing ingWAT and pWAT mass. WAT accumulation in turn leads to impaired insulin sensitivity in PreASKO mice.

To further examine the role of Sox9 at later stages of adipocyte differentiation compared to Pref-1-rtTA/TRE-Cre [23], we also crossed Sox9 floxed mice with FABP4-Cre mice (ASKO mice) (Figure 12A).

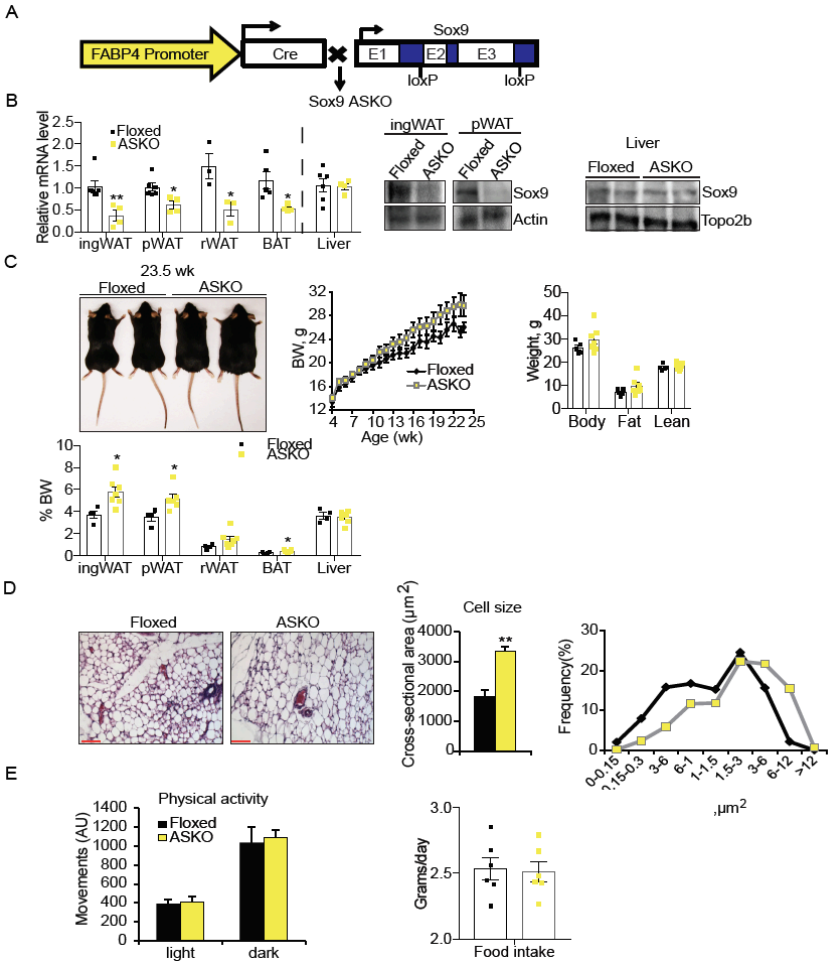

Figure 12. Sox9 ablation using FABP4-Cre increases adiposity. (A) ASKO mice were generated by crossing FABP4-Cre mice with Sox9 floxed mice. (B) RT-qPCR (left) and immunoblotting (right) for Sox9 in floxed and ASKO mice of 23.5 wk-old female mice (n=6-4). (C) Left: Representative image of 23.5 wk-old female mice. Center: Body weight of female mice (n=6-8). Right: Weight determined by EchoMRI. Bottom: Representative average tissue weight expressed as %BW in 23.5 wk-old female mice (n=5-8). (D) H&E staining of slides from ingWAT of 5 wk-old male mice (left) and average cell size and cell size distribution (center and right), scale bar-100μm (n=300-550 cells analyzed). (E) Physical activity and food intake of 22 wks old male floxed or ASKO mice (n=8-5).

We observed a 60-50% lower Sox9 mRNA and protein levels in ingWAT and pWAT, but not in the liver of ASKO mice (Figure 12B). Notably, ASKO mice on chow diet showed a trend of higher body weight and higher ingWAT, pWAT and BAT weights with an increase in adipocyte size assessed by H&E staining of ingWAT (Figure 12C-E). These results support that Sox9 ablation using FABP4-Cre also leads to an increase in body weight due to increase in adipocyte size and adipose tissue mass. However, the phenotype of mice with Sox9 ablation by using FABP4-Cre was milder than that by Pref-1-rtTA/TRE-Cre, clearly due to the later activation of FABP4 promoter during adipogenesis in comparison to Pref-1 promoter that is active in very early adipose precursors (Figure 13).

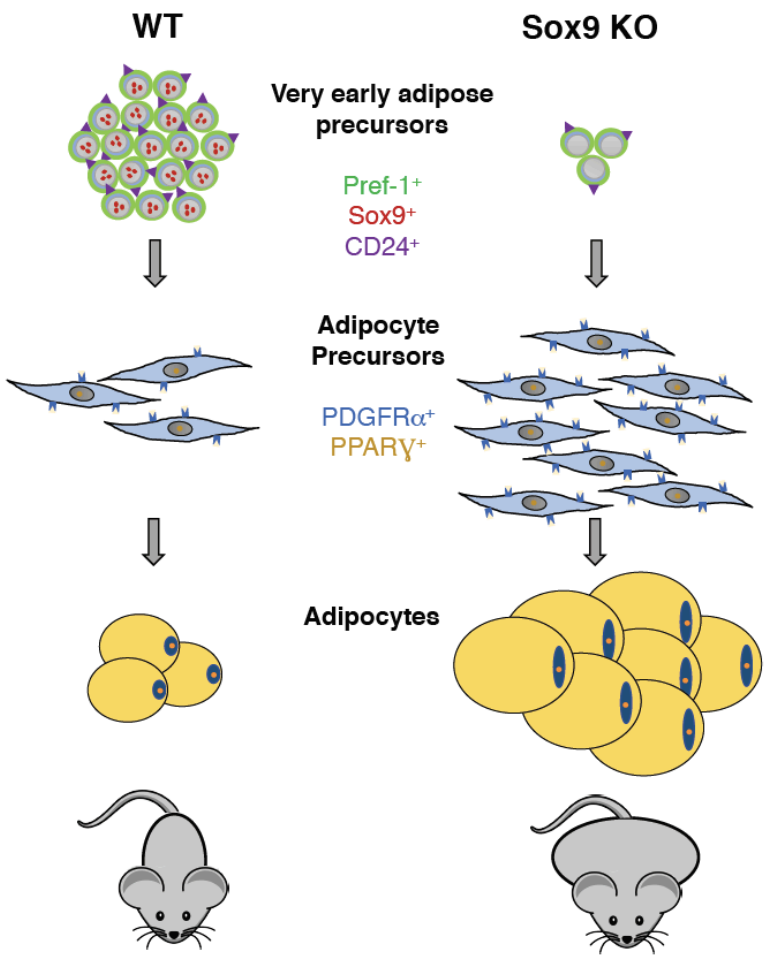

Figure 13. Schematic representation of hierarchy of various precursors in adipogenic pathway and the result of Sox9 ablation form early adipose precursors.

Discussion

Despite attempts in characterizing precursor populations in white adipose tissue, it is not clear whether adipocyte precursors in SVF of WAT, isolated and characterized using various markers, represent a single population. If not, what is the relationship of the different precursor populations during adipogenic pathway? We originally identified Pref-1 as a factor that is expressed and secreted from SVF cells but and not from adipocytes, and lineage tracing showed that Pref-1 marks very early adipose precursors. Here, we examined the relationship during adipogenic process between Pref-1$^+$:Sox9$^+$ cells and PDGFRα$^+$ cells by ablating Sox9 specifically in Pref-1$^+$ cells. Pref-1 expression in adult tissues is restricted to adipose precursors, therefore its promoter in combination with rtTA system provides us with a unique tool for conditional ablation. In this regard, promoters of various other genes were used to mark precursors or drive gene ablation in adipose tissue, such as FABP4 [24,25] and PPARγ [5], and more recently, PDGFRα [19] and Prx1 [26]. However, use of these promoters have their limitations as they are not specific for adipose tissue or they mark various types of cells within adipose tissue which will not allow to study the relationship between different adipose precursors. Indeed, FABP4 is a late marker of adipogenesis and is expressed

also in the brain, endothelial cells and macrophages [19,24,25], PPARγ is expressed also in macrophages and dendritic cells [27,28], and PDGFRα is expressed in preadipocytes but also in neural crest cells [29], developing intestine [30], testes [31], heart [32] and bone marrow stem cells [33]. Thus, inducible version of PDGFRα-Cre also targets oligodendrocyte precursors in the brain [34] and fibroblast-like cells in the skin [35], whereas Prx1-Cre is highly expressed in mesenchymal cells of the limb during embryogenesis [26]. While adipose specific, AdipoQ is expressed in mature adipocytes exclusively, making it unsuitable for studying gene function in adipose precursors.

By using our Pref-1-rtTA/TRE-Cre system, we found that Sox9 inactivation reduces the Pref-1$^+$ very early adipose precursor pool. Gene expression analysis at the global level indicate that Sox9 maintains an undifferentiated and highly proliferative stem cell population in WAT and, Sox9 inactivation drives these early precursor cells towards a more differentiated state in adipogenesis. However, with increased proliferation, we did not observe an increase in the number of nGFP$^+$ cells due to the transient nature of the Pref-1-rtTA/TRE-Cre/TRE-GFP system, in which any cells that lose Pref-1 expression also lose nGFP expression. However, by examining the effect of Sox9 ablation on PDGFRα$^+$ cells, we could compare and position PDGFRα$^+$ cells and Pref-1$^+$ cells in the adipogenic pathway. Since Pref-1 and PDGFRα were not detected in the same population of cells, sorting for PDGFRα allowed us to capture different cell population that was not included in nGFP-Seq due to the loss Pref-1 expression. RNA-Seq of PDGFRα$^+$ cells revealed that Sox9 ablation affects a set of genes that differ from those affected by Sox9 ablation in nGFP$^+$ cells. We also detected an increase in PDGFRα$^+$ population in PreASKO mice. Additionally, PDGFRα$^+$ PreASKO cells showed an increase in negative regulators of proliferation and early genes of adipocyte differentiation, accompanying enhanced differentiation potential in culture. Moreover, by performing RNA-Seq in mGFP$^+$ cells from mT/mG reporter, we examined not only those cells actively expressing Pref-1 but also Pref-1-derived progenies that may also include PDGFRα$^+$ cells. Indeed, the results showed that PreASKO mGFP$^+$ cells had mixed phenotype of PDGFRα$^+$ PreASKO and nGFP$^+$ PreASKO cells, sharing similarities in expression pattern affected by Sox9 inactivation (data not shown). Interestingly, a population of CD9^{high}, PDGFRα$^+$ proliferative cells that highly express Pref-1 was found recently to drive adipose tissue fibrosis upon high fat diet feeding [36]. In this study CD9^{low} PDGFRα$^+$ cells highly expressed PPARγ and C/EBPα but not Pref-1 and did not proliferate, most likely representing preadipocytes. We conclude that Pref-1 and Sox9 are highly expressed in very early adipose precursors that proliferate and express CD24 and, as cells lose Pref-1 and Sox9 expression, they acquire PDGFRα and lose proliferation capacity to undergo adipogenic differentiation.

We have previously shown that global Pref-1 KO mice have increased adiposity, but also growth retardation and skeletal abnormality [37]. In this regard, Sox9 inactivation from adipose precursors in mice prenatally or at birth induces early adipogenic program that leads to adipose expansion and higher fat pad weight, contributing to higher body weight albeit without differences in food intake or physical activity. We did not observe an effect of Sox9 ablation on growth or skeletal development in PreASKO mice given Dox at P1, since bone formation occurs earlier during embryogenesis. Additionally, Pref-1 KO mice may exhibit skeletal system abnormalities, due to lack of Pref-1 action on other targets that regulate skeletogenesis. Similarly, Sox9 ablation from FABP4

expressing cells resulted in similar phenotype with adiposity. However, the phenotype of Sox9 ablated mice using FABP4-Cre was less pronounced than that from using Pref-1-Cre, probably due to the FABP4 promoter which is known to be activated at a later stage of adipocyte differentiation, consistent with a notion that Sox9 and Pref-1 are highly expressed in early adipose precursors.

Overall, the use of our Pref-1-rtTA/Tre-Cre to ablate Sox9 showed presence of heterogeneous population of adipose precursors in SVF of WAT and allowed us to establish a relationship between these precursor populations, demonstrating that Pref-1^{+}:$Sox9^{+}$ cells are the earliest adipogenic precursors while PDGFRα cells are those further progressed through adipogenic pathway. These results also reveal a critical role of Sox9 in maintaining very early adipose precursors, requiring its inactivation for adipose development and expansion *in vivo*. Our study also establishes that this system is effective for adipose-specific and inducible ablation in adipose precursors at the very early stage in adipogenesis.

Experimental procedures

Animals

All animal studies were carried out in accordance with UC Berkeley ACUC and OLAC regulations. Generation of Pref-1-rtTA mice was described previously [8]. Tg(tetO-HIST1H2BJ/GFP)47Efu/J (pTRE-H2BGFP, stock no. 005104), B6.Cg-Tg(tetO-CRE)1Jaw/J (TRE-CRE, stock no. 006234), *Gt(ROSA)26Sor*$^{tm4(ACTB-tdTomato,-EGFP)Luo}$/J. (mT/mG, stock no.007576), B6.129S7-Sox9^{tm2Crm}/J (Sox9^{flox}, stock no. 013106), B6.Cg-Tg(Fabp4-Cre)1Rev/J (aP2-CRE, stock no. 005069) were purchased from the Jackson Laboratory. Mice were housed in a 12:12 light-dark cycle and chow and water were provided *ad libitum.* Dox was provided in chow at 600mg/kg. Sox9 floxed indicates mice homozygous for floxed allele. For experiments with PreASKO mice, floxed controls were Sox9 floxed littermates with Pref-1-rtTA only or with TRE-Cre only. For experiments with PreASKO-TRE-GFP mice: PreASKO refers to Sox9 floxed mice with rtTA, TRE-Cre and TRE-GFP, whereas floxed controls refer to Sox9 floxed mice with rtTA and TRE-GFP but no Cre expression.

Metabolic measurements

Fat and lean mass was determined by echoMRI-100V. CT Scan was performed on Trifoil eXplore RS9 microCT system. Insulin tolerance test was performed on 6 h fasted mice and insulin (Humulin-R, Eli Lilly) was injected at 1.25U/kg of body weight. Glucose tolerance test was performed on overnight fasted mice, glucose was injected at 1mg/kg of body weight. Blood from mouse tail was taken and glucose levels were measured using Contour glucometer (Bayer). Metabolic cage experiments to measure physical activity were carried out on CLAMS System (Columbus). Liver TAG content was assessed using Triglyceride Colorimetric kit (Cayman).

Cell culture

Adipocyte differentiation of SVF cells was performed as previously described [21]. For Dox treatment *in vitro,* 1μg/ml of doxycycline chloride (RPI) was added to the medium. Cells were then harvested for RNA isolation or protein extraction or fixed with

formalin for ORO staining. For CRISPR experiments, 3T3-L1 cells were transfected with Lipofectamine 3000 (Thermo Fisher) and plasmid pCRISPR-CG01containing Cas9, RFP and 2 independent sgRNA targeting mouse Sox9 (Genecopoeia) (sgRNA sequences can be found in Table 1). RFP^+ cells were then isolated using FACS, expanded as a single cell or a pool and used for differentiation experiments. CRISPR-mediated KO was confirmed by sequencing of 10-20 random clones of fragment of Sox9 gene that was PCRed and subcloned into Teasy vector, and by immunoblotting for Sox9. Post-confluent 3T3-L1 cells were differentiated with media containing 1mM DEX, 0.5mM MIX and 1.67mM insulin with or without 1 μM Rosiglitazone. For adenoviral transduction- subconfluent cells were transduced with GFP (ViraQuest) or Sox9 (VectorBiolabs) adenovirus with 0.5μg/ml polyLysine at MOI=500.

Separation of SVF and Adipocyte fraction

SVF fractionation was carried out as previously described [21]. Briefly, mouse WAT was minced and digested with Collagenase type II (Sigma) in KREBs buffer at 37° C for 45 min with shaking. Cell suspension was then passed through 100μm mesh, span at 300g for 5 min, floating adipocyte fraction was collected for RNA or DNA extraction, whereas cell pellet was resuspended in KREBS buffer, passed through 70μm and 40μm mesh and subjected to FACS or *in vitro* differentiation or lysed with RIPA buffer for Western blot analysis or TRIzol for RNA isolation.

RNA isolation and RT-qPCR

Total RNA from SVF cells was extracted using TRIzol and RNA from adipose tissue was extracted using RNeasy Lipid kit (Qiagen). Reverse transcription was performed with 1μg of total RNA using Superscript II (Invitrogen) or with 10-100ng from sorted cells using Superscript Villo (Invitrogen). RT-qPCR was performed on ABI PRISM 7500 (Applied Biosystems). Statistical analysis was performed using ddct method with U36B4 primers as control (see primer sequences in Supplementary Table ST1). Microarray hybridization and scanning as well as library generation for RNA sequencing was carried out at the Functional Genomics Laboratory at UC Berkeley.

DNA isolation and PCR

DNA was extracted from WAT piece or SVF cells from WAT using DNeasy Kit (Qiagen). PCR to detect Sox9 Floxdel utilized primers flanking loxP cites of Sox9 floxed allele as described previously [11]. Myogenin primers were used as a control.

Western Blot analysis and Immunostaining

For Western blot- tissues or cells were lysed in RIPA buffer. Proteins (5-100μg) were separated on SDS-PAGE gel, transferred on a nitrocellulose membrane and incubated with indicated antibodies (see Table 2 for list of antibodies). For immunostaining tissues were fixed with paraformaldehyde, embedded in paraffin, sectioned in 10μm sections using Leica microtome and collected on glass slides and stained with H&E. Alternatively, slides were baked in buffer3 for antigen retrieval as previously described [38], blocked and stained with indicated antibodies. For whole mount imaging a 1mm piece of WAT was excised, incubated with LipidTOX Green Reagent (Thermo Fisher) and DAPI, immobilized on a slide with mounting medium and imaged

using confocal microscope. Cell number and size was calculated using ImageJ software.

FACS

SVF cells were incubated with indicated antibody for 20min in dark, washed, span at 300g for 5 min, resuspended in FACS buffer (1x PBS+0.5% BSA) and passed through 40μm filter prior to FACS analysis. FACS was performed on BD Influx cell sorter. Cells were initially chosen based on forward and side scatter (FFS and CCS) and trigger pulse width. Cells that were not incubated with antibody were used as a control to determine background fluorescence levels. Cells were collected in TRIzol LS (Thermo Fisher) for RNA isolation or in DMEM+10%FBS for cell culture or proliferation assessment using Quick Cell Proliferation Kit (Abcam).

Statistical analysis

Statistical analysis was performed using two tailed t-test. The error bars represent standard error mean (s.e.m). Data is expressed as mean +/- s.e.m, p value <0.05 was considered statistically significant. Number of mice or replicates used in each experiment is indicated in figure legends.

Acknowledgements

We thank Jon Dempersmier for proofreading of the manuscript. The work was supported in part by NIDDK grant to H.S.S. Imaging was supported in part by NIH S10RR026866-01. The content is solely the responsibility of the authors and does not necessarily represent the official views of the NIH. The authors declare no competing financial interests.

Table 1. Primer sets used in RT-qPCR and sgRNA sequences used for CRISPR KO

	List or primer used for RT-qPCR		
Gene Symbol	**Primers**		**Amplicon (bp)**
AdipoQ	F	GCACTGGCAAGTTCTACTGCAA	122
	R	GTAGGTGAAGAGAACGGCCTTGT	
Adora3	F	CCCTGGTTGTCATGTGTGTC	272
	R	AGGGTTCATCATGGAGTTCG	
Bmp5	F	ACCTCTTGCCAGCCTACATG	169
	R	TGCTGCTGTCACTGCTTCTC	
C/EBPα	F	TGGACAAGAACAGCAACGAG	360
	R	AATCTCCTAGTCCTGGCTTG	
C/EBPβ	F	GCCAAGAAGACGGTGGACAA	205
	R	ACAAGTTCCGCAGGGTGCT	
C/EBPδ	F	GAACCCGCGGCCTTCTAC	189
	R	GAAGAGTTCGTCGTGGCACA	
Camp	F	CTTCAACCAGCAGTCCCTAGACA	51
	R	TCCAGGTCCAGGAGACGGTA	
Cdkn2b	F	GGGTGCAGTCAGTACCTTCC	240
	R	CAGGCATCAAGGCAACTGTG	
Col5a1	F	AAGCGTGGGAAACTGCTCTCCTATA	118
	R	AGCAGTTGTAGGTGACGTTCTGGT	
Cre	F	GAACCTGATGGACATGTTCAGG	250
	R	AGTGCGTTCGAACGCTAGAGCCTGT	
Erdr1	F	GGTCAAGATGTATGTGCCACC	130
	R	GCTTCTACGTGTGTGCTTTCG	
FABP4	F	ACACCGAGATTTCCTTCAAACTG	88
	R	CCATCTAGGGTTATGATGCTCTTCA	
FAS	F	CAAGTGTCCACCAACAAGCG	120
	R	GGAGCGCAGGATAGACTCAC	
Fgf18	F	TGAACACGCACTCCTTGCTAGT	76
	R	GAATTCTACCTGTGTATGAACCGAAA	
Fzd10	F	TGGTGTGTGTTATGTGGGCA	157
	R	GTTCTCCCCACCCGTTTTCA	
Gas1	F	CGAACACTGCAGGTCCACCAAG	273
	R	TCGCACACGCAGTCGTTGAG	
Glut4	F	TCATTGTCGGCATGGGTTT	69
	R	CGGCAAATAGAAGGAAGACGTA	

Id2	F	GGACCA CAGCTTGGGCAT	74
	R	CGTTCATGTTGTAGAGCAGACTCAT	
Il1b	F	AAGGAGAACCAAGCAACGACAAAA	213
	R	TGGGGAACTCTGCAGACTCAAACT	
Leptin	F	TGCTCCAGCAGCTGCAAGGTGCAAG	550
	R	TCAGCATTCAGGGCTAACATCCAACTGT	
Meis1	F	GCAAAGTATGCCAGGGGAGTA	235
	R	TCCTGTGTTAAGAACCGAGGG	
PDGFRα	F	CAAACCCTGAGACCACAATG	235
	R	TCCCCCAACAGTAACCCAAG	
Plin1	F	GGCCTGGACGACAAAACC	120
	R	CAGGATGGGCTCCATGAC	
Plin4	F	CTGCTCCAACCTTCTGAACAG	121
	R	GGACCATTCCTTTTGCAGCAT	
PPARγ2	F	ACTGCCTATGAGCTCTTCAC	448
	R	CAATCGGATGGTTCTTCGGA	
Prtn3	F	TCCTATGCCGGGAACACAAC	127
	R	CGGATCACGAAGGAGTCCAC	
Prx1a	F	TTACCCGGATGCTTTTGTTC	263
	R	AAGTAGCCATGGCGCTGTA	
Prx1b	F	TTACCCGGATGCTTTTGTTC	287
	R	GCCCCTCGTGTAAACAACAT	
Resistin	F	TCTCCTCCAGAGGGAAGTTGG	99
	R	TTTCTTCACGAATGTCCCACG	
Sca1	F	CTCTGAGGATGGACACTTCT	404
	R	GGTCTGCAGGAGGACTGAGC	
Sirt1	F	GCAGATTAGTAAGCGGCTTGAGG	244
	R	AGCACATTCGGGCCTCTCCGTA	
Six1	F	CACCAGTTCTCGCCTCACA	117
	R	CACCCGATATTTGCCCAC	
Sox4	F	CCTCGCTCTCCTCGTCCT	67
	R	TCGTCTTCGAACTCGTCGT	
Tbx6	F	CCTGACTCTCCTGCCACTG	339
	R	CCTCTTCACACGGGCATCC	
Tgfb3	F	ATTCGACATGATCCAGGGAC	101
	R	TCTCCACTGAGGACACATTGA	
Tlr13	F	GGAGCGCCTTGATCTAACTAACA	80
	R	TCAGGTGGGTCAGAGAAACCA	

U36B4	F	AGATGCAGCAGATCCGCA	59
	R	GTTCTTGCCCATCAGCACC	

TaqMan probes (Life Technologies):

Sox9- Mm00448840_m1

Pref-1- Mm00494477_m1

18s rRNA- Mm03928990_g1

eGFP -Mr04097229_mr

sgRNA sequences for CRISPR:

Sox9 sgRNA A: TTCATGGGTCGCTTGACGTG
Sox9 sgRNA B: TTCAGATCCGGCTCGCCCTT

Table 2. List of antibodies used for FACS and immunoblotting

	List of antibodies used		
Antibody	**Vendor**	**Catalog number**	**Concentration**
βActin	Cell Signaling	4967S	1:1000
Topo2β	Santa Cruz	SC-48429	1:1000
αTubulin	Abcam	Ab52866	1:1000
FABP4	Cell Signaling	3544S	1:1000
FAS	Santa Cruz	SC-55580	1:1000
GAPDH	Santa Cruz	SC-25778	1:1000
Pref-1	Cell Signaling	2069S	1:1000
PDGFRα-PE	Molecular Probes	A18351	1:200
Sca1-V450	BD Horizon	560653	1:1000
Na+/K+ pump	Thermo	MA3926	1:500
C/EBPβ	Santa Cruz	SC-7962	1:500
C/EBPδ	Santa Cruz	SC-636	1:500
Pol2	Santa Cruz	SC-899	1:500
Sox9	Millipore	A65535	1:1000
CD24	Molecular Probes	A14790	1:100
CD31-APC	BD Biosciences	561814	1:100
CD46-APC	BD Biosciences	561018	1:10000
Ter119-APC	BD Biosciences	561033	1:100

References

1. Rosen, E. D. & Spiegelman, B. M. What we talk about when we talk about fat. *Cell* **156,** 20–44 (2014).
2. Farmer, S. R. Transcriptional control of adipocyte formation. *Cell Metab.* **4,** 263–273 (2006).
3. Gregoire, F. M., Smas, C. M. & Sul, H. S. Understanding adipocyte differentiation. *Physiol. Rev.* **78,** 783–809 (1998).
4. Smas, C. M. & Sul, H. S. Pref-1, a protein containing EGF-like repeats, inhibits adipocyte differentiation. *Cell* **73,** 725–734 (1993).
5. Tang, W. *et al.* White fat progenitor cells reside in the adipose vasculature. *Science* **322,** 583–586 (2008).
6. Wang, W. & Seale, P. Control of brown and beige fat development. *Nat Rev Mol Cell Biol* **17,** 691–702 (2016).
7. Hepler, C., Vishvanath, L. & Gupta, R. K. Sorting out adipocyte precursors and their role in physiology and disease. *Genes Dev.* **31,** 127–140 (2017).
8. Hudak, C. S. *et al.* Pref-1 Marks Very Early Mesenchymal Precursors Required for Adipose Tissue Development and Expansion. *Cell Rep* **8,** 678–687 (2014).
9. Rodeheffer, M. S., Birsoy, K. & Friedman, J. M. Identification of white adipocyte progenitor cells in vivo. *Cell* **135,** 240–249 (2008).
10. Berry, R. & Rodeheffer, M. S. Characterization of the adipocyte cellular lineage in vivo. *Nat Cell Biol* **15,** 302–308 (2013).
11. Akiyama, H., Chaboissier, M.-C., Martin, J. F., Schedl, A. & de Crombrugghe, B. The transcription factor Sox9 has essential roles in successive steps of the chondrocyte differentiation pathway and is required for expression of Sox5 and Sox6. *Genes Dev.* **16,** 2813–2828 (2002).
12. Liu, C.-F. & Lefebvre, V. The transcription factors SOX9 and SOX5/SOX6 cooperate genome-wide through super-enhancers to drive chondrogenesis. *Nucleic Acids Res.* **43,** 8183–8203 (2015).
13. Ohba, S., He, X., Hojo, H. & McMahon, A. P. Distinct Transcriptional Programs Underlie Sox9 Regulation of the Mammalian Chondrocyte. *Cell Rep* **12,** 229–243 (2015).
14. Adam, R. C. *et al.* Pioneer factors govern super-enhancer dynamics in stem cell plasticity and lineage choice. *Nature* **521,** 366–370 (2015).
15. Mori–Akiyama, Y. *et al.* SOX9 Is Required for the Differentiation of Paneth Cells in the Intestinal Epithelium. *Gastroenterology* **133,** 539–546 (2007).
16. Furuyama, K. *et al.* Continuous cell supply from a Sox9-expressing progenitor zone in adult liver, exocrine pancreas and intestine. *Nat Genet* **43,** 34–41 (2011).
17. Kadaja, M. *et al.* SOX9: a stem cell transcriptional regulator of secreted niche signaling factors. *Genes Dev.* **28,** 328–341 (2014).
18. Bi, W. *et al.* Haploinsufficiency of Sox9 results in defective cartilage primordia and premature skeletal mineralization. *PNAS* **98,** 6698–6703 (2001).
19. Jeffery, E. *et al.* Characterization of Cre recombinase models for the study of adipose tissue. *Adipocyte* **3,** 206–211 (2014).
20. Majka, S. M. *et al.* Analysis and Isolation of Adipocytes by Flow Cytometry. *Methods Enzymol* **537,** 281–296 (2014).

21. Wang, Y. & Sul, H. S. Pref-1 regulates mesenchymal cell commitment and differentiation through Sox9. *Cell Metab.* **9,** 287–302 (2009).
22. Todaro, G. J. & Green, H. Quantitative studies of the growth of mouse embryo cells in culture and their development into established lines. *J. Cell Biol.* **17,** 299–313 (1963).
23. Shan, T., Liu, W. & Kuang, S. Fatty acid binding protein 4 expression marks a population of adipocyte progenitors in white and brown adipose tissues. *FASEB J* **27,** 277–287 (2013).
24. Lee, K. Y. *et al.* Lessons on Conditional Gene Targeting in Mouse Adipose Tissue. *Diabetes* **62,** 864–874 (2013).
25. Mullican, S. E. *et al.* A Novel Adipose-Specific Gene Deletion Model Demonstrates Potential Pitfalls of Existing Methods. *Mol Endocrinol* **27,** 127–134 (2013).
26. Sanchez-Gurmaches, J., Hsiao, W.-Y. & Guertin, D. A. Highly Selective In Vivo Labeling of Subcutaneous White Adipocyte Precursors with Prx1-Cre. *Stem Cell Reports* **4,** 541–550 (2015).
27. Nagy, L., Tontonoz, P., Alvarez, J. G., Chen, H. & Evans, R. M. Oxidized LDL regulates macrophage gene expression through ligand activation of PPARgamma. *Cell* **93,** 229–240 (1998).
28. Szatmari, I. *et al.* PPARgamma regulates the function of human dendritic cells primarily by altering lipid metabolism. *Blood* **110,** 3271–3280 (2007).
29. Soriano, P. The PDGF alpha receptor is required for neural crest cell development and for normal patterning of the somites. *Development* **124,** 2691–2700 (1997).
30. Karlsson, L., Lindahl, P., Heath, J. K. & Betsholtz, C. Abnormal gastrointestinal development in PDGF-A and PDGFR-(alpha) deficient mice implicates a novel mesenchymal structure with putative instructive properties in villus morphogenesis. *Development* **127,** 3457–3466 (2000).
31. Brennan, J., Tilmann, C. & Capel, B. Pdgfr-alpha mediates testis cord organization and fetal Leydig cell development in the XY gonad. *Genes Dev.* **17,** 800–810 (2003).
32. Chong, J. J. H. *et al.* Adult cardiac-resident MSC-like stem cells with a proepicardial origin. *Cell Stem Cell* **9,** 527–540 (2011).
33. Morikawa, S. *et al.* Prospective identification, isolation, and systemic transplantation of multipotent mesenchymal stem cells in murine bone marrow. *Journal of Experimental Medicine* **206,** 2483–2496 (2009).
34. Rivers, L. E. *et al.* PDGFRA/NG2 glia generate myelinating oligodendrocytes and piriform projection neurons in adult mice. *Nat. Neurosci.* **11,** 1392–1401 (2008).
35. Driskell, R. R. *et al.* Distinct fibroblast lineages determine dermal architecture in skin development and repair. *Nature* **504,** 277–281 (2013).
36. Marcelin, G. *et al.* A PDGFRα-Mediated Switch toward CD9(high) Adipocyte Progenitors Controls Obesity-Induced Adipose Tissue Fibrosis. *Cell Metab.* **25,** 673–685 (2017).
37. Moon, Y. S. *et al.* Mice lacking paternally expressed Pref-1/Dlk1 display growth retardation and accelerated adiposity. *Mol. Cell. Biol.* **22,** 5585–5592 (2002).
38. Long, D. J. & Buggs, C. Microwave oven-based technique for immunofluorescent staining of paraffin-embedded tissues. *J Mol Histol* **39,** 1–4 (2008).

Chapter 3:
Cold–inducible Zfp516 Activates UCP1 Transcription to Promote Browning of White Fat and Development of Brown Fat

Cold–inducible Zfp516 Activates UCP1 Transcription to Promote Browning of White Fat and Development of Brown Fat

Abstract

Uncoupling protein 1 (UCP1) mediates non-shivering thermogenesis and, upon cold exposure, is induced in BAT and subcutaneous white adipose tissue (iWAT). Here, by high-throughput screening using the UCP1 promoter, we identify Zfp516 as a novel transcriptional activator of UCP1 as well as PGC1α thereby promoting a BAT program. Zfp516 itself is induced by cold and sympathetic stimulation through the cAMP-CREB/ATF2 pathway. Zfp516 directly binds to the proximal region of the UCP1 promoter, not to the enhancer region where other transcription factors bind, and interacts with PRDM16 to activate the UCP1 promoter. Although ablation of Zfp516 causes embryonic lethality, knockout embryos still show drastically reduced BAT mass, while overexpression of Zfp516 in adipose tissue promotes browning of iWAT even at room temperature, increasing body temperature, energy expenditure, and preventing diet-induced obesity. Zfp516 may represent a future target for obesity therapeutics.

Introduction

Whereas white adipose tissue (WAT) is the primary energy storage organ, brown adipose tissue (BAT) is specialized to perform nonshivering thermogenesis to maintain body temperature in mammals. Although the contribution of white fat to thermogenesis is not fully understood, inguinal WAT (iWAT) but not visceral WAT can undergo browning upon acute cold exposure. Non-shivering thermogenesis requires uncoupling protein-1 (UCP1), which dissipates the mitochondrial proton gradient to produce heat rather than ATP. Recently, metabolically relevant amounts of functional BAT or BAT-like tissue have been shown to be present in adult humans (Cypess et al., 2009; Farmer, 2009; van Marken Lichtenbelt et al., 2009; Virtanen et al., 2009). This finding has generated considerable interest as an increase in BAT activity in mice has been shown to have anti-obesity and anti-diabetic effects (Cederberg et al., 2001; Leonardsson et al., 2004).

Lineage-tracing has shown that brown adipocytes may arise from $Myf5^{+}$/$Sca\text{-}1^{+}$/$Pax7^{+}$ cells of the dermomyotome, progenitors of skeletal muscle, cartilage, and dermis (Gensch et al., 2008; Lepper and Fan, 2010; Schulz et al., 2011; Seale et al., 2008). In addition to BAT, upon cold exposure, brown adipocyte-like cells termed “brite” or “beige” cells, which originate mainly from $Myf5^{-}$ cells, may arise in inguinal WAT (iWAT) depots or there may be interconversion between white and brown adipocytes (Rosenwald et al., 2013; Wu et al., 2012). Contrary to classic BAT cells, brown adipocyte-like cells express very low levels of UCP1 and other BAT-enriched genes in non-stimulated conditions and are induced greatly following cold exposure (Waldén et al., 2012; Wu et al., 2012). As the thermogenic program in classic BAT and emergence of brown adipocyte-like cells in iWAT are both induced by cold, a common regulatory mechanism may operate.

For transcriptional activation of UCP1, several transcription factors and coregulators, including PPARs, PGC1α, and ATF2, have been implicated, but are found in both WAT and BAT as well as in other tissues (Collins et al., 2010; Kang et al., 2005). These factors have been shown to act through the well-characterized enhancer element located 2.5kb upstream of the UCP1 gene. In this regard, brown fat specific expression of UCP1 *in vivo* has been demonstrated by using a construct that contained the UCP1 proximal promoter region as well as the enhancer region (Ricquier and Bouillaud, 1997). Therefore, a yet to be identified cold inducible transcription factor(s) may bind the proximal promoter region to participate in activating UCP1 and other thermogenic genes.

Here, by performing high throughput screening of putative transcription factors for activation of the UCP1 promoter, we report that Zfp516, a novel, cold inducible transcription factor enriched in BAT compared to WAT, binds to the promoter region of UCP1. Zfp516 directly interacts with PRDM16 for transcriptional activation of thermogenic genes. Whereas ablation of Zfp516 causes embryonic lethality with drastically diminished BAT, overexpression of Zfp516 in adipose tissue causes browning of iWAT, increasing body temperature and energy expenditure to prevent diet induced obesity.

Results

To identify potential transcriptional activators of the UCP1 gene, we screened over 1100 transcription factor expression vectors representing two-thirds of known or putative transcription factors (Fulton et al., 2009). These expression vectors were individually cotransfected with a GFP reporter driven by the -5.5kb UCP1 promoter. Previous studies have shown that the -4.55kb promoter region to be sufficient for BAT-specific and regulated expression in transgenic mice (Cassard-Doulcier et al., 1993). Positive clones, identified by the detection of GFP signal, were subjected to a secondary screen employing luciferase instead of GFP as a reporter to quantitate promoter activation. During screening, known transcriptional activators of UCP1 that are widely expressed, such as CREB and ATF2, were identified as positives demonstrating the effectiveness of our screening. We identified 18 candidate genes independently capable of activating the UCP1 promoter more than 3-fold. We further selected those that were expressed at higher levels in BAT compared to WAT by RT-qPCR (data not shown). Here, we studied one of the best candidates, the previously uncharacterized Krüppel-like zinc finger transcription factor, Zfp516 (Gene ID: 329003), for its role in the transcriptional regulation of UCP1.

Zfp516 directly binds and activates UCP1 promoter

As Zfp516 activity or function has not been studied previously, we performed a motif analysis of Zfp516, which identified ten C2H2-type zinc fingers, widespread DNA binding motifs of eukaryotic transcription factors (Figure 14A top) (Laity et al., 2001). Cell fractionation experiments to examine the localization of Zfp516 in the brown preadipocyte cell line, HIB-1B, showed that Zfp516 was present exclusively in the nucleus (Figure 14A bottom). As detected in the initial screening, we established that Zfp516 robustly activated the UCP1 promoter-GFP reporter (Figure 14B top). As

compared to empty vector control, cotransfection of Zfp516 with the -5.5kb UCP1 promoter-luciferase resulted in a 4-fold activation of the UCP1 promoter (Figure 14B bottom). This degree of UCP1 promoter activation was similar to that observed by cotransfection of CREB. We found that by both RT-qPCR and immunoblotting that Zfp516 was enriched in BAT in comparison to WAT depot (Figure 14C top). When BAT was fractionated into adipocytes and stromal vascular fraction (SVF) that contain brown preadipocytes, as expected, we detected UCP1 expression to be 30-fold higher in adipocytes than SVF. We found that Zfp516 expression was 6-fold higher in adipocytes compared to the SVF (Figure 14C bottom).

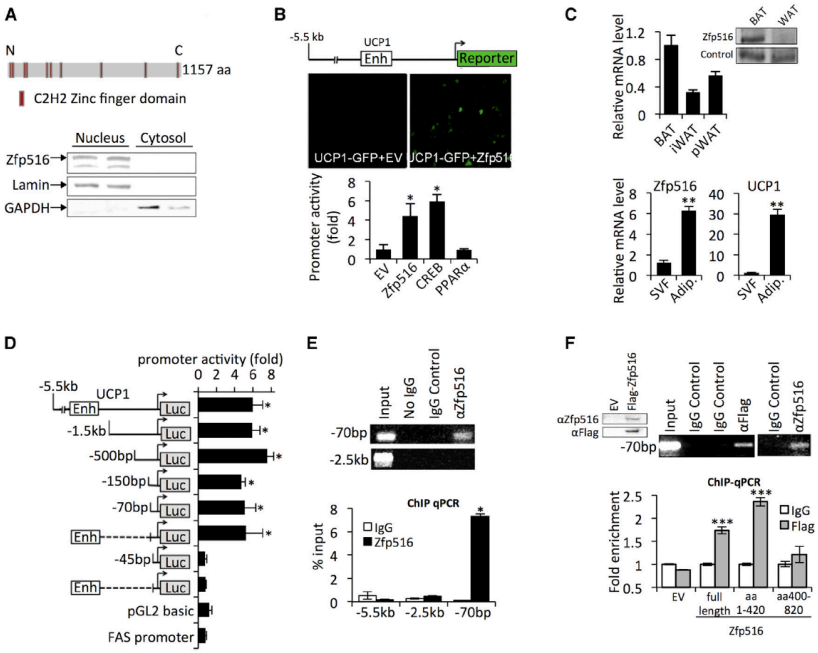

Figure 14. Zfp516 is a Brown Fat- Enriched Transcription Factor that binds and activates UCP1 promoter.

(A) Top, diagram of Zfp516 structure. Bottom, immunoblotting in nuclear and cytosolic fractions of HIB-1B cells. (B) Top, GFP fluorescence of 293FT cells transfected with -5.5kb UCP1-GFP and either empty vector (EV) or Zfp516. Bottom, relative luciferase activity of 293FT cells cotransfected with -5.5kb UCP1-Luc. (C) Top and inlay, RT-qPCR and immunoblotting for Zfp516 mRNA and protein levels in BAT and WAT tissues from 6 week-old C57BL/6 mice. Bottom, RT-qPCR for Zfp516 and UCP1 mRNA levels in the adipocyte fraction and SVF from BAT **(**D) Schematic representation of 5' deletion constructs of the UCP1 promoter-luciferase and relative luciferase activity in 293FT cells cotransfected with indicated promoter construct and Zfp516 (expressed as fold of vector control). (E) Top, ChIP for Zfp516 association to the UCP1 promoter in BAT. Bottom, qPCR for the ChIP DNA for Zfp516 (n=4 mice). F. Top-left, immunoblotting of lysates from 293FT cells transfected with -5.5kb UCP1-GFP with FLAG-Zfp516 or vector. Top-right, ChIP for FLAG-Zfp516 association to the UCP1 promoter using both αFLAG and αZfp516 antibodies. Middle, gel shift assay performed with nuclear extracts from 293FT cells transfected with full length Zfp516 or truncations of Zfp516 containing AA1-420 or AA400-820. Bottom, qPCR quantification of ChIP DNA for the association of full length Zfp516 or truncations of Zfp516 to the UCP1 promoter in 293FT cells. *p<0.05; **p<0.01; ***p<0.001

To start defining how Zfp516 activates the UCP1 promoter, 5' deletions of the UCP1 promoter driving a luciferase reporter were generated and cotransfected along with Zfp516 into 293FT cells. Contrary to the majority of known transcriptional activators

of UCP1 that act at the enhancer element at -2.5kb upstream of the transcription start site (Cassard-Doulcier et al., 1998; Kozak et al., 1994), activation of the UCP1 promoter by Zfp516 was maintained even after deletion of the -2.5kb enhancer element (Figure 14D). Further, all UCP1 promoter constructs deleted down to -70bp showed over 4.5-fold activation upon Zfp516 cotransfection. However, UCP1 promoter activation by Zfp516 was lost when the promoter was deleted to -45bp indicating that Zfp516 worked through the sequence from -70 to -45bp. Linking the -2.5kb UCP1 enhancer element to the -70bp and -45bp sequence did not show any further effect (Figure 14D). Gel mobility shift assay showed a complex formation between Zfp516 and -70 to -45bp sequence, which could be supershifted by Zfp516 antibodies (data not shown). Chromatin immunoprecipitation (ChIP) of interscapular BAT from C57BL/6 mice showed clear evidence of Zfp516 binding to the proximal UCP1 promoter region *in vivo* (Figure 14E). We conclude that Zfp516 functions through the sequence from -70 to -45bp. As indicated in Figure14A, Zfp516 contains 10 Zinc fingers primarily at the N-terminus. Therefore in addition to full length, we generated truncations of Zfp516 containing either the first one third (AA1-420) (contains 7 Zn fingers) or second third (AA400-820) (contains 2 Zn fingers) to use in ChIP assays. As expected, use of the Flag antibody showed the binding of full length Zfp516 at the proximal UCP1 promoter region. ChIP using Zfp516 antibody showed the same results (Figure 14F top). ChIP qPCR showed that in addition to full length Zfp516, the first one third of the N-terminus (AA1-420) but not the second third (AA400-820) showed binding to the UCP1 promoter indicating that Zfp516 interacted with UCP1 promoter through the first third from the N-terminus (Figure 14F bottom). Similarly, gel shift assay showed that full-length Zfp516 and Zfp516 (AA1-420) but not Zfp516 (AA400-820) form DNA-protein complexes (data not shown). These data indicate that Zfp516, through its N-terminal domain binds to the UCP1 promoter region from -70 to -45bp to activate transcription.

In addition to UCP1, we also examined several BAT-enriched gene promoters for sequence similarity to -70 to -45 of UCP1 promoter. Indeed, several of BAT-enriched genes contained the DNA sequence, CCACT, present in the UCP1 promoter. We chose PGC1α and Cox8b, which contained sequences with the highest alignment score, for further examination. ChIP analysis of the 293FT cells transfected with Zfp516 and the PGC1α or Cox8b promoter-reporters showed that, indeed, Zfp516 was bound to the -2.4kb region of the PGC1α promoter and -2.8kb region of Cox8b promoter. Cotransfection of Zfp516 with the -2.5kb PGC1α promoter-luciferase construct in 293FT cells resulted in a 15-fold activation of the PGC1α promoter (data not show). These results show that Zfp516 binds and activates not only UCP1 but other BAT gene promoters as well.

Zfp516 interacts with PRDM16

Next, we asked whether Zfp516 interacts with known transcription factors or cofactors have been reported to be involved in UCP1 activation. PGC1α, PPARγ, C/EBPβ, and PRDM16 were cotransfected with Zfp516 and immunoprecipitated with the Zfp516 antibody. Immunoblotting with antibodies against these transcription factors identified PRDM16, but not other factors, as an interacting partner of Zfp516 (Figure 15A top-left). Interaction between Zfp516 and PRDM16 was confirmed by using Flag-tagged Zfp516 and V5-tagged PRDM16 as well as using endogenous proteins from

mouse BAT (Figure 15A top-right, bottom-left). Use of various GST-PRDM16 fusion proteins indicated that Zfp516 can directly interact with PRDM16 AA881-1038, a region shown to interact with other transcription factors (Kajimura et al., 2008) (Figure 15A bottom-right). To examine the functional significance of Zfp516 and PRDM16 interaction in the activation of UCP1 and other BAT-enriched genes, we cotransfected Zfp516 and PRDM16 with the -5.5kb UCP1-luciferase reporter construct. Zfp516 and PRDM16 individually activated the UCP1 promoter 13- and 10- fold, respectively while, cotransfection of both resulted in a 25-fold activation (Figure 15B left). Cotransfection of Zfp516 and PRDM16 together with the PGC1α promoter caused a robust 200-fold increase in promoter activity whereas Zfp516 and PRDM16 individually activated the PGC1α promoter 15- and 3-fold respectively (Figure 15B right). These data show that Zfp516 and PRDM16, upon their interaction, further activate transcription of BAT genes. Since the DNA binding activity of PRDM16 is not required for BAT gene induction, Zfp516 may recruit PRDM16 to the promoter regions of BAT-enriched genes. In this regard, Re-Chip indicated that Zfp516 and PRDM16 were bound to the UCP1 promoter in the similar region (data not shown).

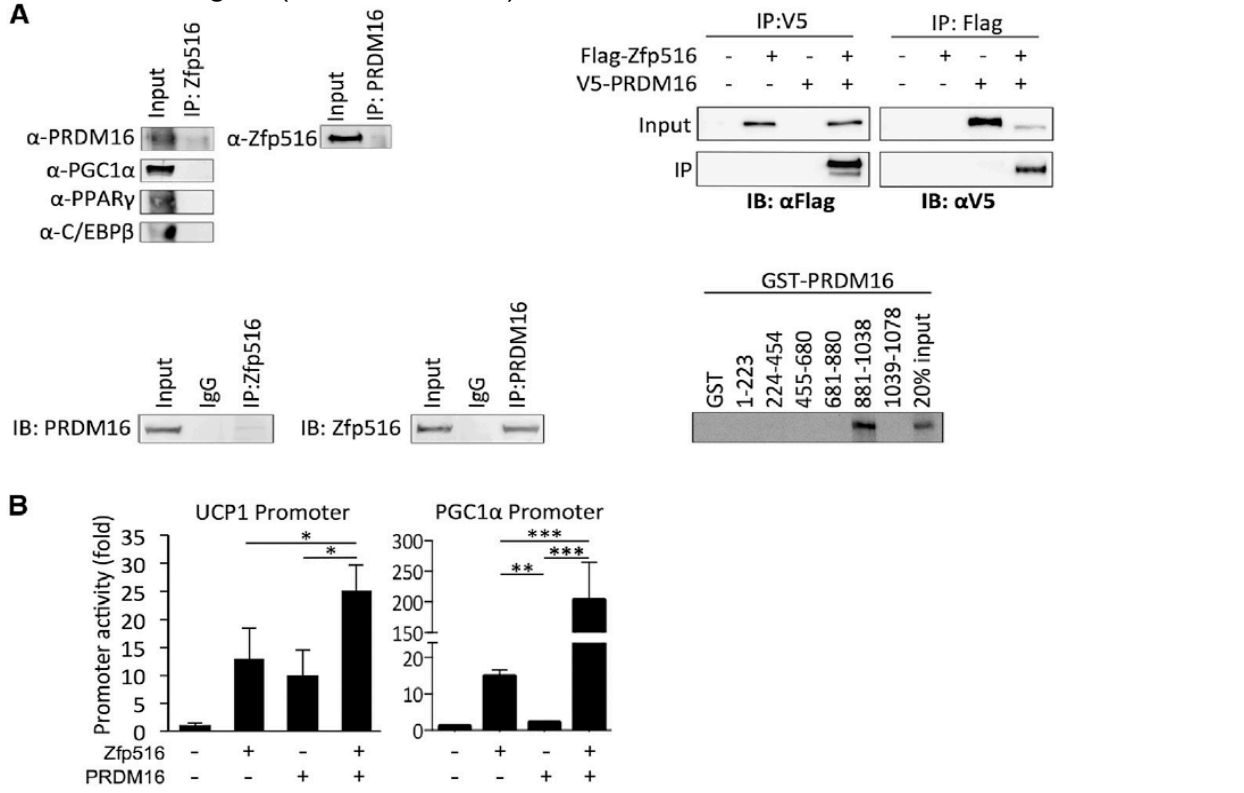

Figure 15. Zfp516 directly interacts with PRDM16.
(A) Top-left (left column), immunoblot for various brown fat specific transcription factors after IP with αZfp516 antibody in 293FT cells. Top-left (right side), immunoblot for Zfp516 protein after IP with αPRDM16 of lysates coexpressing Zfp516 and PRDM16. Top-right, immunoblot with αV5 or αFLAG after IP with either FLAG or V5 respectively of 293FT lysates. Bottom-left, immunoblot for either Zfp516 or PRDM16 after IP with indicated antibody of 50μg of BAT nuclear extracts. Bottom-right, Autoradiograph of GST pulldown using GST fusion proteins containing the indicated domains of PRDM16 and ^{35}S-labelled *in vitro* translated Zfp516. (B) Left, luciferase activity of 293FT cells cotransfected with the -5.5kb UCP1 promoter with Zfp516 and PRDM16 either together or separately. Right, luciferase activity of 293 FT cells cotransfected with the -2.5kb PGC1α promoter. *p<0.05; **p<0.01; ***p<0.001

Zfp516 is cold induced via cAMP-CREB/ATF pathway

Expression of many BAT-enriched genes as well as BAT development are known to be induced by cold (Bachman et al., 2002; Cannon and Nedergaard, 2004; Farmer, 2008; Nedergaard and Cannon, 2010). Therefore, we next assessed possible regulation by the β-adrenergic receptor-cAMP pathway of Zfp516 itself. We treated HIB-1B cells with IBMX, Isoproterenol, or Forskolin, agents that can increase intracellular cAMP levels. Treatment of cells with the β-adrenergic agonist, isoproterenol resulted in approximately 2-fold increase in both Zfp516 and UCP1 mRNA levels. Other known cold responsive genes such as PGC1α and Dio2 were also induced while PRDM16 remained unchanged (Figure 16A top-left). Treatment of HIB-1B cells with IBMX, a phosphodiesterase inhibitor, resulted in a rapid increase in Zfp516 mRNA level reaching maximal increase of 2-fold after 6 h treatment which was maintained up to 24h.

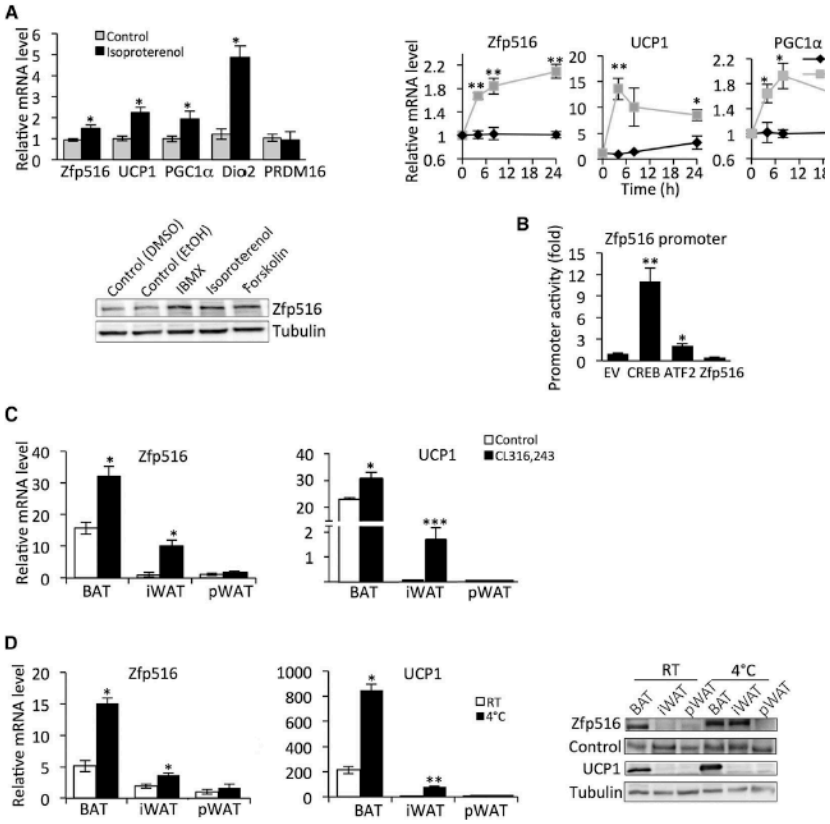

Figure 16. Zfp516 is regulated by Cold through CREB/ATF.
(A) Top-left, RT-qPCR for selected genes in HIB-1B cells with or without 4 h treatment with 10μM isoproterenol. Top-right, RT-qPCR for Zfp516, UCP1, and PGC1α mRNA in HIB-1B cells during 500μM IBMX treatment. Bottom, immunoblotting for Zfp516 or tubulin in HIB-1B cells treated with vehicle or indicated compound for 12 hours. Values are normalized to nontreated cells. (B) Relative luciferase activity of 293FT cells transfected with the -2.0kb Zfp516-Luc and indicated transcription factor expression vector. (C) RT-qPCR for Zfp516 and UCP1 mRNA in various tissues of wild-type mice following 10 days of intraperitoneal injection with either CL316,243 or saline. (D) RT-qPCR for Zfp516 and UCP1 mRNA (left and center) and immunoblotting for indicated proteins (right) in various adipose depots of wild-type mice exposed to cold (4°C) for 6 h. *p<0.05; **p<0.01; ***p<0.001

Expression of other known targets such as UCP1 and PGC1α showed similar pattern during IBMX treatment but increased by 13- and 2-fold, respectively (Figure 16A top-right). Treatment with these agents resulted in increased Zfp516 protein levels in all treatment conditions (Figure 16A bottom). We next generated a reporter construct linking the -2.0kb of the Zfp516 promoter to a luciferase reporter and cotransfected it with CREB, ATF2, and other known BAT transcription factors. Motif search of the proximal -2.0kb of Zfp516 promoter region revealed two half CREs at -1.1kb and -1.8kb upstream of Zfp516 transcription start site. Indeed, cotransfection of CREB or ATF2 with the Zfp516 promoter-reporter construct increased the luciferase activity by 11- and 2-fold, respectively, whereas other transcription factors, such as PRDM16, C/EBPβ, PGC1α, PPARα, and PPARγ, did not show any effect (Figure 16B). These data show that Zfp516 is induced via cAMP-CREB/ATF2 pathway.

To test cAMP pathway *in vivo* we treated mice with the β-adrenergic agonist, CL316,243 for 10d. Expression of UCP1and Zfp516 was increased 1.5- to 2-fold, respectively in BAT (Figure 16C). There was no change in UCP1 or Zfp516 expression levels in perigonadal WAT (pWAT), a visceral WAT depot. In contrast, in iWAT, UCP1 and Zfp516 were drastically increased by 30- and 10-fold, respectively (Figure 16C). Overall, these results indicate that Zfp516 expression in iWAT, although its absolute levels are still lower than in BAT, is induced to a greater extent by β-adrenergic agonist treatment.

Next, we subjected mice to a 6h cold challenge. Similarly to β-adrenergic agonist treatment, we detected an increase of UCP1 and Zfp516 mRNA and protein levels in BAT upon cold exposure. Zfp516 expression in pWAT was lower and remained low, even after cold exposure. In iWAT, UCP1 and Zfp516 expression increased 40- and 2.5-fold, respectively, with Zfp516 expression approaching the expression levels detected in BAT at room temperature (Figure 16D). Overall, we conclude that although Zfp516 level is higher in BAT than WAT, the degree of induction by β-agonist or cold exposure was much higher in iWAT compared to BAT while there was no change in pWAT. These data suggest that Zfp516 may be involved in the browning of iWAT.

Zfp516 promotes browning of white adipose tissue

Next, to test the effect of Zfp516 overexpression in adipose tissue *in vivo*, we generated transgenic mouse lines expressing Zfp516 driven by the -5.4kb aP2 promoter. Although endogenous Zfp516 expression is significantly higher in BAT than WAT, the fold increase of Zfp516 in iWAT and pWAT of transgenic mice was greater than in BAT (50-fold versus 10-fold) (Figure 17A). Zfp516 expression in other tissues was unaffected (Figure S5H). Similarly, Zfp516 protein levels were elevated in two independent transgenic lines in all adipose depots compared to wild-type mice. We then examined UCP1 levels by immunoblotting. UCP1 levels were increased approximately 3-4-fold in BAT of aP2-Zfp516 mice compared to wild-type littermates. Strikingly, although its level was lower than that in BAT, the fold increase of UCP1 was more drastic in iWAT, but not pWAT, of aP2-Zfp516 mice even in the absence of cold or adrenergic stimuli (Figure 17B). Noticeably, iWAT of aP2-Zfp516 mice that were maintained at room temperature showed large clustered populations of cells with smaller multilocular lipid droplets, a characteristic of the browning of WAT depots whereas pWAT of aP2-Zfp516 mice showed no difference in morphology compared to

wild-type littermates (Figure 17B). UCP1 immunostaining of UCP1 in iWAT sections from aP2-Zfp516 mice maintained at room temperature also showed robust UCP1 staining (Figure 17B), while no significant staining was observed in wild type littermates.

To examine overall gene expression changes in iWAT, RNA from iWAT of wild-type and aP2-Zfp516 mice were subjected to Affymetrix microarray analysis. We found that transgenic expression of Zfp516 led to upregulation of a broad program of BAT-enriched genes while common adipocyte markers were not affected significantly (Figure 17C left). RT-qPCR analysis of these samples showed that expression levels of BAT-enriched genes, such as UCP1, PGC1α, and Cox8b, were all significantly elevated in

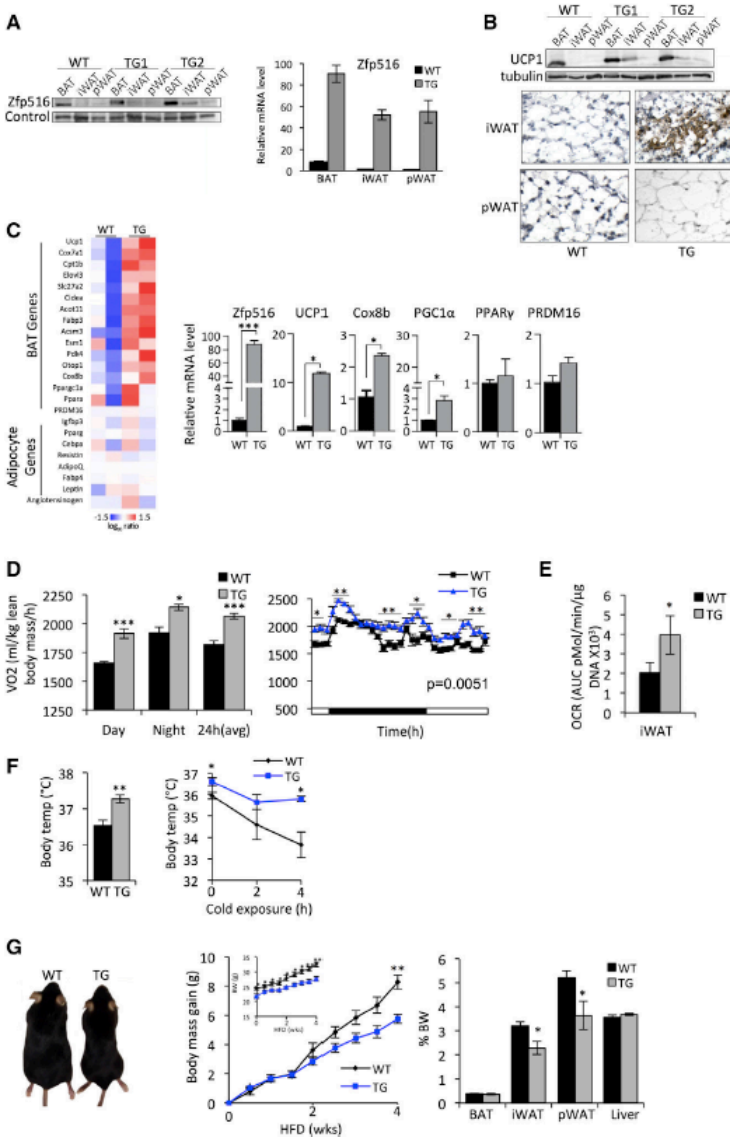

Figure 17. Zfp516 Promotes Browning of WAT.
(A) Left, immunoblotting for Zfp516 in adipose depots of WT and aP2-Zfp516 mice with different transgene copy number. Right, RT-qPCR for Zfp516. (B) Top, immunoblotting for UCP1 in adipose depots of WT and TG mice. Bottom, immunostaining for UCP1 in sections of iWAT and pWAT from WT and TG mice. (C) Left, microarray analysis from iWAT of WT or TG mice. Right, RT-qPCR of genes from microarray in WT or TG mice (n= 3 per group). (D) VO_2 assayed by indirect calorimetry in WT and TG mice on chow diet (CD) (n=6 mice per group). (E) Oxygen consumption rate of iWAT from WT or TG mice. (F) Rectal temperature measured in 15 wk old WT and TG mice fed CD at room temperature (left) and after 4 h cold exposure (right) (n=7-8 mice per group). (G) Left, representative photograph of 26 wk old WT or TG mice fed HFD for 16 wk. Center, body mass gain for the mice from left. Inlay, body weight in WT and TG mice fed HFD starting at 6 wk old (n=6-8 mice per group). Right, mass of each adipose tissue depot and liver represented in percentage of body weight in the mice mentioned above. *p<0.05; **p<0.01; ***p<0.001

iWAT of aP2-Zfp516 mice, while PPARγ and PRDM16 remain unaffected (Figure 17C top-right).

Considering the striking increase in UCP1 levels as well as extensive browning of iWAT of aP2-Zfp516 mice, we next assessed the metabolic effect in the transgenic animals. We observed 10% higher oxygen consumption rate (VO_2) in transgenic mice

during both day and night cycles (Figure 17D). We next tested whether changes in respiratory activity in iWAT could contribute to the altered respiratory activity in these transgenic mice. Indeed, upon using a Seahorse XF-24 Extracellular flux analyser, we found a 70% increase in oxygen consumption rate (OCR) in iWAT of transgenic mice (Figure 1E7). We did not detect significant alterations of OCR in BAT of transgenic mice (data not shown). Strikingly, aP2-Zfp516 mice fed a standard chow diet and maintained at room temperature had 0.7°C higher core body temperature than their wild-type littermates, although its implication in thermogenesis is not clear (Nedergaard and Cannon, 2014) (Figure 17F). However, when subjected to an acute cold exposure, these transgenic mice showed rectal temperature to be dropped by 1°C after 4h at 4°C, whereas the wild-type mice showed drop of 3°C, showing improved thermogenic capacity in Zfp516 transgenic mice. Taken together, these data show that Zfp516 overexpression causes browning of iWAT that results in increase in oxygen consumption and increased cold resistance.

We next subjected aP2-Zfp516 transgenic mice to high-fat diet (HFD) to test whether the increase in thermogenesis results in protection from diet-induced obesity. Interestingly, aP2-Zfp516 transgenic mice have significantly smaller body weight compared to wild type littermates on chow diet at room temperature, despite no change in food intake or activity level in these mice. When subjected to HFD feeding, aP2-Zfp516 transgenic mice gained 30% less weight than their wild-type littermates (Figure 17G). Noticeably, the iWAT and pWAT depots of transgenic mice had approximately 30% lower weights than wild-type littermates, even when normalized to body weight while BAT as well as other organs such as liver was unaffected (Figure 17G right). These data suggest that Zfp516 overexpressing mice are protected from diet induced obesity. After 4 wks on HFD, mice were subjected to glucose and insulin tolerance tests. We found that Zfp516 transgenic mice had improved glucose tolerance and insulin sensitivity as compared to wild-type littermates. Taken together, these data show that overexpression of Zfp516 causes an increase in UCP1 and browning iWAT resulting in increased energy expenditure, improved cold tolerance, as well as protection against diet-induced obesity.

Ablation of Zfp516 impairs BAT development *in vivo*

To further examine Zfp516 function in BAT program *in vivo*, we ablated Zfp516 in mice by using embryonic stem cells containing a gene trap inserted in intron 1 of the Zfp516 gene. Mice homozygous for the Zfp516 gene-trap were found to die immediately after birth due to a yet to be defined role of this gene during development. Therefore, we examined $Zfp516^{-/-}$ embryos at E20.5 when the presence of BAT, but not WAT, can be easily detected. RT-qPCR showed that Zfp516 expression was undetectable in $Zfp516^{-/-}$ embryos compared to wild-type littermates confirming Zfp516 ablation. Although $Zfp516^{-/-}$ embryos were somewhat smaller at E17.5, they were visibly indistinguishable from their wild-type littermates in terms of size at E20.5, yet the defective BAT formation was easily detected (Figure 18A). UCP1 staining on transverse sections of embryos showed a complete absence of UCP1 in the $Zfp516^{-/-}$ presumptive BAT (Figure 18B top). Haematoxylin and eosin (H&E) staining of the WAT/BAT boundary indicated abnormal cell morphology in the presumptive BAT of Zfp516 deficient embryos, while nearby WAT showed decreased cell size (Figure 18B upper-middle). Oil Red O staining of

presumptive BAT from Zfp516$^{-/-}$ embryos revealed a near complete loss of lipid staining (Figure 18B lower-middle). Furthermore, transmission electron microscopy revealed that mitochondria from presumptive BAT from Zfp516$^{-/-}$ embryos have randomly-oriented cristae as compared to the classic laminar cristae found in wild-type littermates (Figure 18B bottom).

We next examined gene expression in presumptive BAT of our Zfp516 ablated embryos at the global level by performing Affymetrix microarray analysis. Clustering of significantly affected genes into functionally related gene groups revealed down

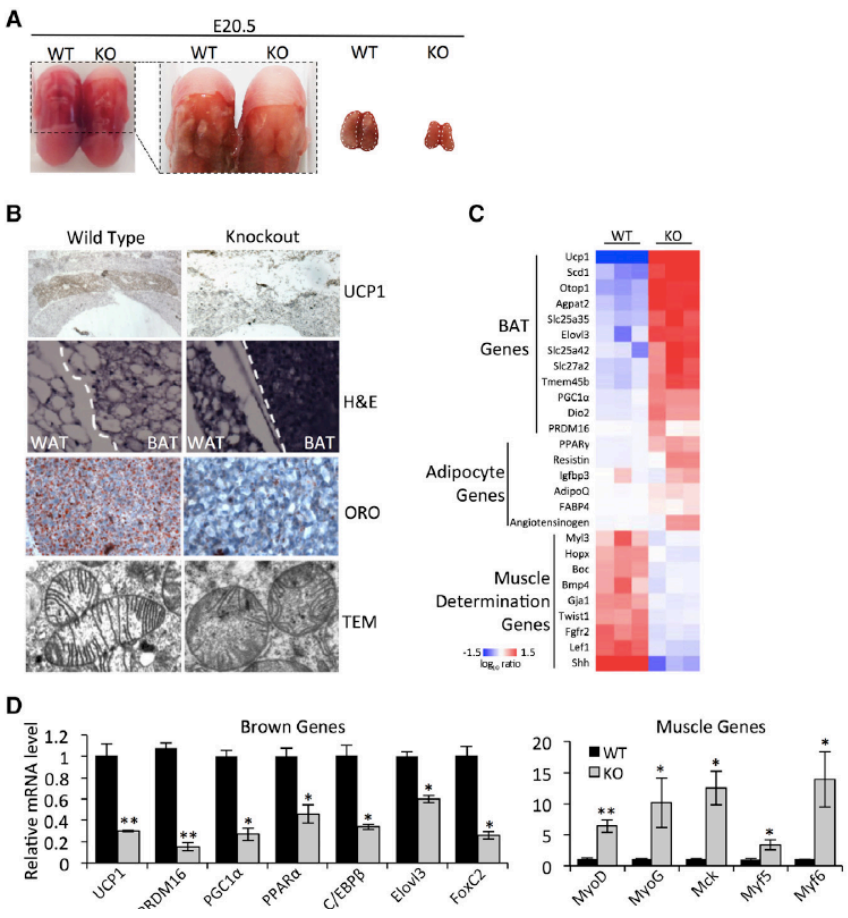

Figure 18. Zfp516 ablation blocks brown fat development in mice. (A) Left, E20.5 WT and Zfp516 KO embryos from back view. White dots delineate area of BAT or presumptive BAT. Right, cropped image from left. (B) Top, immunostaining for UCP1 in BAT or presumptive BAT in WT and KO embryos. Top middle, H&E staining of the BAT/WAT border in WT and KO mice. Bottom middle, ORO staining of WT or KO BAT. Bottom, transmission electron microscopy of WT and KO BAT mitochondria. (C) Microarray analysis from BAT or presumptive BAT of WT or KO E20.5 embryos. (D) RT-qPCR for BAT enriched (left) and muscle (right) genes in BAT from E17.5 WT or KO embryos (n=3). *p<0.05; **p<0.01; ***p<0.001.

regulation of a broad program of genes required for BAT function, whereas expression of muscle genes was elevated (Figure 18C). Common adipocyte markers were not significantly altered (data not shown). The gene expression analysis of BAT from Zfp516$^{-/-}$ embryos by RT-qPCR revealed that expression of BAT-enriched genes, such as UCP1, PRDM16, PGC1α, PPARα, C/EBPβ, Elovl3, and FoxC2, was all significantly lower by 40-85% (Figure 18D left). In contrast, myogenic genes, such as MyoD, MyoG, Mck, Myf5, and Myf6, were significantly upregulated by 3- to 14-fold (Figure 18D right). We conclude that Zfp516 ablation abrogates the induction of UCP1 and other BAT genes during normal BAT development.

Zfp516 promotes brown adipogenesis and suppresses myogenesis *in vitro*

As stated above, BAT develops from Myf5^{+} precursors that can differentiate to both muscle and BAT.

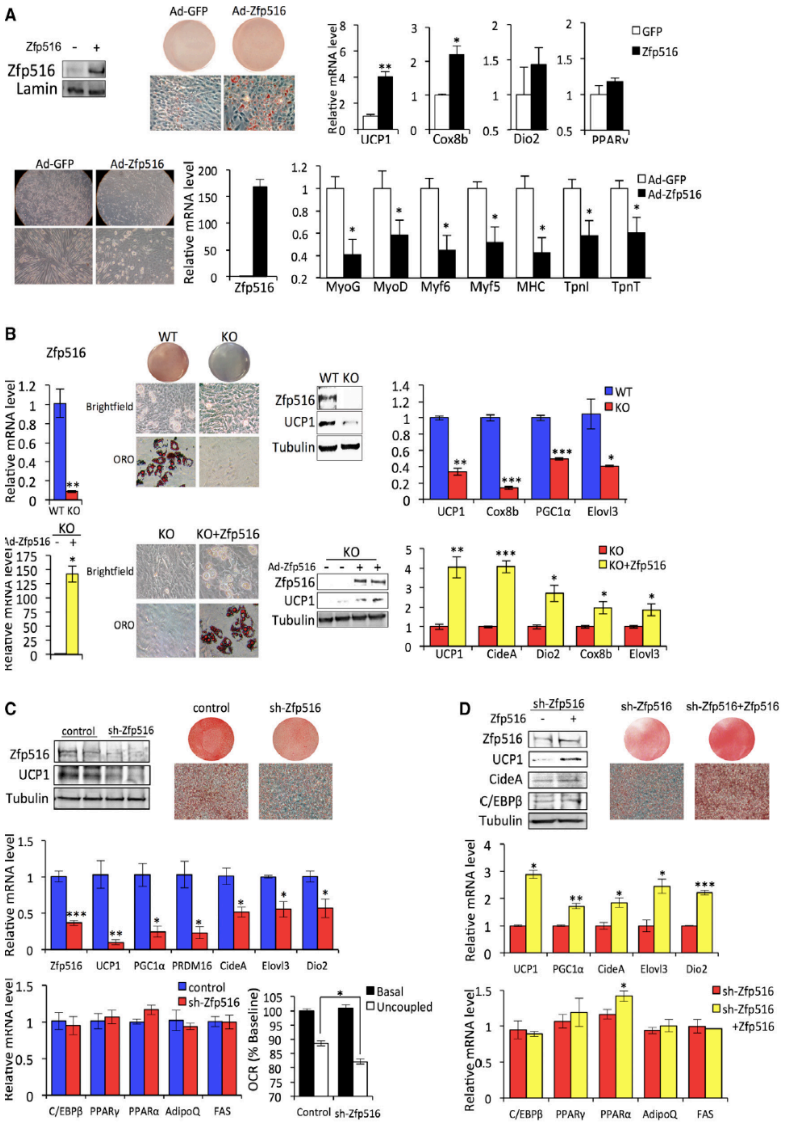

Figure 19. Zfp516 promotes brown adipogenesis and suppresses myogenesis.
(A) Top, immunoblotting (left), ORO staining (center) and RT-qPCR (right) in C2C12 cells after 6 days of brown adipogenic differentiation. Bottom, Brightfield view at 20X (top left) and 40X (bottom left) magnification, RT-qPCR (center and right) in C2C12 cells transduced with GFP or Zfp516 adenovirus after 6 days of myogenic differentiation. (B) Top, RT-qPCR (left), ORO staining and brightfield view pictures (center left), immunoblotting (center right) and RT-qPCR for BAT enriched genes (right) in WT and KO MEFs after 5 days of adipogenic differentiation. Bottom, RT-qPCR (left) ORO staining and brightfield view pictures (center left), immunoblotting (center right) and RT-qPCR for BAT enriched genes (right) in KO MEFs after 5 days of adipogenic differentiation. (C) Top-left, immunoblotting in HIB-1B cells after 5 days of adipogenic differentiation. Top-right, ORO staining. Middle, RT-qPCR in cells from Figure 19B. Bottom-left, RT-qPCR for common adipogenic genes. Bottom-right, Relative OCR rates in cells from Figure 19B before and after oligomycin treatment. OCR measurements before drug injection in the control cells were set as 100%. (N=9 or 10). (D) Top-left, Immunoblotting sh-Zfp516 HIB-1B cells or rescued cells. Top-right, ORO staining at day 5 of differentiation. Middle and bottom, RT-qPCR in these

Since we detected an increase in myogenic genes accompanied by decrease in BAT enriched genes in presumptive BAT of Zfp516$^{-/-}$ embryos, we employed C2C12 cells to test the ability of Zfp516 to induce UCP1 and other thermogenic genes to promote brown adipocyte differentiation. C2C12 cells were transduced with adenovirus expressing Zfp516 and treated with brown adipogenic cocktail. Endogenous expression of Zfp516 in C2C12 was very low but was substantially increased by adenoviral infection as verified at the protein level by immunoblotting (Figure 19A top-left) and at the mRNA level by RT-qPCR (data not shown). Upon infection with Zfp516, we observed an activation of the brown adipogenic program in C2C12 cells as evidenced

by enhanced lipid accumulation (Figure 19A top-center) and increased expression of UCP1 and Cox8b (respectively by 4- and 2- fold; Figure 6A top-right). In contrast, in myogenic conditions, Zfp516-overexpressing cells failed to undergo efficient myogenic differentiation, exhibiting a rounded cell shape, whereas control C2C12 cells underwent drastic morphological modifications toward multinucleated and elongated characteristic of myotubes (Figure 19A bottom-left). Consistent with the cell morphology, in comparison to control C2C12 cells, ectopic Zfp516 expressing cells had a significant reduction in the expression of myogenic genes, including myogenic transcription factors, MyoG, MyoD, Myf6 and Myf5, as well as late markers MHC, TpnI and TpnT (Figure 19A bottom right). These data show that ectopic expression of Zfp516 represses the myogenic program and drives transcription of a BAT gene program to promote brown adipocyte differentiation in C2C12 cells.

Next, we tested whether ablation of Zfp516 causes impairment of brown adipocyte differentiation *in vitro* by using mouse embryo fibroblasts (MEFs) isolated from Zfp516 $^{-/-}$embryos (Tseng et al., 2008). In contrast to wild-type that accumulated lipid droplets, knockout MEFs failed to differentiate as evidenced by lack of Oil red O (ORO) staining (Figure 19B center-left). While the wild-type MEFs underwent a morphological change to the rounded polygonal shape characteristic of brown adipocytes, the knockout MEF retained fibroblast-like morphology (Figure 19B center-left). UCP1 at both the protein and mRNA levels was greatly lower in the knockout MEFs (Figure 19B center-left). Expression levels of other BAT-enriched genes, such as Cox8b, PGC1α, and Elovl3, were 50-80% lower in the knockout compared to wild-type MEFs (Figure 19B top right). We next performed a rescue experiment using Zfp516 adenovirus in knockout MEFs. Compared to Zfp516 $^{-/-}$ MEFs, transduction with Zfp516 adenovirus completely rescued the phenotype in regard to morphological changes, lipid accumulation, and expression of BAT-enriched genes (Figure 19B bottom). These data show that Zfp516 expression is necessary for differentiation of multipotent MEFs to brown adipocytes.

We next investigated whether knockdown of Zfp516 can inhibit BAT gene expression in brown preadipocyte cell line. HIB-1B cells were transduced with sh-Zfp516 or control lentivirus and the cells selected for stable integration were subjected to brown adipocyte differentiation. Zfp516 knockdown cells, which had approximately 50% lower Zfp516 mRNA (Figure 19C center) and protein levels (Figure 19C top-left) at confluence, showed drastically lower ORO staining after 5 days of differentiation (Figure 19C top-right). Similarly, Zfp516 knockdown resulted in a marked decrease in the expression of various BAT genes, including UCP1, PRDM16, PGC1α decreased by 70-90% and CideA, Elovl3 and Dio2 by 40% (Figure 19B middle) further indicating inhibition of brown adipocyte differentiation by Zfp516 knockdown. Gene expression levels of PPARα, PPARγ, AdipoQ and FAS, common markers for both WAT and BAT, were not affected (Figure 19C bottom-left). Using Seahorse XF-24 Bioanalyzer, we next measured the respiratory rates of the Zfp516 knockdown cells after differentiation, to test if there was altered uncoupling in Zfp516 knockdown cells. While the basal respiratory rates were similar, the Zfp516 knockdown cells had significantly reduced uncoupling following oligomycin treatment, as compared to control cells (Figure 19C bottom-right). These data show that Zfp516 is required for proper brown adipocyte differentiation *in vitro*, which can be reflected in mitochondrial uncoupling. Furthermore,

in order to eliminate off-target effects of our shRNA knockdown, we performed a rescue experiment by infecting Zfp516 knockdown cells with adenoviral Zfp516. We observed a rescue of differentiation as evidenced by enhanced lipid accumulation (Figure 19D top-right), increased expression of BAT enriched genes such as UCP1, CideA, PGC1α, Elovl3 and Dio2 at the mRNA level (Figure 19D center) as well as at the protein level (UCP1 and CideA are shown), while common adipocyte markers were unaffected (Figure 19D bottom). Together these studies demonstrate that Zfp516 transcriptionally activates UCP1 and other BAT genes resulting in cell autonomous brown adipocyte differentiation.

Discussion

Due to its potential as a target of anti-obesity therapeutics, arising from evidenced presence of BAT like cells in humans, BAT development and activity have recently become an area of intense interest. While widely expressed transcription factors, such as PRDM16, PGC1α, C/EBPβ, and EBF2, have been identified to promote the BAT program, specific brown fat enriched transcription factors may operate to activate BAT genes and BAT development (Rajakumari et al., 2013). By unbiased genome-wide transcription factor library screening, we identified the zinc-finger protein, Zfp516, as a novel brown fat enriched, cold-inducible DNA-binding transcriptional activator of UCP1 and other BAT genes, which promotes browning of iWAT and is required for BAT development. Importantly, we show that Zfp516 is induced by sympathetic signaling, which to our knowledge, represents the first sympathetically regulated BAT-enriched transcription factor promoting a BAT program.

The above-mentioned transcriptional activators act through the well-characterized enhancer element at -2.5kb upstream of UCP1 promoter. Indeed, the enhancer region found at -2.5kb along with the proximal -400bp of the UCP1 promoter has been found to be sufficient to drive reporter expression in a tissue specific and sympathetically regulated manner (Ricquier and Bouillaud, 1997). Here, we identified Zfp516 as a novel activator of the UCP1 promoter, through binding at the proximal promoter region. Interestingly, CREB has previously been identified to interact with the proximal promoter region at -140bp to activate the UCP1 promoter. However, even the proximal -120bp of the UCP1 promoter that does not contain a CRE has still shown to respond to sympathetic stimuli (Rim and Kozak, 2002) clearly suggesting presence of a yet to be identified cold responsive transcription factors to function through binding to the proximal promoter region. Our finding that expression of Zfp516 is induced by cold and sympathetic stimulation and binds -70 to -45bp proximal region may represent such a transcription factor. In addition, Zfp516 can also bind PGC1α and Cox8b promoter regions for transcriptional activation. Zfp516 clearly acts as a transcriptional activator by binding to the promoter regions of BAT-enriched genes.

Recent research on the transcriptional factors critical for BAT development has centered on PRDM16. However, PRDM16 is broadly expressed and promotion of a BAT program by PRDM16 is independent of its DNA-binding activity (Ohno et al., 2013; Seale et al., 2007). Thus, PRDM16 must act through other transcription factors that bind promoter regions of BAT-enriched genes. In this regard, PPARγ and C/EBPβ, which bind to the -2.5kb enhancer region, have been reported to function with PRDM16 to

activate a BAT program (Kajimura et al., 2009; Seale et al., 2008) but these transcription factors also regulate WAT development and do not respond to cold exposure. Since the BAT program is induced upon cold exposure, DNA binding transcription factor(s) that are enriched in BAT and also cold inducible may act by interacting with PRDM16. We found that Zfp516, which binds to proximal promoter region of UCP1, directly interacts with PRDM16. In addition Zfp516 interacts with the PRDM16 ZF-2 domain that has been shown to interact with C/EBPβ (Kajimura et al., 2009). The relationship between these transcription factors interacting with PRDM16 needs further studies. Regardless, unlike other PRDM16 interacting proteins, Zfp516 is cold inducible by the classical β-AR-PKA-CREB pathway. Zfp516 expression is induced by β-adrenergic stimulation in both BAT and iWAT depots by cold exposure as well as by CL316,243 treatment. These results suggest that the transcriptional regulation of UCP1 in response to cold stimuli may require Zfp516 activity. Our finding that Zfp516 drives promoter activity of UCP1 and PGC1α, two genes both known to be essential for proper BAT response to cold (Leone et al., 2005; Lin et al., 2004), establishes the key role Zfp516 plays in transcriptional activation of BAT-genes during cold exposure.

We show here that overexpression of Zfp516 *in vivo* causes browning of iWAT even at room temperature. The fact that Zfp516 expression is induced by cold exposure to induce thermogenic genes indicates that Zfp516 may play a critical role in browning of iWAT. Sympathetic stimulation in mice causes an order of magnitude higher Zfp516 levels in iWAT but not in pWAT. However, we did not detect significant alterations in BAT phenotype in our transgenic mice. In this regard, although Zfp516 is also induced in BAT, the fold induction was significantly lower than that detected in iWAT. This may explain the inability of detecting changes in BAT in our transgenic mice. However, it is also possible that the endogenous Zfp516 level in BAT is sufficient for a BAT phenotype. Similar to our aP2-Zfp516 transgenic mice, overexpression of PRDM16 in adipose tissue caused browning of iWAT, without alteration in BAT phenotype (Seale et al., 2011). Zfp516 directly interacts with PRDM16, suggesting that Zfp516 cooperatively works along with PRDM16 for browning of iWAT. Previously PRDM16 presumptive BAT from null embryos was reported to have lower BAT enriched and higher muscle specific gene expression, with higher lipid stores. A recent report of a Myf5-cre PRDM16 conditional KO, however, indicated no defect in early BAT development but impaired BAT function in adults (Harms et al., 2014). Although Zfp516 null embryonic presumptive BAT showed similar gene expression pattern to PRDM16 null, they also showed significantly decreased lipid staining, with altered genome-wide gene expression pattern as well as abnormal mitochondrial morphology. It is also possible that as a DNA binding protein, which often shows more severe phenotype of null mutation than coregulator, Zfp516 may interact with coregulator(s) other than PRDM16 during early BAT development. Regardless, PRDM16 is expressed constitutively and, thus, the cold-inducible nature of Zfp516 could be a key driving BAT-gene program in browning of iWAT. Since iWAT is a predominant adipose depot in humans and is normally devoted to lipid storage rather than dissipation of energy, Zfp516, which induces browning of iWAT even at room temperature preventing diet induced obesity, may represent a compelling target for future anti-obesity therapeutics.

Experimental Procedures

Animals, and cell culture

All protocols for mice studies were approved from the University of California at Berkeley Animal Care and Use Committee. Mice were fed chow diet ad libitum. Oxygen consumption (VO_2) was measured using the Comprehensive Laboratory Animal Monitoring System (CLAMS). Data were normalized to lean body mass as determined by echoMRI. Body temperatures were assessed using a RET-3 rectal probe for mice (Physitemp). CL316,243 (Sigma) was intraperitoneally injected into mice at 1 $mg*kg^{-1}$. GTT and ITT performed upon intraperitoneal injection of 1 mg/g BW of D-glucose or 0.75 mU/g BW of insulin as previously described (Ahmadian et al., 2011). Tail vein blood was collected for measurements. Derivation of mice is described in the supplementary methods. Brown adipocyte differentiation was performed as described in (Kajimura et al., 2009). To induce thermogenic genes, cells were treated for 6 h with 10μM forskolin or 10 μM isoproterenol. For myogenic differentiation, confluent cells were treated with DMEM containing 2% Horse serum and 25mM Hepes, pH 7.4. Primary MEFs were isolated as previously described (Wang and Sul, 2009). All differentiation experiments were carried out using cells at passage 3. Upon reaching confluence, the cells were split into 6-well plates. MEF differentiation was performed as described in (Tseng et al., 2008). Cellular and tissue explant respiration was measured using a XF24 Analyzer (Seahorse Bioscience).

Functional Screen

cDNA clones in pCMV-Sport6 vector from the Mammalian Genome Collection (Invitrogen) were screened for activation of the -5.5kb UCP1 promoter-eGFP-N1 construct. 100 ng of -5.5kb UCP1-eGFP-N1, 1ng of lipofectamine2000 (Invitrogen), and 44.8 μl Optimem (Gibco) were added to 40 ng of test vector in 48-well plates. Complexes were added to7.5×10^4 293FT cells. Cells were assayed for GFP signal at 24 and 48 h post-transfection. Each plate contained positive (pCMV-Sport6-CREB) and negative (pCMV-Sport6) controls. For secondary screening, 100 ng of -5.5kb UCP1-Luciferase, 0.5 ng pRL-CMV, and 1.2 μl Lipofectamine2000 were diluted to 45 μl in Optimem before addition of 50 ng of each of the positive clone from the initial screen in 48-well plates in triplicates. 7.5×10^4 293FT cells were added to transfection mixtures and incubated for 24 h. Cells were assayed for luciferase activity using Dual-Luciferase Reporter assay system (Promega).

Oil red O staining

Wells were washed once with phosphate-buffered saline and subsequently fixed for 30 min in 10% formalin. Cells were then stained with freshly prepared 0.3% Oil Red O working solution for 1h. Cells were washed twice with distilled water prior to visualization.

RT-PCR Analysis and Western blotting

Total RNA was extracted using TRIzol reagent (Invitrogen). Reverse transcription was performed with 1 μg of total RNA using SuperScript II (Invitrogen). RT-qPCR was performed with an ABI PRISM 7500 sequence detection system (PE Applied

Biosystems) to quantify the relative mRNA levels for various genes. Statistical analysis of the qPCR was obtained using the ΔΔCt method with U36B4 as the internal control. Experiments were performed in triplicate. Primer sets used are listed in Table S1. Microarray hybridization and scanning were performed by the Functional Genomics Laboratory core facility using Affymetrix Mouse Genome 430A 2.0 Gene Chip arrays. Microarray data for both KO and TG mice are available at http://dx.doi.org/10.6084/m9.figshare.1009210 and http://dx.doi.org/10.6084/m9.figshare.1009211. For western blot analysis, total cell lysates were prepared using RIPA buffer and nuclear extracts were isolated using the NE-PER Nuclear and Cytoplasmic Extraction kit (Thermo). Proteins were separated by SDS-PAGE, transferred to nitrocellulose membrane and probed with the indicated antibodies.

Luciferase Assays

293FT cells were transfected with 300 ng Zfp516 or empty vector and/or 300 ng PRDM16 or empty vector in cotransfection assays together with 100 ng of indicated luciferase reporter construct and 0.5 ng pRL-CMV in 24-well plates. Cells were lysed 24h post-transfection and assayed for luciferase activity as above.

Electrophoretic Mobility Shift Assay

Nuclear extracts of 293FT cells transfected with full length Zfp516, Zfp516 (AA1-420), or Zfp516 (AA400-820) fragment were used in electrophoretic mobility shift assay (EMSA). Sense (5'-CCTGGGCCGGCTCAGCCACTTCCCCCAGTC-3') and antisense (5'-GACTGGGGGAAGTGGCTGAGCCGGCCCAGG-3') oligonucleotides were end-labeled by γ ^{32}P-ATP using T4 Polynucleotide kinase (NEB) and annealed. Samples were separated by 5% native PAGE before autoradiography.

Transmission electron microscopy

WT and KO BAT were fixed in 2% glutaraldehyde in 0.1 M phosphate buffer, pH 7.3, at 4°C overnight, then postfixed in 1% OsO_4 and embedded in an Epon-Araldite mixture. Ultrathin sections (0.2 μm) mounted on 150-mesh copper grids were stained with lead citrate and observed under a FEI Tecnai 12 transmission electron microscope.

Statistical analysis

Data are expressed as means ± standard errors of the means (SEM). The statistical differences in mean values were assessed by Student's *t* test. All experiments were performed at least twice and representative data are shown.

Acknowledgements

We thank Dr. S. Kajimura for GST-PRDM16 constructs and Dr. P. Tontonoz for the V5-PRDM16 construct. We thank D. Hunerdosse, J. Niliwat, W. Orenella, N. Chien, J. Zheng, X. Liang, E. Esquivel and J. Chong for technical assistance. The work was supported in part by DK095338 to H.S.S.

References

1. Ahmadian, M., Abbott, M.J., Tang, T., Hudak, C.S.S., Kim, Y., Bruss, M., Hellerstein, M.K., Lee, H.-Y., Samuel, V.T., Shulman, G.I., et al. (2011). Desnutrin/ATGL is regulated by AMPK and is required for a brown adipose phenotype. Cell Metab. *13*, 739–748.
2. Bachman, E.S., Dhillon, H., Zhang, C.-Y., Cinti, S., Bianco, A.C., Kobilka, B.K., and Lowell, B.B. (2002). βAR Signaling Required for Diet-Induced Thermogenesis and Obesity Resistance. Science *297*, 843–845.
3. Cannon, B., and Nedergaard, J. (2004). Brown adipose tissue: function and physiological significance. Physiol. Rev. *84*, 277–359.
4. Cassard-Doulcier, A.M., Gelly, C., Fox, N., Schrementi, J., Raimbault, S., Klaus, S., Forest, C., Bouillaud, F., and Ricquier, D. (1993). Tissue-specific and beta-adrenergic regulation of the mitochondrial uncoupling protein gene: control by cis-acting elements in the 5'-flanking region. Mol. Endocrinol. Baltim. Md *7*, 497–506.
5. Cassard-Doulcier, A.M., Gelly, C., Bouillaud, F., and Ricquier, D. (1998). A 211-bp enhancer of the rat uncoupling protein-1 (UCP-1) gene controls specific and regulated expression in brown adipose tissue. Biochem. J. *333 (Pt 2)*, 243–246.
6. Cederberg, A., Grønning, L.M., Ahrén, B., Taskén, K., Carlsson, P., and Enerbäck, S. (2001). FOXC2 is a winged helix gene that counteracts obesity, hypertriglyceridemia, and diet-induced insulin resistance. Cell *106*, 563–573.
7. Collins, S., Yehuda-Shnaidman, E., and Wang, H. (2010). Positive and negative control of Ucp1 gene transcription and the role of β-adrenergic signaling networks. Int. J. Obes. 2005 *34 Suppl 1*, S28–33.
8. Cypess, A.M., Lehman, S., Williams, G., Tal, I., Rodman, D., Goldfine, A.B., Kuo, F.C., Palmer, E.L., Tseng, Y.-H., Doria, A., et al. (2009). Identification and importance of brown adipose tissue in adult humans. N. Engl. J. Med. *360*, 1509–1517.
9. Farmer, S.R. (2008). Molecular determinants of brown adipocyte formation and function. Genes Dev. *22*, 1269–1275.
10. Farmer, S.R. (2009). Obesity: Be cool, lose weight. Nature *458*, 839–840.
11. Fulton, D.L., Sundararajan, S., Badis, G., Hughes, T.R., Wasserman, W.W., Roach, J.C., and Sladek, R. (2009). TFCat: the curated catalog of mouse and human transcription factors. Genome Biol. *10*, R29.
12. Gensch, N., Borchardt, T., Schneider, A., Riethmacher, D., and Braun, T. (2008). Different autonomous myogenic cell populations revealed by ablation of Myf5-expressing cells during mouse embryogenesis. Dev. Camb. Engl. *135*, 1597–1604.
13. Harms, M.J., Ishibashi, J., Wang, W., Lim, H.-W., Goyama, S., Sato, T., Kurokawa, M., Won, K.-J., and Seale, P. (2014). Prdm16 Is Required for the Maintenance of Brown Adipocyte Identity and Function in Adult Mice. Cell Metab. *19*, 593–604.
14. Kajimura, S., Seale, P., Tomaru, T., Erdjument-Bromage, H., Cooper, M.P., Ruas, J.L., Chin, S., Tempst, P., Lazar, M.A., and Spiegelman, B.M. (2008).

Regulation of the brown and white fat gene programs through a PRDM16/CtBP transcriptional complex. Genes Dev. *22*, 1397–1409.
15. Kajimura, S., Seale, P., Kubota, K., Lunsford, E., Frangioni, J.V., Gygi, S.P., and Spiegelman, B.M. (2009). Initiation of myoblast to brown fat switch by a PRDM16-C/EBP-beta transcriptional complex. Nature *460*, 1154–1158.
16. Kang, S., Bajnok, L., Longo, K.A., Petersen, R.K., Hansen, J.B., Kristiansen, K., and MacDougald, O.A. (2005). Effects of Wnt signaling on brown adipocyte differentiation and metabolism mediated by PGC-1alpha. Mol. Cell. Biol. *25*, 1272–1282.
17. Kozak, U.C., Kopecky, J., Teisinger, J., Enerbäck, S., Boyer, B., and Kozak, L.P. (1994). An upstream enhancer regulating brown-fat-specific expression of the mitochondrial uncoupling protein gene. Mol. Cell. Biol. *14*, 59–67.
18. Laity, J.H., Lee, B.M., and Wright, P.E. (2001). Zinc finger proteins: new insights into structural and functional diversity. Curr. Opin. Struct. Biol. *11*, 39–46.
19. Leonardsson, G., Steel, J.H., Christian, M., Pocock, V., Milligan, S., Bell, J., So, P.-W., Medina-Gomez, G., Vidal-Puig, A., White, R., et al. (2004). Nuclear receptor corepressor RIP140 regulates fat accumulation. Proc. Natl. Acad. Sci. U. S. A. *101*, 8437–8442.
20. Leone, T.C., Lehman, J.J., Finck, B.N., Schaeffer, P.J., Wende, A.R., Boudina, S., Courtois, M., Wozniak, D.F., Sambandam, N., Bernal-Mizrachi, C., et al. (2005). PGC-1alpha deficiency causes multi-system energy metabolic derangements: muscle dysfunction, abnormal weight control and hepatic steatosis. PLoS Biol. *3*, e101.
21. Lepper, C., and Fan, C.-M. (2010). Inducible lineage tracing of Pax7-descendant cells reveals embryonic origin of adult satellite cells. Genes. N. Y. N 2000 *48*, 424–436.
22. Lin, J., Wu, P.-H., Tarr, P.T., Lindenberg, K.S., St-Pierre, J., Zhang, C.-Y., Mootha, V.K., Jäger, S., Vianna, C.R., Reznick, R.M., et al. (2004). Defects in adaptive energy metabolism with CNS-linked hyperactivity in PGC-1alpha null mice. Cell *119*, 121–135.
23. Van Marken Lichtenbelt, W.D., Vanhommerig, J.W., Smulders, N.M., Drossaerts, J.M.A.F.L., Kemerink, G.J., Bouvy, N.D., Schrauwen, P., and Teule, G.J.J. (2009). Cold-activated brown adipose tissue in healthy men. N. Engl. J. Med. *360*, 1500–1508.
24. Nedergaard, J., and Cannon, B. (2010). The changed metabolic world with human brown adipose tissue: therapeutic visions. Cell Metab. *11*, 268–272.
25. Nedergaard, J., and Cannon, B. (2014). The Browning of White Adipose Tissue: Some Burning Issues. Cell Metab. *20*, 396–407.
26. Ohno, H., Shinoda, K., Ohyama, K., Sharp, L.Z., and Kajimura, S. (2013). EHMT1 controls brown adipose cell fate and thermogenesis through the PRDM16 complex. Nature *504*, 163–167.
27. Rajakumari, S., Wu, J., Ishibashi, J., Lim, H.-W., Giang, A.-H., Won, K.-J., Reed, R.R., and Seale, P. (2013). EBF2 determines and maintains brown adipocyte identity. Cell Metab. *17*, 562–574.
28. Ricquier, D., and Bouillaud, F. (1997). The mitochondrial uncoupling protein: structural and genetic studies. Prog. Nucleic Acid Res. Mol. Biol. *56*, 83–108.

29. Rim, J.S., and Kozak, L.P. (2002). Regulatory motifs for CREB-binding protein and Nfe2l2 transcription factors in the upstream enhancer of the mitochondrial uncoupling protein 1 gene. J. Biol. Chem. *277*, 34589–34600.
30. Rosenwald, M., Perdikari, A., Rülicke, T., and Wolfrum, C. (2013). Bi-directional interconversion of brite and white adipocytes. Nat. Cell Biol.
31. Schulz, T.J., Huang, T.L., Tran, T.T., Zhang, H., Townsend, K.L., Shadrach, J.L., Cerletti, M., McDougall, L.E., Giorgadze, N., Tchkonia, T., et al. (2011). Identification of inducible brown adipocyte progenitors residing in skeletal muscle and white fat. Proc. Natl. Acad. Sci. U. S. A. *108*, 143–148.
32. Seale, P., Kajimura, S., Yang, W., Chin, S., Rohas, L.M., Uldry, M., Tavernier, G., Langin, D., and Spiegelman, B.M. (2007). Transcriptional control of brown fat determination by PRDM16. Cell Metab. *6*, 38–54.
33. Seale, P., Bjork, B., Yang, W., Kajimura, S., Chin, S., Kuang, S., Scimè, A., Devarakonda, S., Conroe, H.M., Erdjument-Bromage, H., et al. (2008). PRDM16 controls a brown fat/skeletal muscle switch. Nature *454*, 961–967.
34. Seale, P., Conroe, H.M., Estall, J., Kajimura, S., Frontini, A., Ishibashi, J., Cohen, P., Cinti, S., and Spiegelman, B.M. (2011). Prdm16 determines the thermogenic program of subcutaneous white adipose tissue in mice. J. Clin. Invest. *121*, 96–105.
35. Tseng, Y.-H., Kokkotou, E., Schulz, T.J., Huang, T.L., Winnay, J.N., Taniguchi, C.M., Tran, T.T., Suzuki, R., Espinoza, D.O., Yamamoto, Y., et al. (2008). New role of bone morphogenetic protein 7 in brown adipogenesis and energy expenditure. Nature *454*, 1000–1004.
36. Virtanen, K.A., Lidell, M.E., Orava, J., Heglind, M., Westergren, R., Niemi, T., Taittonen, M., Laine, J., Savisto, N.-J., Enerbäck, S., et al. (2009). Functional brown adipose tissue in healthy adults. N. Engl. J. Med. *360*, 1518–1525.
37. Waldén, T.B., Hansen, I.R., Timmons, J.A., Cannon, B., and Nedergaard, J. (2012). Recruited vs. nonrecruited molecular signatures of brown, “brite,” and white adipose tissues. Am. J. Physiol. Endocrinol. Metab. *302*, E19–31.
38. Wang, Y., and Sul, H.S. (2009). Pref-1 regulates mesenchymal cell commitment and differentiation through Sox9. Cell Metab. *9*, 287–302.
39. Wu, J., Boström, P., Sparks, L.M., Ye, L., Choi, J.H., Giang, A.-H., Khandekar, M., Virtanen, K.A., Nuutila, P., Schaart, G., et al. (2012). Beige adipocytes are a distinct type of thermogenic fat cell in mouse and human. Cell *150*, 366–376.

Chapter 4:

LSD1 Interacts with Zfp516 to Promote UCP1 Transcription and Brown Adipogenesis

LSD1 Interacts with Zfp516 to Promote UCP1 Transcription and Brown Adipogenesis

Abstract

Zfp516 is a brown fat (BAT) enriched and cold inducible transcription factor, which promotes transcription of UCP1 and other BAT-enriched genes for non-shivering thermogenesis. Here, we identify lysine specific demethylase 1 (LSD1) as a direct binding partner of Zfp516. We show that, by interaction with Zfp516, LSD1 is recruited to UCP1 and other BAT-enriched genes, such as PGC1α, and functions as a coactivator by demethylating histone H3, lysine 9 (H3K9). We also show that LSD1, which is cold inducible, is induced during brown adipogenesis and that LSD1 and its demethylase activity are required for brown adipocyte differentiation. Furthermore, BAT-specific deletion of LSD1 in mice via the use of UCP1-Cre impairs the BAT gene program and BAT development making their BAT resemble WAT, reducing thermogenic activity, and promoting obesity.

Introduction

Unlike white adipose tissue (WAT), whose main function is to store energy in the form of triacylglycerol to be used during periods of energy deprivation, brown adipose tissue (BAT) is specialized in heat production for maintenance of body temperature via nonshivering thermogenesis. Since the discovery that active brown adipose-like tissue is present in adults (Cypess et al., 2009) (Farmer, 2009) (van Marken Lichtenbelt et al., 2009) (Virtanen et al., 2009) and that BAT can have anti-obesity and anti-diabetic effects (Lowell et al., 1993) (Enerback et al., 1997) (Bartelt et al., 2011), mechanisms underlying BAT formation and function have attracted a growing interest.

BAT displays high mitochondrial density and contains uncoupling protein 1 (UCP1), a proton transporter that is uniquely expressed in BAT, induced upon cold exposure, and uncouples the mitochondrial proton gradient from ATP synthesis, dissipating energy as heat. UCP1 transcription has been reported to be regulated by various transcription factors, such as PPARγ, PGC1α and ATF2, which bind to an enhancer region of the UCP1 promoter. We recently identified a cold-inducible transcription factor, Zfp516, which is enriched in BAT and activates UCP1 and other BAT-enriched genes, such as PGC1α, to promote a BAT program (Dempersmier et al., 2015). We have shown that Zfp516 activates UCP1 promoter by binding to the proximal region and induces brown adipogenesis. Consequently, ablation of Zfp516 in mice, although embryonically lethal, shows drastically reduced BAT depot formation, whereas overexpression of Zfp516 in adipose tissue causes browning of inguinal white adipose tissue (iWAT) and increases energy expenditure, preventing diet-induced obesity.

In addition to transcription factors and coregulators, histone modifications including methylation, phosphorylation, and acetylation modulate chromatin architecture for epigenetic regulation of gene expression. LSD1 (also called KDM1A or AOF2) was the first identified histone demethylase, which established histone methylation as a

reversible and dynamic regulatory mechanism for transcription. LSD1 catalyzes demethylation through a flavin adenosine dinucleotide (FAD)-dependant oxidative reaction and was initially characterized to target mono- and di-methylated K4 residues of histone H3 (H3K4me1 and me3) (Shi et al., 2004) for transcriptional repression. However, LSD1 has also been shown to promote gene activation through H3K9 demethylation (Metzger et al., 2005). Moreover, LSD1 has been reported to play a role during early stages of white adipocyte differentiation by demethylating H3K9me2 at the C/EBPα promoter region (Musri et al., 2010). Recently, it has also been reported that, LSD1 is not only essential for early steps of white adipocyte differentiation, but also promotes oxidative metabolism by interacting with Nrf1 for mitochondrial biogenesis, thus enhancing browning of WAT (Duteil et al., 2014). However, the function of LSD1 in BAT development and whether it can affect UCP1 or other BAT gene transcription for a BAT program are not known.

Here, we identify LSD1 as a binding partner of Zfp516. LSD1, which is induced during brown adipogenesis and recruited to the UCP1 promoter region via direct interaction with Zfp516 for transcriptional activation via H3K9 demethylation. We also show that LSD1 is required for brown adipogenesis and that BAT specific ablation of LSD1 in mice impairs BAT development and BAT program.

Results

We previously reported Zfp516 as a cold-inducible BAT-enriched transcription factor involved in the BAT gene transcription to promote BAT program. As a DNA binding protein, Zfp516 may interact with other coregulators to promote early BAT development. Thus, we further investigated potential interacting partners of Zfp516 to better understand the molecular mechanisms underlying the transcriptional activation of UCP1 and other BAT-enriched genes to promote a BAT program.

Direct interaction between LSD1 and Zfp516

In order to identify Zfp516 binding partners, we used Tandem Affinity Purification (TAP) followed by mass spectrometry. Lysates from HEK293FT cells overexpressing either TAP alone or TAP tagged-Zfp516 were processed for affinity purification. Eluted proteins from TAP alone (left lane) or TAP-Zfp516 (right lane) samples were then separated by SDS-PAGE and stained with Coomassie blue (data not shown). Bands detected only in TAP-Zfp516 lane were excised and subjected to mass spectrometry. LSD1 was identified as a candidate interacting partner of Zfp516. In order to validate the interaction between LSD1 and Zfp516, we first performed a coimmunoprecipitation (CoIP) using HEK 293FT cells transfected with FLAG tagged-Zfp516 and c-Myc tagged-LSD1 either alone or in combination (Figure 20A top). Indeed, by using FLAG and c-Myc antibodies, we detected an interaction between Zfp516 and LSD1 only when coexpressed together. We then confirmed interaction between endogenous Zfp516 and LSD1, using lysates from differentiated brown adipocytes. Immunoprecipitation with Zfp516 antibody followed by immunoblotting with LSD1 antibody clearly detected interaction between the two proteins (Figure 20C bottom). Next, we asked whether LSD1 binds Zfp516 directly, which we assessed using GST-fused LSD1expressed and purified from E. coli (Figure 20B). Incubating GST-LSD1 fusion protein immobilized on

glutathione agarose beads with *in vitro* translated Zfp516, we indeed detected direct interaction between Zfp516 and LSD1 (Figure 20B).

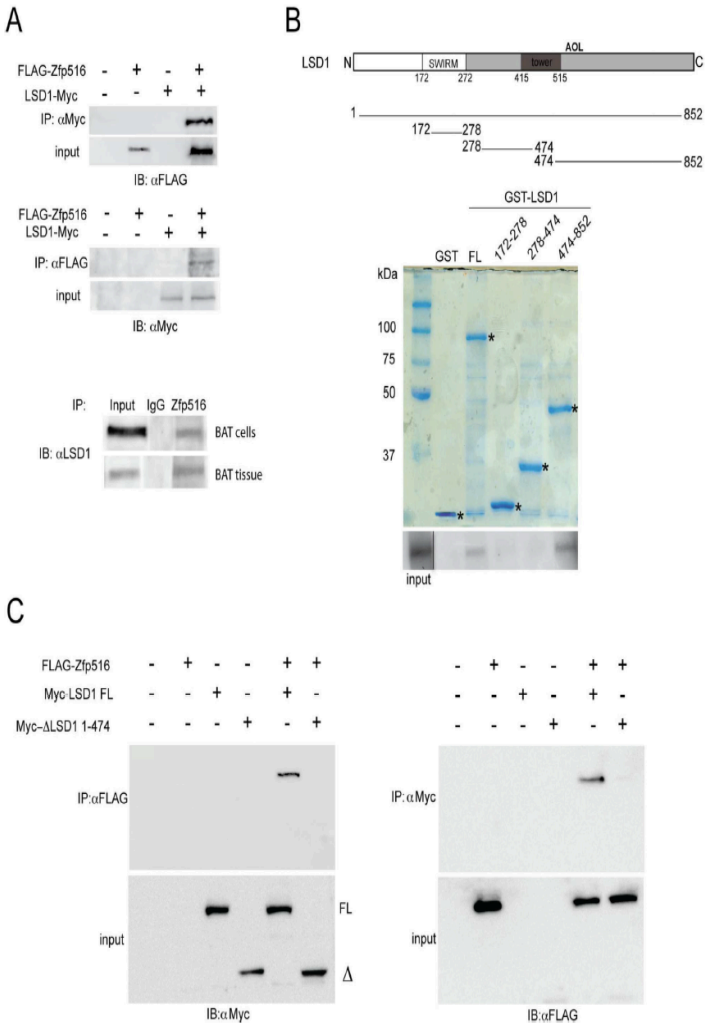

Figure 20. LSD1 directly interacts with Zfp516
(A) Immunoblot using αFLAG (Top) or αMyc (center) after immunoprecipitation with either αMyc or αFLAG, respectively, of HEK 293FT cell lysates. Bottom, immunoblot for after immunoprecipitation of lysates from differentiated BAT cells or BAT tissue with α-Zfp516. (B) Top, schematic representation of GST-LSD1 deletion constructs. Center, Coomassie staining for indicated GST constructs. Bottom, autoradiograph of GST pulldown using GST fusion proteins containing the indicated domains of LSD1 and 35S-labelled in vitro translated Zfp516. (C) Immunoblot using αMyc (top-left) or αFLAG (top-right) after immunoprecipitation with either αFLAG or αMyc respectively, of lysates from 293FT cells transfected with FLAG-Zfp516 and either Myc-LSD1 full length (FL) or deleted Myc-ΔLSD1 1-474 (Δ), together or individually. Immunoblots of input for the corresponding lysate are shown on bottom-left and right.

Furthermore, the use of various GST-LSD1 fragments in this assay indicated that LSD1 directly interacts with Zfp516 through a domain located within the C-terminal region of LSD1, aa474-832, containing a part of the tower and AOL-C-terminal enzymatic domain (Figure 20B). Furthermore, CoIP experiments using a LSD1 construct deleted within the C-terminal region (ΔLSD1 1-474) (Figure 20C) confirmed interaction of Zfp516 with the C-terminal domain of LSD1. Thus, the interaction of LSD1 with Zfp516 was abolished upon deletion of aa474-852 region of LSD1 characterized by GST-LSD1 experiments.

By binding to Zfp516, LSD1 is recruited to and activate the UCP1 promoter

We previously reported that Zfp516 is recruited to the promoter regions of UCP1 and other BAT-enriched genes, such as PGC1α, for promoter activation. Here, we first tested the effect of LSD1 on UCP1 and other BAT genes, by performing luciferase reporter assay using –5.5 kb UCP1 promoter (Figure 21A top) and -2.4 kb PGC1α

promoter (Figure 21A bottom). Along with the luciferase-promoter constructs, Zfp516 and LSD1 were cotransfected, either alone or in combination, into HEK 293FT cells and luciferase activity was measured.

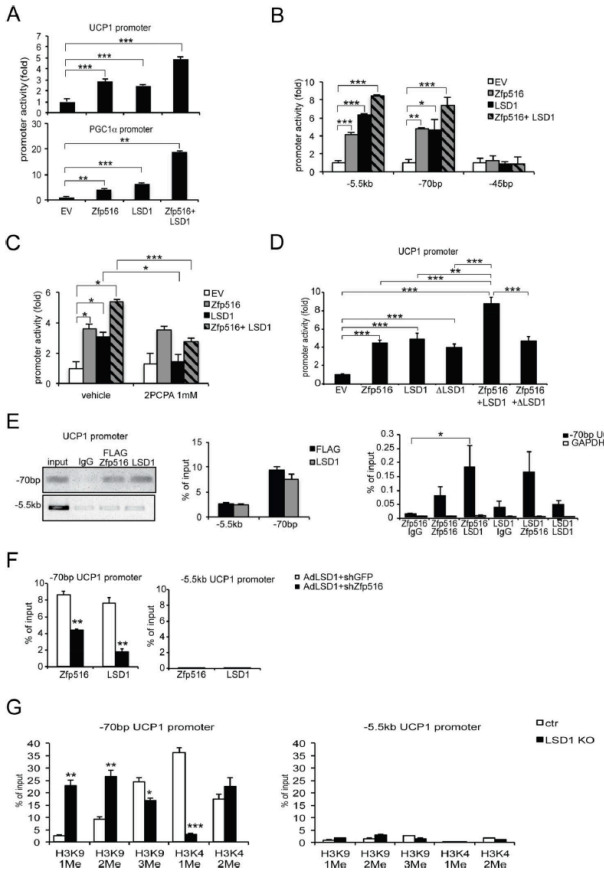

Figure 21. Zfp516 recruits LSD1 to activate the UCP1 promoter.
(A) Luciferase activity in 293FT cells cotransfected with the −5.5kb UCP1 promoter (top) or −2.4kb PGC1α promoter (bottom). (B) Luciferase activity in cells cotransfected with the −5.5kb, −70 bp or −45 bp UCP1 promoter. (C) Luciferase activity in cells cotransfected with the −5.5kb UCP1 promoter and empty vector (EV), along with Zfp516 and LSD1 vectors either together or individually after treatment with LSD1 inhibitor (2PCPA 1mM) or vehicle for 48 h. (D) Luciferase activity with the −5.5kb UCP1 promoter and empty vector (EV), along with Zfp516 and either LSD1 full length (FL) or deleted ΔLSD1 1-474. (E) Left, ChIP for Zfp516 and LSD1 binding at the −70 bp region of UCP1 promoter using both αFlag and αLSD1 for chromatin of BAT cells infected with Zfp516 and LSD1 adenoviruses. Center, qPCR of ChIP DNA. Right, ReChIP for Zfp516 and LSD1 binding to the UCP1 promoter region in BAT cells using IgG, αZfp516 or αLSD1 as indicated. (F) Left, ChIP for Zfp516 and LSD1 binding to the −70 bp region of the UCP1 promoter in BAT cells using both αZfp516 and αLSD1 with LSD1 overexpression and Zfp516 knockdown (shZfp516), compared to negative control (shGFP). (G) ChIP analysis of histone H3 methylations at the −70 bp region of UCP1 promoter (left) or at the GAPDH promoter as a negative control (right) in ChIP of BAT tissue from control (fl/fl) or LSD1 knockout (LSD1KO) mice. Data are represented as mean ± SEM. *p<0.05; **p<0.01; ***p<0.001.

As we previously reported, we observed that Zfp516 activated UCP1 and PGC1α promoter (second panel, Figure 21A top and bottom,). In addition, LSD1 alone could activate these promoters as well (third panel Figure 21A top and bottom). More importantly, cotransfection of the promoter constructs with both Zfp516 and LSD1 further increased promoter activity. Furthermore, LSD1 lacking the domain that interacts with Zfp516 could not activate UCP1 promoter (Figure 21D). These results show that Zfp516 and LSD1 work together to activate BAT genes promoters. We next employed the two shorter constructs of the UCP1 promoter which contain Zfp516 binding sequence but lacking the enhancer region of the UCP1 promoter (-70 bp construct), as well as the UCP1 promoter that does not contain neither Zfp516 binding sequence nor UCP1 enhancer (-45 bp construct) (Figure 21B). We found that promoter activation by Zfp516 and LSD1 was still detected when cotransfected with the -70 bp construct, but not with the -45 bp construct. These results demonstrate requirement of Zfp516 binding sequence for UCP1 promoter activation by LSD1, which in agreement with the interaction between LSD1 and Zfp516 for promoter activation. We also asked whether LSD1-mediated promoter activation requires enzymatic activity of LSD1 by using a

pharmacologic inhibitor of LSD1, 2PCPA, in the reporter assay (Figure 21C). We observed that activation of UCP1 promoter by LSD1 alone or in combination with Zfp516, but not by Zfp516 alone, were greatly reduced in the presence of 2PCPA, indicating the requirement of demethylase activity of LSD1 for its effect on UCP1 promoter activity.

As LSD1 interacts with Zfp516 and promotes UCP1 promoter activity, we predicted that LSD1 should occupy the same region that Zfp516 binds within the UCP1 promoter. We therefore performed chromatin immunoprecipitation (ChIP) assay using BAT cells infected with adenoviral Zfp516 and LSD1 (Figure 21E). Using FLAG (for Zfp516) and LSD1 antibodies, we detected by PCR an enrichment of the -70 bp region of the UCP1 promoter region in comparison to the -5.5 kb region, as a control (Figure 21E left). Quantification by qPCR confirmed a 5- and 4- fold enrichment for Zfp516 and LSD1 binding to the -70 bp UCP1 promoter region, respectively (Figure 21E middle). We then performed reChIP experiment using combinations of Zfp516 and LSD1 antibodies (Figure 21E right). We observed enrichment for the -70 bp region of the UCP1 promoter when we first used Zfp516 antibody followed by LSD1 antibody, whereas no enrichment was observed in the GAPDH promoter. Finally, we tested the requirement of Zfp516 for the LSD1 recruitment to the -70 bp UCP1 promoter region (Figure 21F). We compared LSD1 recruitment to the UCP1 promoter region by ChIP using cells in which Zfp516 is either overexpressed or knocked down using shRNA. We observed a significant decrease in LSD1 binding in Zfp516 knockdown cells (Figure 21F), indicating that Zfp516 is required for LSD1 recruitment to the UCP1 promoter in brown adipocytes.

Transcriptional activation by LSD1 has been shown to be dependent on the demethylation of mono- and di-methylated K9 residue of histone H3 (Metzger et al., 2005). Hence, by ChIP, we assessed methylation status of different lysine residues at the UCP1 promoter region (Figure 21G). We compared samples from BAT of control mice and from mice deleted of LSD1 in BAT-specific manner (described below). We detected higher mono- and di-methylation of H3K9 at the -70 bp region of the UCP1 promoter, but not at the GAPDH promoter region in BAT from LSD1 KO mice (Figure 21G left). In contrast, H3K9-3me and H3K4-2me at the UCP1 promoter region were not significantly affected. These results support the notion that LSD1 participates in the transcriptional activation by modifying histone methylation at the promoter regions of BAT specific genes.

Altogether, we conclude that LSD1 is recruited by, and cooperates with, Zfp516 for the activation of UCP1 promoter. Notably, this activation by LSD1 involves demethylation of H3K9 mono- and di-methylated residues.

LSD1 is induced and is required for brown adipocyte differentiation

We previously reported that Zfp516 not only activates UCP1 and other BAT-enriched genes but also is required for brown adipocyte differentiation. Thus, Zfp516 ablation caused a decrease in BAT mass with a greatly lower expression of UCP1 and other BAT-enriched genes. If Zfp516 recruits LSD1 for its function in BAT gene expression, LSD1 should affect brown adipocyte differentiation also. We first compared LSD1 mRNA levels between the Stromal Vascular Fraction (SVF) containing preadipocytes and adipocyte fraction from BAT of 10 wk-old WT mice (Figure 22A). As

predicted, Pref-1 was found to be higher by 75% in the SVF fraction, whereas UCP1, Perilipin, and Zfp516 were enriched 5-, 5- and 3-fold higher in adipocyte fraction, respectively. We found LSD1 to be enriched by 4-fold in adipocyte fraction compared to the SVF, suggesting an induction of LSD1 expression during brown adipogenesis. We therefore examined LSD1 mRNA and protein levels during brown adipocyte differentiation of BAT cells *in vitro* (Figure 22C). As expected, during brown adipocyte differentiation, we observed an increased expression of BAT-enriched genes, such as PGC1α, PRDM16, and Cox8b (Figure 22C top), as well as common adipocyte differentiation markers, such as PPARγ FABP4 and AdipoQ (Figure 22C top). More importantly, LSD1 mRNA level was significantly increased by 5-fold and LSD protein level was increased as well during brown adipocyte differentiation (Figure 22C bottom). We conclude that LSD1 is enriched in mature brown adipocytes, increasing during brown adipocyte differentiation. We also compared expression of LSD1 and Zfp516 in BAT from wild type mice after a 6 h cold-exposure at 4°C (Figure 22B). As expected, Zfp516, as well as UCP1 and PGC1α mRNA levels in BAT were higher by 2.5- to 10-fold upon cold exposure, whereas PRDM16 did not change. Similar to Zfp516, LSD1 mRNA level in BAT was higher by 3-fold upon cold exposure (Figure 22B). Overall, LSD1 expression pattern is similar to Zfp516 in terms of enrichment in mature brown adipocytes and induction by cold, further supports a cooperative role of LSD1 and Zfp516 in BAT development and function.

Next, we examined the effect of LSD1 inhibition in brown adipocyte differentiation *in vitro*. We treated the cells with two different inhibitors of LSD1 activity, 2PCPA, LSD1i, during brown adipocyte differentiation of BAT cells (Figure 23A). Compared to vehicle-treated control cells, cells treated with LSD1 inhibitors showed lower lipid accumulation (Figure 23A left), as well as expression of BAT-enriched genes, such as PGC1α, Dio2, PRDM16, Cox8b and CideA, by 50 to 80% (Figure 23A right). This indicates that LSD1 activity is required for brown adipocyte differentiation.

To further establish the requirement of LSD1 for brown adipocyte differentiation and to rule out any off-target effects of LSD1 inhibitors, we performed adenoviral shRNA-mediated knockdown of LSD1 (Figure 23B). LSD1 mRNA level was reduced by 70% in LSD1-shRNA infected cells (Figure 23B left). Upon treatment with differentiation cocktail, lipid accumulation was significantly lower in shLSD1 cells compared to the sh-scrambled control cells (Figure 23B center). Expression level of BAT-enriched genes, such as PRDM16, PGC1α and CideA, was lower by 60 to 70% (Figure 23B right top), whereas common adipocyte differentiation markers, PPARγ and FABP4, were not significantly affected (Figure 23B right bottom). Taken together, these results

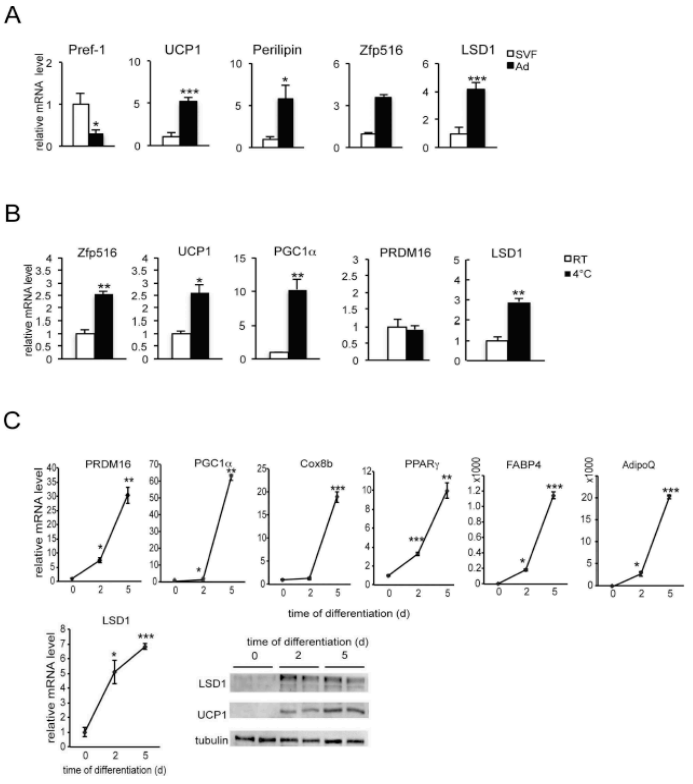

Figure 22. LSD1 is increased during brown adipocyte differentiation and is induced by cold exposure in BAT. (A) RT-qPCR for indicated gene in the adipocyte fraction and SVF from BAT. (B) RT-qPCR for indicated gene in BAT of wild-type mice exposed to cold (4°C) for 6h. (C) Top, RT-qPCR for indicated gene in BAT cells at Day 0, 2 and 5 after the start of differentiation. Bottom, LSD1 mRNA level (top) and immunoblot (bottom) for indicated proteins in BAT cells at Day 0, 2 and 5 of differentiation. Data are represented as mean ± SEM.
*p<0.05; **p<0.01; ***p<0.001

demonstrate that LSD1 expression and its enzymatic activity are required for brown adipocyte differentiation.

It has been previously reported that global LSD1 knockout (KO) is lethal by embryonic day 7.5, which prevents further examination of BAT development or function (Wang et al., 2007). Therefore, to evaluate the role of LSD1 in BAT in vivo, we performed a tissue-specific conditional knockout of LSD1 using the Cre-lox strategy. We first attempted to generate conditional LSD1 KO mice by crossing LSD1 floxed mice with those bearing the Cre recombinase driven by the Myf5 promoter (Tallquist et al., 2000), an established marker of brown adipose precursors (Seale et al., 2008). However, we found that LSD1-Myf5KO resulted in perinatal lethality preventing the study of BAT function in adults. Regardless, we could clearly detect a drastic decrease in the size of BAT depot in Myf5KO newborns compared to control littermates (fl/fl) (Figure 23C left), although the global size of the newborns remained the same (data not shown). LSD1 mRNA level was decreased by 63% in BAT of Myf5KO mice (Figure 23C left). We also detected a significant decrease in mRNA levels of BAT-enriched genes, such as UCP1, PGC1α, C/EBPβ, and Cox8b, by 25 to 60% in BAT of Myf5KO newborns, whereas common adipose markers, such as PPARγ and AdipoQ, were not significantly affected (Figure

23C right). Thus, we conclude that LSD1 ablation in brown adipose precursors impairs embryonic development of BAT in vivo.

LSD1 promotes a BAT gene program and thermogenesis *in vivo*

To further evaluate the role of LSD1 in BAT development and its function *in vivo*, we performed conditional knockout of LSD1 using different Cre mice to overcome perinatal lethality of our Myf5KO model (Figure 23C). Since UCP1 has been shown to express early during BAT development, we next employed UCP1-Cre. Crossing LSD1 floxed mice with mice carrying the UCP1 promoter-Cre (Kong et al., 2014) produced BAT-specific KO mice (BSKO) at room temperature, allowing us to examine the role of LSD1 in BAT. In addition to genotyping, we further validated our mouse model by measuring LSD1 mRNA levels in BAT of LSD1-BSKO and LSD1fl/fl control (fl/fl) mice. LSD1 mRNA level was decreased by 65% in BAT, but not in WAT depots, iWAT and pWAT (Figure 24B top-left). Similarly, LSD1 protein level was reduced only in BAT, but not in liver, iWAT or pWAT (Figure 24B top-right) showing the BAT specificity of the model. LSD1-BSKO mice exhibited

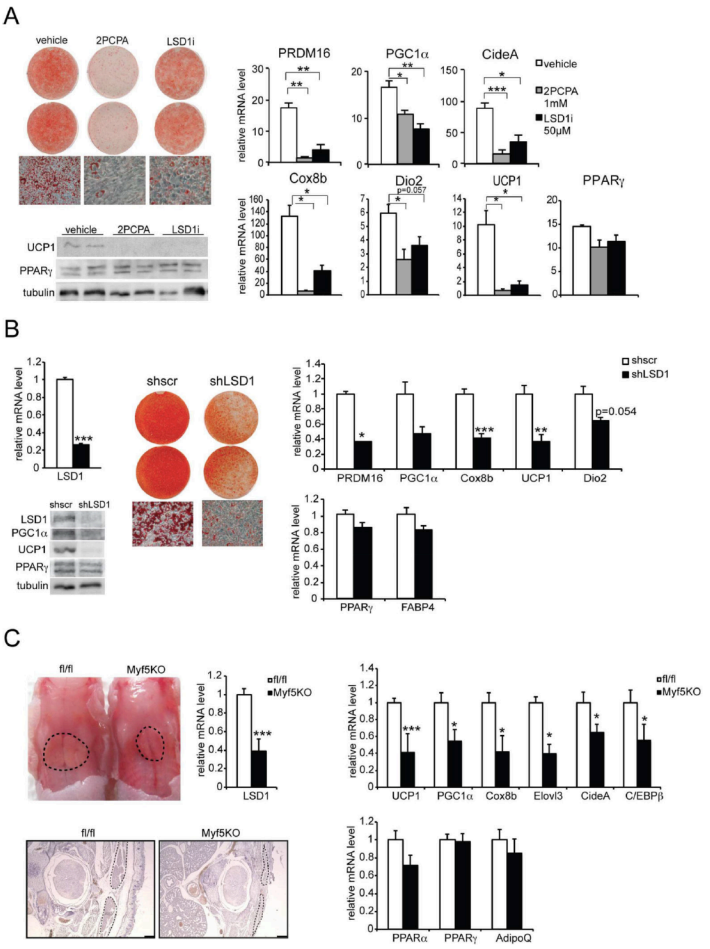

Figure 23. LSD1 is required for the BAT program and BAT development.
(A) Left-top, ORO staining and brightfield view of BAT cells treated with vehicle (left panel) or LSD1 inhibitors: 2PCPA (center panel) and LSD1i (right panel), at Day 6 of differentiation. Left-bottom, immunoblotting of BAT cells at Day 6. Right, RT-qPCR in BAT cells treated with vehicle (left panel) or LSD1 inhibitors at Day 6. (B) Left, RT-qPCR for LSD1 mRNA in BAT cells infected with scrambled (shscr) or shLSD1 adenovirus at Day 6 (top). Immunoblot in BAT cells at Day 6 (bottom). Center, ORO staining and brightfield image of BAT cells infected with control or shLSD1 adenovirus at Day 6. Right, RT-qPCR in these cells. (C) Top-left, representative image of control (fl/fl) and $LSD1^{fl/fl}$-Myf5Cre (Myf5KO) newborn embryos (P0) from back view. Black dots delineate area of BAT. RT-qPCR in BAT of control and Myf5KO embryos (n=8–9 embryos per group). Bottom-left, H&E staining of representative transversal sections of the interscapular region of control and Myf5 KO embryos (P0). Black dots delineate area of BAT. Right, RT-qPCR for BAT-enriched (top) and common adipose genes (bottom) in BAT of control or Myf5KO embryos (n=8–9 embryos per group). Data are represented as mean ± SEM.*p<0.05; **p<0.01; ***p<0.001.

by approximately 4g than control littermates (Figure 24A top) at 14 wk, while food intake was not affected (data not shown). Their BAT depot was bigger but pale (right), in comparison to control mice (left) (Figure 24A top). Body composition analysis indicated that, whereas fat mass was increased, lean mass remained the same in BSKO mice (Figure 24A center and bottom). Histological analysis of the BAT depot from BSKO mice had noticeable morphological differences. Hematoxylin and eosin (H&E) staining showed BAT of BSKO mice exhibited bigger lipid droplets in comparison to control littermates (Figure 24C center). Interestingly, while BAT from control mice presented brown adipocytes with small lipid droplets which is typical of BAT, BAT from BSKO mice exhibited adipocytes containing bigger lipid droplets. Morphology of WAT, as demonstrated with H&E staining of pWAT sections, was unchanged (Figure 24C top). Furthermore, expression levels of BAT-enriched genes, such as PGC1α, UCP1, CideA, and Cox8b, were lower by 55 to 30% (Figure 24B center), whereas common adipocyte markers, PPARγ, FABP4, AdipoQ, and Perilipin, were not affected (Figure 24B bottom). Immunoblots showed a strong reduction of UCP1 at the protein level only in BAT and not in WAT, whereas PPARγ remained unchanged (Figure 24B top-right). Similarly, immunostaining for UCP1 showed a correspondingly lower staining in BSKO compared to control mice (Figure 24C bottom). Collectively, BAT of LSD1-BSKO mice lost the major BAT phenotypic characteristics of brown coloration, presence of multiple lipid droplets within smaller adipocytes, and BAT gene expression pattern. Moreover, not only did we observe a loss of BAT characteristics, but we also observed a switch towards a more white adipose specific morphology of bigger lipid droplet size with increased lipid content. Overall, these results demonstrate that LSD1 ablation causes a whitening of BAT, establishing in vivo requirement of LSD1 for a normal BAT program.

Considering that LSD1-BSKO mice had no change in food intake but exhibited a higher body weight, we next investigated whether energy expenditure could be altered. We first evaluated thermogenic capacity by measuring body temperature. We found that LSD1-BSKO mice had a lower body temperature than control mice at room temperature and this difference in body temperature was further enhanced after a 6h cold exposure (Figure 24D). These results suggest an impaired thermogenic function of BSKO mice. Indeed, indirect calorimetry showed that oxygen consumption (VO2) was significantly reduced in BSKO mice compared to wild type mice at room temperature, while respiratory ratio and locomotor activity were unchanged (Figure 24E left). Similar reduction in oxygen consumption was observed at thermoneutrality (30°C), as well as at 4°C (data not shown). Taken together we conclude that energy expenditure estimated by oxygen consumption was decreased in LSD1-BSKO mice compared to control mice. To examine the contribution of BAT to the altered energy expenditure in BSKO mice, we next measured oxygen consumption rate (OCR) of BAT dissected out from these LSD1-BSKO mice (Figure 24E right). Indeed, we found significantly lower OCR in BAT from BSKO mice by 35% in comparison to that from control mice. In line with these results, BSKO mice gained more body weight on high fat diet (HFD) than their control littermates, demonstrating a propensity for obesity upon BAT-specific LSD1 deletion (Figure 24F left).

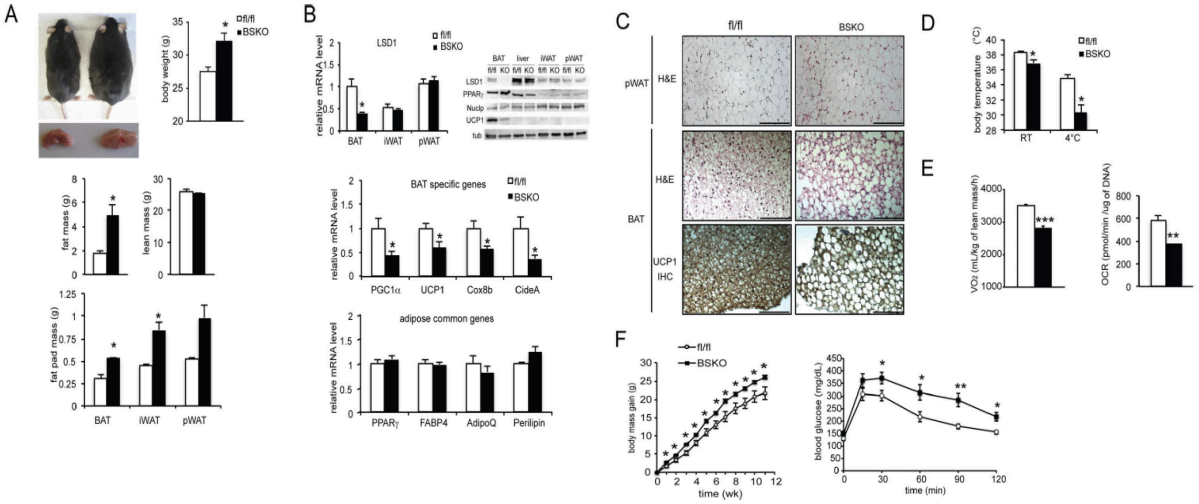

Figure 24. LSD1 promotes a BAT gene program *in vivo.*
(A) Top-left, representative photograph of control and LSD1 BSKO 17 wk-old mice and their BAT depot. Top-right, body weight of 14 wk-old control and LSD1 BSKO mice. Center, fat and lean mass of 14 wk-old control and LSD1 BSKO mice determined using EchoMRI. Bottom, mass of adipose depots from mice described above. (B) Top, RT-qPCR for LSD1 mRNA in adipose tissue depots of control and LSD1 BSKO mice (left) and immunoblot for indicated proteins BAT, liver, iWAT and pWAT of control and LSD1 BSKO mice (right). Center, RT-qPCR for BAT-enriched genes in BAT of control and LSD1 BSKO mice. Bottom, RT-qPCR for common adipose genes in BAT of control and LSD1 BSKO mice. (C) H&E staining of pWAT sections from control and LSD1 BSKO mice (top). H&E staining (center) and immunostaining for UCP1 (bottom) of BAT sections from control and LSD1 BSKO mice. (D) Top, body temperature consumption measured by indirect calorimetry in control and LSD1 BSKO mice on chow diet (NCD) at room temperature (23°C) (n=7 mice per group). (E) Oxygen Consumption Rate (OCR) of BAT from control and LSD1 BSKO mice. (F) Left, body mass gain of control and BSKO mice under high fat diet (HFD) starting at 6 wks of age (n=6–8 mice per group). Right, Glucose tolerance test (GTT) on 16wk-old control and BSKO mice under HFD for 10 wk (n=6–8 mice per group). Scale bars represent 200μm. Data are represented as mean ± SEM. *p<0.05; **p<0.01; ***p<0.001. from control and LSD1 BSKO mice at 23°C and after a 6h cold exposure at 4°C. E. Left, VO2

In addition, blood glucose level of BSKO mice on HFD measured in the course of a glucose tolerance test (GTT) was significantly higher than in control littermates (Figure 24F right), indicative of an impaired glucose tolerance. Collectively, these data establish a defective BAT function in BSKO mice and that LSD1 ablation reduced thermogenic capacity in vivo. Furthermore, in evaluating the role of LSD1 in BAT, we also generated LSD1 conditional KO mice by mating the LSD1 floxed mice with AdipoQ-Cre mice (Eguchi et al., 2011) for LSD1 knockout in all adipose tissue depots BAT, iWAT and pWAT (data not shown). We found the phenotype of these KO mice to be quite similar to that in BSKO mice (data not shown), thus further confirming the critical role of LSD1 for BAT function.

In vivo requirement of LSD1-Zfp516 interaction

To demonstrate the significance of LSD1-Zfp516 interaction, we tested LSD1 requirement in the context of Zfp516-induced browning of iWAT. In this regard, we previously have shown that overexpression of Zfp516 in adipose tissue causes browning of iWAT. In testing the requirement of LSD1 on Zfp516-induced browning, we performed a LSD1 knockdown in 3T3-L1 cells overexpressing Zfp516 (AdZfp516) or a

control empty GFP vector (AdGFP) (Figure 25A). We verified Zfp516 overexpression and LSD1 knockdown at both mRNA (35–40 fold and 70%, respectively) and protein levels (Figure 25A top).

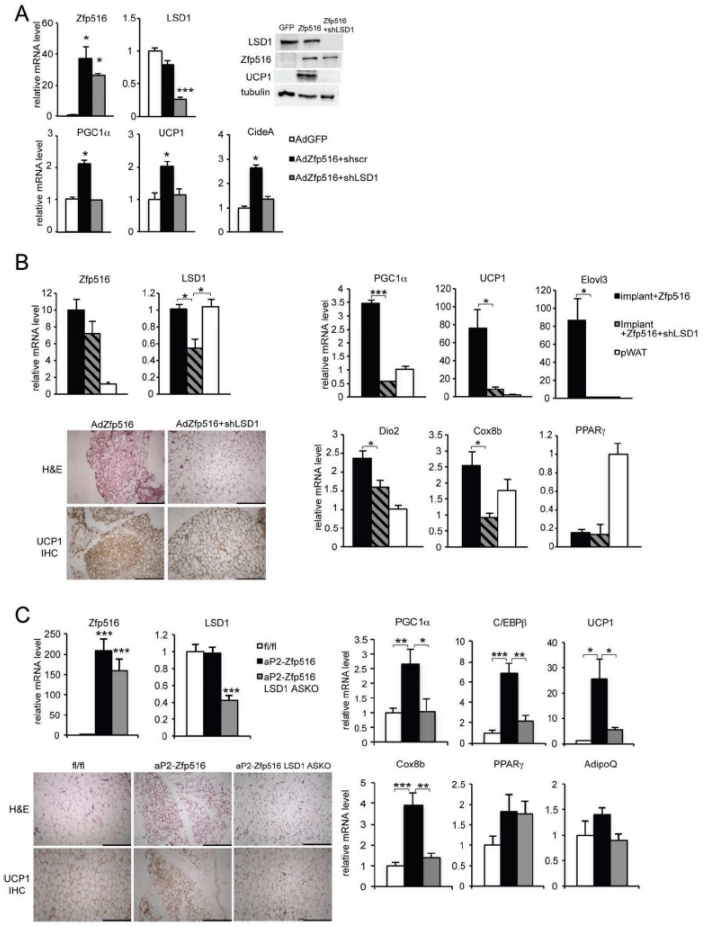

Figure 25. Zfp516-LSD1 interaction is required for browning of iWAT. (A) Top, RT-qPCR for LSD1 and Zfp516 mRNA in 3T3-L1 cells coinfected with either control AdGFP or AdZfp516 and control shscr or shLSD1 adenovirus at Day 7 of differentiation (left). Immunoblot for indicated proteins in lysates from infected 3T3-L1 cells at Day 7 (right). Bottom, RT-qPCR for BAT-enriched genes in infected 3T3-L1 cells at Day 7. (B) Left, RT-qPCR for LSD1 and Zfp516 mRNA in implants and pWAT from mice implanted with 3T3-L1 cells infected with either AdZfp516 + shscr (control) or AdZfp516 + shLSD1 (top). H&E staining (upper panels) and immunostaining for UCP1 (lower panels) of sections of implants described above (bottom). Right, RT-qPCR for BAT-enriched genes and adipose common genes in implants and pWAT described above. (n=6 mice per group). (C) Left, RT-qPCR for LSD1 and Zfp516 mRNA in iWAT from 8 wk-old control (fl/fl), aP2-Zfp516 and aP2-Zfp516 ASKO mice (n=6–8 mice per group). H&E staining (upper panels) and immunostaining for UCP1 (lower panels) in sections of iWAT from mice described above. Scale bars represent 200μm. Right, RT-qPCR for BAT-enriched or common adipose genes in iWAT from mice described above. Data are represented as mean ± SEM.*p<0.05; **p<0.01; ***p<0.001.

We observed that induction of BAT-enriched genes by Zfp516 overexpression was impaired in LSD1 shRNA knockdown cells (shLSD1) compared to control shRNA (shscr) cells, as indicated by approximately 50% decrease in mRNA levels for PGC1α, UCP1 and CideA (Figure 25A bottom), as well as strong reduction of UCP1 at protein level (Figure 25A top-right).

Next, to evaluate the requirement of LSD1 within in vivo setting, we performed implantation experiments using Zfp516 overexpressing 3T3-L1 cells coinfected with shLSD1 or control shscr (Figure 25B). After 7 days, implants along with pWAT as a control were collected and analyzed. Zfp516 overexpression and LSD1 knockdown were validated at the mRNA levels, as indicated by 8–10-fold increase in Zfp516 mRNA level and 55% decrease in LSD1 in knockdown implants (Figure 25B left-top). The expression of BAT-enriched genes such as PGC1α, UCP1, Elovl3 and Dio2 was greatly

reduced in shLSD1 knockdown implants compared to control, at a level close to that in pWAT depot (Figure 25B right-top). However, we did not observe any difference in PPARγ expression between these implants (Figure 25B right-bottom). Moreover, histological analysis of implant sections showed a global increase in adipocyte size, as well as decreased UCP1 staining in shLSD1 implants (Figure 25B left-bottom). These results suggest that Zfp516 and LSD1 cooperate together to activate BAT-enriched genes in white adipocytes, thereby changing their characteristics toward a brown morphology. Furthermore, upon exposure of LSD1-ASKO mice at 4°C for 6h, we observed expression of BAT-enriched genes, such as PGC1α, UCP1, and Cox8b, was lower not only in BAT (data not shown) but also iWAT of ASKO mice in comparison to control littermates (data not shown). These results demonstrate a role for LSD1 in cold-induced browning of iWAT, in addition to promotion of thermogenic program in BAT as shown above.

To address the relevance of Zfp516-LSD1 interaction for iWAT browning in a more physiologically relevant system, we generated an additional mouse model by crossing aP2-Zfp516 transgenic mice overexpressing Zfp516 in all adipose depots with LSD1-ASKO mice with LSD1 ablation in all adipose depots (Figure 25C). We verified Zfp516 overexpression and LSD1 ablation in iWAT of aP2-Zfp516, aP2-Zfp516 ASKO and their control littermates (fl/fl). We detected a 160- to 200–fold increase in Zfp516 expression and 60% lower LSD1 expression, respectively, in these mice (Figure 25C left-top). Zfp516 overexpression and LSD1 KO in iWAT were confirmed at the protein level (data not shown). We found that induction of BAT-enriched genes, including UCP1, Cox8b and PGC1α, by Zfp516 in iWAT was blunted upon LSD1 ablation, whereas adipose common markers for WAT and BAT, such as PPARγ and AdipoQ, remained unchanged (Figure 25C right). Histological analysis of iWAT sections showed that LSD1 ablation prevented morphological changes (smaller lipid droplets) and UCP1 staining arising from Zfp516 overexpression in aP2-Zfp516-LSD1-ASKO mice (Figure 25C left-bottom). In comparison, there was no drastic change in either morphology or UCP1 staining in pWAT (data not shown). Moreover, as expected, LSD1 ablation also reduced the expression of BAT-enriched genes in BAT of aP2-Zfp516 mice (data not shown). Collectively, these results demonstrate the role of LSD1 in the induction of the BAT program and browning of iWAT in vivo and, more importantly, the biological significance of LSD1-Zfp516 interaction in these processes.

Discussion

In the present study, we demonstrate that Zfp516, previously established as a transcriptional activator of UCP1 and other BAT-enriched genes, directly interacts with LSD1. Zfp516 recruits LSD1 on the promoter regions of BAT genes and they work together for transcriptional activation of BAT genes. In this context, LSD1 works as a coactivator for the regulation of BAT genes through its demethylase activity on H3K9. We establish both in vitro and in vivo that LSD1 is crucial for the BAT program for proper development and function of BAT. Altogether our data establish that LSD1 is a cold-induced histone modifier interacting with Zfp516, a BAT-enriched transcription factor, for its recruitment and thereby regulates transcription of BAT genes. We

demonstrate here the requirement of LSD1 for Zfp516 function in inducing a BAT program to promote thermogenic function of BAT and also browning of iWAT.

Whereas LSD1 has been initially described as a component of a repressor complex by removing active epigenetic marks by demethylating H3K4 (H3K4-1me and -2me), it has also been reported that LSD1 can act as a coactivator by demethylating H3K9 (H3K9-1me and - 2me). We show here that, in the context of BAT gene regulation, LSD1 works as a coactivator recruited by Zfp516 and we detected increased H3K9-1me and H3K9-2me, but not of H3K4-1me and H3K4-2me, at the promoter region of UCP1 in BAT of LSD1 KO mice. We observed no increase, but rather, a decrease in H3K4-1me in LSD1 BSKO BAT, which may have resulted from altered expression or activity of other methylase(s) due to impaired brown adipogenesis. In this regard, G9a methyltranferase has been reported to induce PPARγ expression during both white and brown adipogenesis by methylating H3K9-1me (Wang et al., 2013). EHMT1, a methyltransferase that has recently been shown to regulate brown adipose cell fate, may also affect histone modification (Ohno et al., 2013). Considering that many methylases and demethylases act together to regulate histone methylation for transcriptional activation, the decrease observed in H3K4-1me is likely an indirect effect of LSD1 KO on other histone methylases at the same region of UCP1 promoter. Notably, it has been reported that LSD1 affects histone methylation status in association with SETDB1 histone methylase on C/EBPα promoter during white adipogenesis (Musri et al., 2010). Regardless, histone demethylases and methyltransferases may target the same residues to maintain a tightly regulated balance between activating and repressive epigenetic marks on BAT gene promoters.

Our results suggest that LSD1 activates UCP1 and other BAT genes, such as PGC1α, probably by demethylating H3K9-1me and H3K9-2me, which are known to be epigenetic repressive marks. It remains unclear how LSD1 mediates transcription repression or activation, either by demethylating H3K4 or H3K9, respectively. Recently, it has been reported that an isoform of LSD1, LSD1+8a arising from alternative splicing, does not retain any enzymatic activity toward H3K4-2me and hence regulates neuronal differentiation solely through demethylation of H3K9-2me (Laurent et al., 2015). Another study documented LSD1+8a to demethylate H4K20, which was associated with memory and learning process (Wang et al., 2015). Regardless, we could not detect LSD1+8a isoform either in BAT or in differentiated BAT cells (data not shown). Such a versatile substrate specificity of LSD1 remains to be elucidated. We propose that Zfp516 controls LSD1 specificity by recruiting it to chromatin to demethylate H3K9 at the promoter regions for BAT development and function.

We show here that Zfp516 directly interacts with LSD1thereby recruiting it to the promoter regions of UCP1 or other BAT-enriched genes. Thus, LSD1 activates thermogenic genes, such as UCP1 and PGC1α, for BAT program. Interestingly, Duteil et al, globally overexpressed LSD1 in mice and reported that LSD1 promotes oxidative capacities in WAT by interaction with nuclear respiratory factor 1 (Nrf1) for mitochondrial biogenesis (Duteil et al., 2014). In the same study, LSD1 was reported also to induce Nrf1 expression for the observed effect. Due to the global overexpression of LSD1 in these mice, however, specific role of LSD1 in WAT was not clear. In this regard, we previously have shown that Zfp516 overexpression in adipose tissue causes browning of iWAT. We cannot rule out that LSD1 may function by interacting with multiple

partners. However, since LSD1 directly interacts with Zfp516 and both of these genes are cold-inducible, iWAT browning may be mediated by LSD1-Zfp516 interaction. Indeed, we found that knockdown of LSD1 in 3T3-L1 cells prevented Zfp516-induced BAT gene activation, indicating involvement of Zfp516-LSD1 interaction in this process (Figure 6A). LSD1 ablation prevents Zfp516-induced browning of implanted 3T3-L1 cells (Figure 6B) but also of iWAT in aP2-Zfp516 LSD1 ASKO mice (Figure 6C). Hence, we show here that LSD1 is required for browning of iWAT through its interaction with Zfp516. Not only LSD1 but Zfp516 also have multiple interacting partners. We previously reported that Zfp516 directly interacts with PRDM16 for transcriptional activation of UCP1 and other BAT-enriched genes, such as PGC1α. Here, we confirmed that LSD1 interacts with PRDM16 (Figure S1 B). More importantly, we demonstrate that Zfp516 function requires interaction with LSD1. Therefore, we propose that multiple coregulators, such as LSD1 and PRDM16, interact with Zfp516 in inducing BAT genes for BAT program and thermogenesis.

In order to examine the role of LSD1 during BAT development in vivo, we first attempted at generating LSD1 conditional KO in brown adipose precursors using Myf5-Cre mice. However, LSD1 Myf5KO mice were found to die perinatally. Such an early lethality might have resulted from the fact that, besides brown adipose precursors, Myf5+ cells are early mesenchymal progenitors giving rise to myocytes, cartilage, and dermis. Interestingly, LSD1 has been shown to regulate myogenesis through regulation of MyoD and Mef2 expression (Choi et al., 2010) as well as thyroid hormone signaling (Ambrosio et al., 2013). We propose that survival of LSD1 Myf5KO pups was probably compromised not only by impaired thermoregulation but also by defects in development of other tissues. Unlike previously characterized ASKO mice using aP2 promoter which were shown to be devoid of WAT (Duteil et al., 2014), our ASKO mice with Adiponectin-Cre promoter exhibited an increase in WAT mass. Considering that AdipoQ is expressed later than aP2/FABP4 during development, LSD1 may be crucial only for early steps of WAT development, which is in accordance with previously reported in vitro studies (Duteil et al., 2014). We predict that impaired BAT development and function in these mice may have caused increase in lipid content and depot size of WAT as a compensatory mechanism. Regardless, we cannot rule out other roles of LSD1 in WAT, such as that reported by Duteil et al. As is the case of coregulators in general, LSD1 may function with other transcription factors, such as Nrf1, in WAT to alter FA oxidation and thus lipid content. The use of UCP1-Cre allows ablation of LSD1 in BAT (UCP1+ cells specifically), when mice are maintained at room temperature. Upon cold exposure, LSD1 could be ablated in subcutaneous WAT depots of BSKO mice also, with the appearance of UCP1 expressing beige cells. BAT-conditional KO (BSKO mice) shows a stronger phenotype in BAT and WAT than Myf5-PRDM16KO. Indeed, Harms et al., reported that Myf5-PRDM16 KO mice exhibit a late-onset decrease of thermogenic markers in BAT suggesting that PRDM16 is dispensable for early BAT development but required for BAT identity maintenance. However, they suggested compensatory activity of PRDM3 in PRDM16 KO mice and reported a stronger phenotype in PRDM16/PRDM3 double KO mice. Similarly, UCP1 KO mice (Enerbäck et al.,1997) phenotype is milder than LSD1 BSKO. However, only UCP1 is deleted and, as the authors indicated, UCP2 was induced for compensation. These points may explain the differences in phenotype severity. However, we also suggest that, because of

Zfp516-LSD1 interaction, the phenotype we observed in LSD1 BSKO is also due to the impaired Zfp516 function for activation of UCP1 and BAT-enriched genes and BAT development

In conclusion, our results support the idea that BAT development and function require the concerted action of transcriptional regulators as well as chromatin modifiers. We establish that, not only is LSD1 required for BAT development but is also a major activator of BAT-enriched genes through its interaction with Zfp516, thereby regulating thermogenesis. As both Zfp516 and LSD1 are cold inducible, it reinforces the idea that their interplay is essential for cold adaptation. Thus, Zfp516 directly interacts with LSD1, recruits it to BAT gene promoters where it demethylates H3K9 residues. Together, they promote a BAT gene program and regulate both development and thermogenic function of BAT as well as browning of iWAT.

Experimental procedures

Plasmid constructs and antibodies

The following antibodies were used: Anti-Flag M2 and Anti-c-Myc-Peroxidase antibody (Sigma), Anti-UCP1 and Anti-KDM1/LSD1 (Sigma); Anti-KDM1/LSD1 (abcam, ab17721), Anti-Histone H3K9-2me (ab1220), Anti-Histone H3K9-1me (ab9045), Anti-Histone H3K9-3me (ab8898), Anti-Histone H3K4-2me (ab32356) from Abcam; Anti-Zfp516, Anti-LSD1 and IgG mouse and rabbit (Santa Cruz). The cMyc-LSD1 expression vector was from obtained from Sinobiological (ref). The FLAG-Zfp516 expression vector, the -5.5kb UCP1-Luc, -70bp UCP1-Luc, -45bp UCP1-Luc and -2.4bp PGC1α-Luc were previously described.

Cell culture and viral transduction

Brown adipocyte cell line (BAT) was obtained from Prof.S Kajimura, 3T3-L1 were obtained from ATCC. Brown adipocyte differentiation was induced by treating confluent cells in DMEM containing 10% FBS, 850nM insulin, 0.5mM isobutyl-methylxanthine, 1µM dexamethasone, 1nM T3, 125 nM indomethacin and 1µM rosiglitazone. After 48h of induction, cells were switched to a maintenance medium containing 10% FBS, 850nM insulin, 1nM T3 and 1µM rosiglitazone. To stimulate thermogenesis, cells were treated 6h with 10µM forskolin. GFP, Zfp516 and LSD1 recombined adenoviruses were purchased from Viraquest. For adenoviral infection of BAT cells, subconfluent cells were incubated overnight with scramble shRNA or shLSD1 (MOI 500) adenoviruses. For adenoviral infection of 3T3-L1 cells, confluent cells were incubated 24h with GFP, Zfp516 and/or LSD1 (MOI 250) adenoviruses pre-incubated with DMEM containing polyLysine. Then, viral medium is replaced by induction medium for brown adipogenic conditions. Adenoviruses scrambled (shscr) Ad-U6-RNAi-GFP; Ad-U6-mKDM1-shRNA: Ad-GFP-mKDM1 were obtained from Vector Biolabs. The following inhibitors were used throughout differentiation: LSD1i 489476 (EMD Millipore), 2PCPA (*trans*-2-Phenylcyclopropylamine hydrochloride, Sigma). For Oil Red O staining, cells were washed once with phosphate-buffered saline and subsequently fixed for 1h in 10% formalin. Cells were then stained with freshly prepared 0.5% Oil Red O solution for 1 h for lipid visualization.

RT-qPCR and Western blotting

Total RNA was extracted using TRIzol reagent (Invitrogen). Reverse transcription was performed with 1 µg of total RNA using SuperScript II (Invitrogen). RT-qPCR was performed using SYBR green fluorescent dye with an ABI PRISM 7500 sequence detection system (Applied Biosystems) to quantify the relative mRNA levels for various genes. Statistical analysis of the qPCR was obtained using the $2^{-\Delta\Delta Ct}$ method with U36B4 as the internal control. Experiments were performed in triplicates (biological replicates) for each sample. For western blot analysis, total cell lysates were prepared using Ripa buffer and nuclear/cytosolic extracts were isolated using the NE-PER Nuclear and Cytoplasmic Extraction kit (Thermo). Proteins were separated by SDS-PAGE, transferred to nitrocellulose membrane (Bio-Rad) and probed with the indicated antibodies.

Reporter assays

HEK 293FT cells were transfected with 150ng of Zfp516 or empty vector and/or 150 ng of LSD1, dLSD1 1-474, or empty vector together with 50 ng of indicated luciferase reporter construct and 0.5 ng of renilla construct pRL-CMV in 48-well plates using Lipofectamin (Invitrogen). Cells were lysed 48 h post-transfection and assayed for luciferase activity using Dual-Luciferase Reporter assay system (Promega). Firefly luciferase reporter gene measurements were normalized to Renilla luciferase activity

Co-Immunoprecipitation

For Co-IP experiments using tagged constructs, HEK 293FT cells were transfected using Lipofectamine2000 to express FLAG-tagged Zfp516 and/or Myc-tagged LSD1 or LSD1 1-474 construct. Cells were lysed in IP buffer containing 20 mM Tris, pH 7.4, 150 mM NaCl, 1mM EDTA, 10% glycerol, 1% NP-40 supplemented with proteases inhibitors. Total cell lysates were incubated 2 h at 4°C with anti-FLAG M2 or anti-c-Myc-agarose affinity gels, antiZfp516 or anti-LSD1. Agarose beads were washed 3 times and bound proteins were eluted by boiling in Laemmli sample buffer and analysed by immunoblotting using the indicated antibodies. For Co-IP in BAT cells, nuclear extraction was carried out using the NE-PER Nuclear and Cytoplasmic Extraction kit (Thermo). Equal amounts of nuclear extracts were incubated with the specific antibodies and protein A/G agarose beads overnight at 4°C, washed and proteins separated by SDS-PAGE, transferred onto nitrocellulose membranes for immunoblotting.

***In vitro* Binding Assays**

GST-fused to various LSD1 fragments (described in reference[29]) were expressed in BL21 by IPTG induction for 3 h at 37°C, purified on glutathione sepharose beads and eluted with elution buffer containing reduced glutathione. [^{35}S]-labeled Zfp516 protein was produced by using TNT coupled transcription/translation kit (Promega). Twenty µg of GST fusion proteins were incubated overnight at 4°C with *in vitro* translated proteins and glutathione sepharose beads in a binding buffer containing 20mM Hepes, pH 7.7, 300mM KCl, 2.5mM $MgCl_2$, 0.05% NP40, 1mM DTT, and 10% glycerol. The sepharose beads were then washed 3 times with binding buffer. Bound proteins were eluted by

boiling in Laemmli sample buffer, separated by SDS-PAGE and analysed by autoradiography.

ChIP and reChip

For ChIP analysis using 293FT cells, cells were transfected with 10 µg of either pcDNA3.1-FLAG-Zfp516 or Zfp516 truncations or pcDNA3.1 and 5 ug of either -5.5kb UCP1-Luciferase or -2kb PGC1α-Luciferase using calcium phosphate method. At 48 h post-transfection, cells were crosslinked for 10 min by adding 1% formaldehyde in DMEM at room temperature. Cross-linking was stopped by the addition of glycine to a final concentration of 0.125 M. After sonication, DNA sizes were 0.3–0.9kb. For HIB-1B cells, cells were cultured to confluence before crosslinking and sonication as above. For ChIP experiments in BAT, tissues were minced on ice and crosslinked using 1% formaldehyde in phosphate-buffered saline for 10 min. Crosslinking was stopped using glycine as before. Samples were dounced, washed twice, centrifuged and resuspended in RSB buffer, containing 10mM Tris pH 7.4, 10mM NaCl, 3mM $MgCl_2$, prior to sonication. Nuclei were released by douncing on ice and collected by centrifugation. Nuclei were then lysed in nuclei lysis buffer containing 50mM Tris, pH 8.0, 1% SDS 10mM EDTA supplemented with protease inhibitors, followed by sonication. Chromatin samples were diluted 1:10 with the dilution buffer, containing 16.7mM Tris, pH 8.1, 0.01% SDS 1.1 % Triton X-100 1.2mM EDTA and 1.67mM NaCl and proteinase inhibitors. Soluble chromatin was quantified by absorbance at 260 nm, and equivalent amounts of input DNA were immunoprecipitated using 2.5 µg of indicated antibodies or normal mouse IgG and protein A/G magnetic beads (ref). After the beads were washed and cross-linking was reversed, DNA fragments were extracted with purification kit. DNA was precipitated and resuspended in water. Samples were analyzed by endpoint and qPCR. ReChIP was performed as in Truax et al., using 10ug of chromatin isolated from BAT cell line cells and 3ug of anti-LSD1 (Abcam), anti-Znf516 (Santa Cruz) [p-12 sc85244x], or Rabbit IgG (Sigma) as indicated.

Animals

Mice carrying floxed LSD1 alleles (KDM1a $^{fl/fl}$) and UCP1-Cre transgenic mice were obtained from Jackson laboratories. KDM1a $^{fl/fl}$ were crossed with UCP1-Cre mice and the progeny was intercrossed to generate KDM1a $^{fl/fl}$ mice carrying Cre transgene, that were used as conditional BAT specific LSD1 KO (BSKO) mice. KDM1a $^{fl/fl}$ mice (fl/fl) were used as control. All protocols for mice studies were approved from the University of California at Berkeley Animal Care and Use Committee. Mice were fed a chow diet or a high fat diet (45% calorie from fat, ResearchDiet) ad libitum. Body weight and food intake were measured weekly.

Body composition and histology

Body composition was measured in non-anesthetized mice using EchoMRI. For histology, fresh dissected adipose tissues were fixed in 4% paraformaldehyde, embedded in paraffin, sectioned in 5uM thick sections and then stained with Hematoxilin and Eosin. For immunohistochemistry, fresh dissected adipose tissues were fixed in 7% glutaraldehyde, included in OCT and sectioned on Leica CM3050S Cryostat in 20µm thick section. Briefly, slides were allowed to warm to room

temperature for 5 minutes, fixed with 4% formalin phosphate buffered saline for 30 minutes at room temperature, blocked with 5% BSA in PBS containing 0.025% Triton X-100 (PBST), and incubated with the UCP1 antibody (Sigma) diluted in 2.5% BSA in PBST overnight at 4°C. Slides were washed 3 times in PBST, and incubated with secondary antibody for 2 h at room temperature. Slides were then washed twice in PBST, and then stained with hematoxylin (bright field) for 30 s. Slides were washed and mounted in 15% glycerol in PBS with glass coverslips.

Indirect Calorimetry, Explant Respiration, and Body Temperature

Oxygen consumption (VO_2) was measured using the Comprehensive Laboratory Animal Monitoring System (CLAMS, Colombus Instruments). Data were normalized to body weights or lean body mass determined by EchoMRI. Tissue explant respiration was measured using a XF24 Analyzer (Seahorse Bioscience). Briefly, tissues we excised and placed directly into KREB's-Heslinger buffer (121mM NaCl, 4.9mM KCl, 1.2mM $MgSO_4$, 0.33mM $CaCl_2$, 12mM Hepes, 25mM glucose, 10mM Sodium Pyruvate, 1% fatty acid free BSA, pH 7.4). 3-5µg pieces of tissue were put in XF-24 plates and secured using an islet capture screen. Tissues were incubated for 1 hr at 37°C without CO_2 prior to analysis on the XF24 Analyzer. Body temperatures were assessed using a RET-3 rectal probe for mice (Physitemp).

Statistical analysis

Data are expressed as means ± standard errors of the means (SEM). The statistical differences in mean values were assessed by Student's *t* test. The sample size is 6-8 per genotype for animal studies and 3–6 for protein and transcript. All experiments were performed at least three times and representative data are shown.

Acknowledgments

We thank Prof. Y Shi and Prof. J Lingner for GST-LSD1 constructs. We thank Prof S. Kajimura for brown preadipocyte cell line (BAT). We thank T. Do and S. Yoo for technical assistance. The work was supported in part by NIH-DDK to H.S.S.

References

1. Bartelt, A., Bruns, O.T., Reimer, R., Hohenberg, H., Ittrich, H., Peldschus, K., Kaul, M.G., Tromsdorf, U.I., Weller, H., Waurisch, C*., et al.* (2011). Brown adipose tissue activity controls triglyceride clearance. Nature medicine *17*, 200-205.
2. Cypess, A.M., Lehman, S., Williams, G., Tal, I., Rodman, D., Goldfine, A.B., Kuo, F.C., Palmer, E.L., Tseng, Y.H., Doria, A*., et al.* (2009). Identification and importance of brown adipose tissue in adult humans. The New England journal of medicine *360*, 1509-1517.
3. Dempersmier, J., Sambeat, A., Gulyaeva, O., Paul, S.M., Hudak, C.S., Raposo, H.F., Kwan, H.Y., Kang, C., Wong, R.H., and Sul, H.S. (2015). Cold-inducible Zfp516 activates UCP1 transcription to promote browning of white fat and development of brown fat. Molecular cell *57*, 235-246.
4. Duteil, D., Metzger, E., Willmann, D., Karagianni, P., Friedrichs, N., Greschik, H., Gunther, T., Buettner, R., Talianidis, I., Metzger, D*., et al.* (2014). LSD1 promotes oxidative metabolism of white adipose tissue. Nature communications *5*, 4093.
5. Enerback, S., Jacobsson, A., Simpson, E.M., Guerra, C., Yamashita, H., Harper, M.E., and Kozak, L.P. (1997). Mice lacking mitochondrial uncoupling protein are cold-sensitive but not obese. Nature *387*, 90-94.
6. Farmer, S.R. (2009). Obesity: Be cool, lose weight. Nature *458*, 839-840.
7. Laurent, B., Ruitu, L., Murn, J., Hempel, K., Ferrao, R., Xiang, Y., Liu, S., Garcia, B.A., Wu, H., Wu, F*., et al.* (2015). A specific LSD1/KDM1A isoform regulates neuronal differentiation through H3K9 demethylation. Molecular cell *57*, 957-970.
8. Lowell, B.B., V, S.S., Hamann, A., Lawitts, J.A., Himms-Hagen, J., Boyer, B.B., Kozak, L.P., and Flier, J.S. (1993). Development of obesity in transgenic mice after genetic ablation of brown adipose tissue. Nature *366*, 740-742.
9. Metzger, E., Wissmann, M., Yin, N., Muller, J.M., Schneider, R., Peters, A.H., Gunther, T., Buettner, R., and Schule, R. (2005). LSD1 demethylates repressive histone marks to promote androgen-receptor-dependent transcription. Nature *437*, 436-439.
10. Musri, M.M., Carmona, M.C., Hanzu, F.A., Kaliman, P., Gomis, R., and Parrizas, M. (2010). Histone demethylase LSD1 regulates adipogenesis. The Journal of biological chemistry *285*, 30034-30041.
11. Ohno, H., Shinoda, K., Ohyama, K., Sharp, L.Z., and Kajimura, S. (2013). EHMT1 controls brown adipose cell fate and thermogenesis through the PRDM16 complex. Nature *504*, 163-167.
12. Shi, Y., Lan, F., Matson, C., Mulligan, P., Whetstine, J.R., Cole, P.A., Casero, R.A., and Shi, Y. (2004). Histone demethylation mediated by the nuclear amine oxidase homolog LSD1. Cell *119*, 941-953.
13. van Marken Lichtenbelt, W.D., Vanhommerig, J.W., Smulders, N.M., Drossaerts, J.M., Kemerink, G.J., Bouvy, N.D., Schrauwen, P., and Teule, G.J. (2009). Cold-activated brown adipose tissue in healthy men. The New England journal of medicine *360*, 1500-1508.
14. Virtanen, K.A., Lidell, M.E., Orava, J., Heglind, M., Westergren, R., Niemi, T., Taittonen, M., Laine, J., Savisto, N.J., Enerback, S*., et al.* (2009). Functional

brown adipose tissue in healthy adults. The New England journal of medicine *360*, 1518-1525.
15. Wang, J., Scully, K., Zhu, X., Cai, L., Zhang, J., Prefontaine, G.G., Krones, A., Ohgi, K.A., Zhu, P., Garcia-Bassets, I.*, et al.* (2007). Opposing LSD1 complexes function in developmental gene activation and repression programmes. Nature *446*, 882-887.
16. Wang, J., Telese, F., and Tan, Y. (2015). LSD1n is an H4K20 demethylase regulating memory formation via transcriptional elongation control.
17. Wang, L., Xu, S., Lee, J.E., Baldridge, A., Grullon, S., Peng, W., and Ge, K. (2013). Histone H3K9 methyltransferase G9a represses PPARgamma expression and adipogenesis. The EMBO journal *32*, 45-59.

Supplement:

Identification of The Novel Protein Critical for BAT Function

Supplement:
Identification of the novel protein critical for BAT function

In order to identify new proteins that are critical for BAT function, I performed a screening by RT-qPCR in WAT, BAT and cold exposed (CE) BAT. Figure 26A demonstrates induction of expression of control genes such as UCP1, Dio2, Elovl3, PGC1α, but not PRDM16 or Sox9 upon cold exposure (CE) to demonstrate that 6h CE time point was sufficient to induce known thermogenic markers and therefore, appropriate to test unknown genes for responsiveness to CE. After searching through microarray databases obtained by our laboratory over the years, several genes were selected for initial screening based on their expression in adipose tissue. Among the genes measured, C11orf54 or C11, appeared to be highly expressed in BAT than WAT and was upregulated by cold exposure indicating that it might be involved in BAT thermogenic function. Next step was to test expression of these genes over the course of BAT cell line (CL) and WAT cell line, 3T3-L1, differentiation. Most of the genes measured were induced by 2-5- fold during BAT CL differentiation, and two of them demonstrated the greater magnitude of induction-C11 and H2-Q10 (induced 20- and 90-fold respectively). Interestingly, C11 and H2-Q10 were not changed during white fat cell line differentiation pointing to the BAT-specific role. H2-Q10 is a component of major histocompatibility complex, and further experiments did not produce any conclusive results on its role in BAT (data not shown), so C11 was chosen for further detailed analysis. Human C11orf54 homolog or PTDO12 has been annotated as an ester hydrolase. This gene is conserved among species, demonstrating around 88% homology between mouse and human. There is only one publication available regarding the human PTD012 gene, in which authors crystallized its structure and predicted its localization in the nucleus (although some online databases indicate its localization to the cytoplasm). It was shown to be coordinated by Zinc atom and based on structural similarities, the authors compared PTDO12 with other enzymes coordinated by Zinc such as- carbonic anhydrase, carboxypeptidase and β-lactamase but were unable to detect any of these enzymatic activities of this protein, so its physiological function remains unknown.

To determine the role of C11 in BAT, I first performed RT-qPCR and immunoblotting analysis to measure its levels in different murine tissues and found its highest expression in kidney, BAT and liver (Figure 26B). The specificity of C11 antibody (designed against the human version of this protein), was tested it in 293FT cells transfected with C11-HA. C11 was detected as a 37 kDa protein by immunoblotting with C11 antibody in the 293 FT whole cell lysate (WCL), but not in conditioned medium (CM). Thus, it was concluded that C11 must be an intracellular protein. Next, I performed a more careful analysis of C11 protein levels among different tissues using 2 different antibodies and again detected highest abundance in BAT, kidney and liver but not in WAT or other tissues. Since BAT is heterogeneous tissue that contains adipocytes and other types of cells in SVF, I found that it was enriched in adipocyte fraction similar to UCP1 and AdipoQ, whereas Pref-1 and Sox9 are highly expressed in SVF as expected. All together, these data indicated that C11 is highly expressed in BAT compared to WAT and therefore might play a critical role in BAT function requiring further investigation.

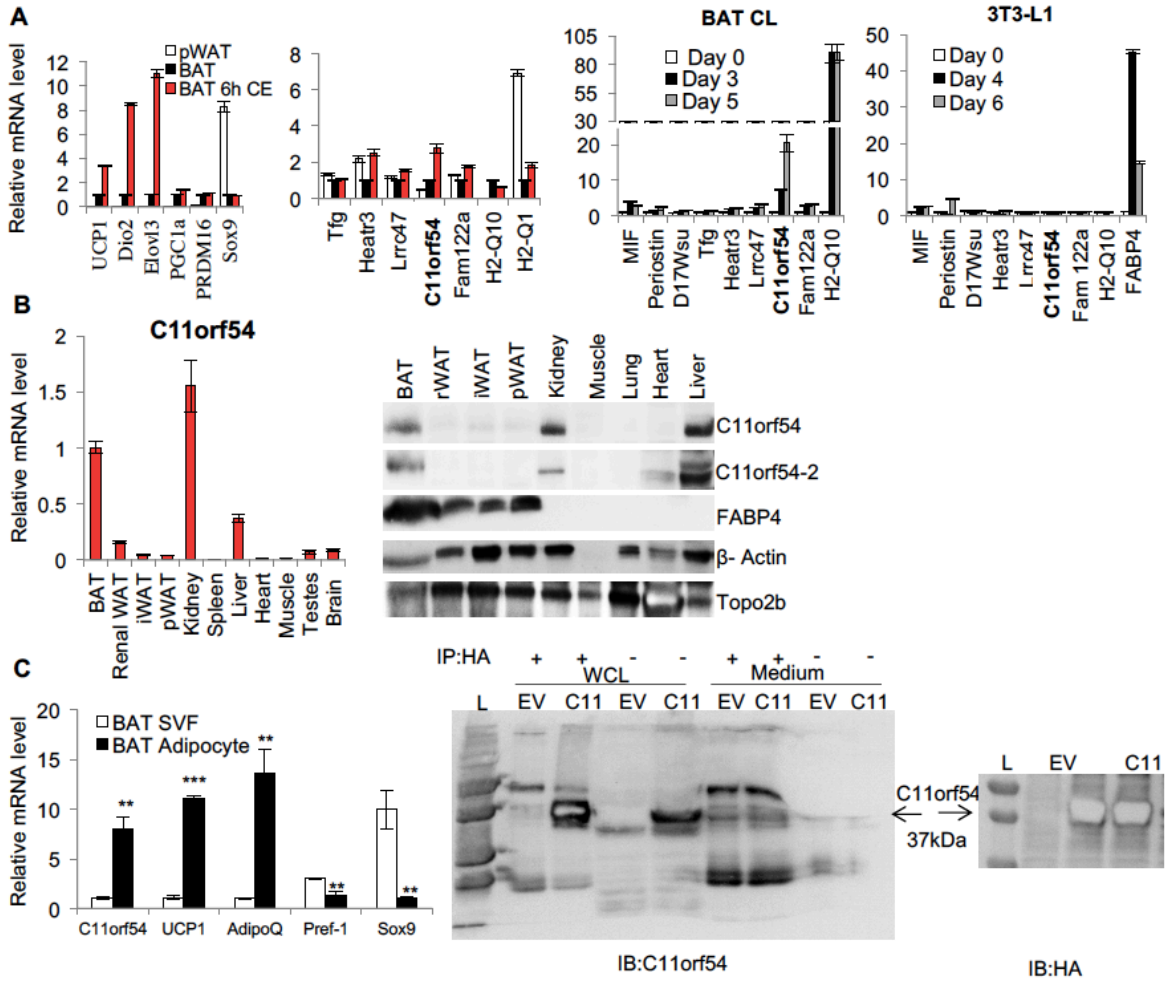

Figure 26. Identification of a novel factor for BAT function.
(A) RT-qPCR screening in pWAT, BAT, BAT after 6h cold exposure (CE) (left) and in brown fat cell line (BAT CL) and 3T3-L1 cells during differentiation. (B) RT-qPCR (left) and immunoblotting using 2 antibodies for C11orf54 (C11) (right) for tissue distribution. (C) RT-qPCR for C11 and controls in SVF and adipocytes from BAT (left) and immunoblotting for C11 and C11-HA in 293FT cells transfected with EV or C11-HA in WCL or conditioned medium. *-p value<0.05, **-p value<0.01, ***-p value<0.005

Next, I looked at subcellular localization of C11 to further narrow down its function. Immunoblotting revealed that in Cos7 cell transfected with C11-HA, it could be detected in both nucleus and cytosol but not in mitochondria or ER (Figure 27A left). Interestingly, in differentiated BAT CL and in BAT tissue C11 was detected exclusively in the cytoplasm (figure 27A center and right). Immunostaining analysis in Cos7 cells transfected with C11-eGFP revealed ubiquitous presence of C11 in a cell both in the nucleus and in the cytoplasm. In transfected BAT CL, C11 was similarly detected in the cytoplasm and nucleus and was not co localized with lipid droplets stained by Lipid Tox. These experiments reveled that C11 is predominantly localized in the cytoplasm, at least in BAT, proposing its potential enzymatic function.

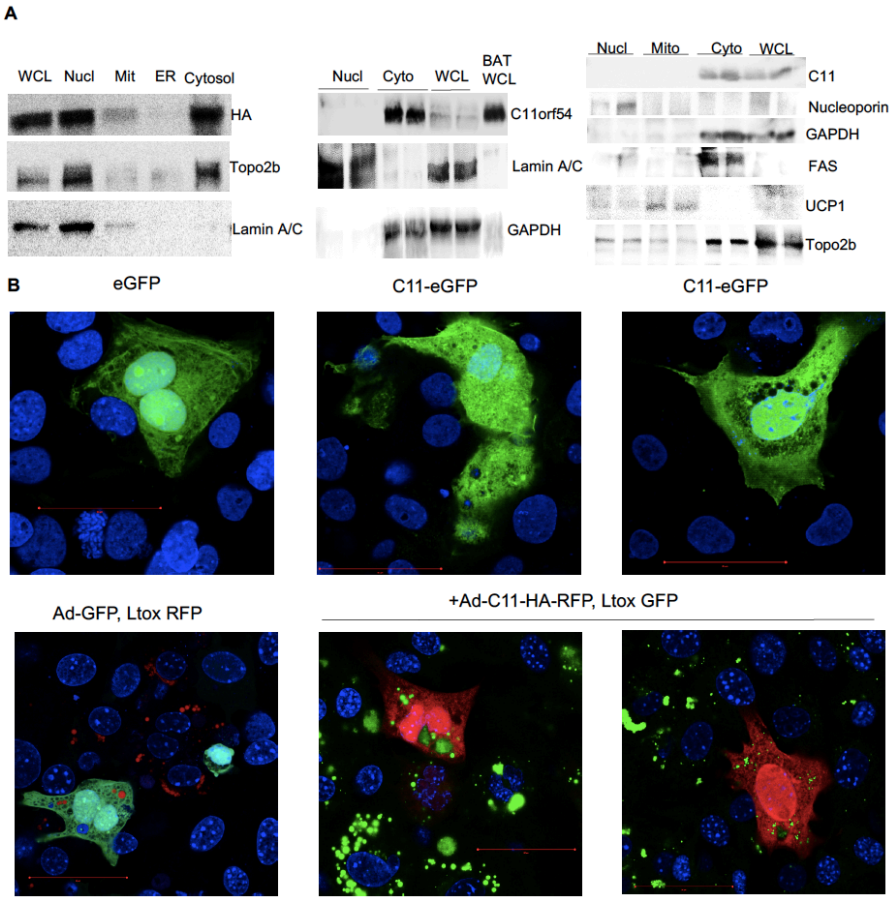

Figure 27. Subcellular localization of C11 in Cos7 cells, BAT CL and BAT tissue. (A) Immunoblotting for C11 and controls in various subcellular fractions of Cos7 cells transfected with C11-HA (left), BAT CL (center), BAT tissue (right). (B) Immunostaining for localization of C11 in Cos7 cells transfected with eGFP or C11-GFP (top) or in BAT CL transduced with Ad-GFP stained with Lipidtox RFP for lipids or C11-HA Adenovirus and stained with aHA-GFP antibody and Lipidtox-GFP for lipids (bottom).

Next, I assessed C11 expression during cold exposure in adipose tissue and during BAT CL differentiation and found that C11 was dramatically and gradually induced in BAT and to a lesser extent in iWAT upon cold exposure similar to UCP1. During BAT CL differentiation, cells accumulate lipids as evident from ORO staining (Figure 28B top) and acquired adipogenic genes expression indication successful adipogenic differentiation process (figure 26B middle). C11 was dramatically induced during differentiation as evident from mRNA and protein levels (Figure 28B middle and bottom), demonstrating importance of this protein in BAT cells.

To determine its function, I performed CRISPR-mediated KO of C11 in the BAT CL. Various sgRNAs aligning to different parts of C11 gene were used to assess off target effects of a single sgRNA (Figure29A). For one of the sgRNA “C”, 2 lines were generated and they showed virtually no C11 mRNA or protein (Figure 29B and 29C). Surprisingly, upon differentiation KO BAT CL lines in the absence of Rosiglitozone (a chemical agent known to dramatically enhance BAT CL differentiation) showed a dramatic reduction in adipogenic markers as well as thermogenic markers. Addition of rosiglitozone enhanced differentiation in both control and KO lines, making the difference less pronounced.

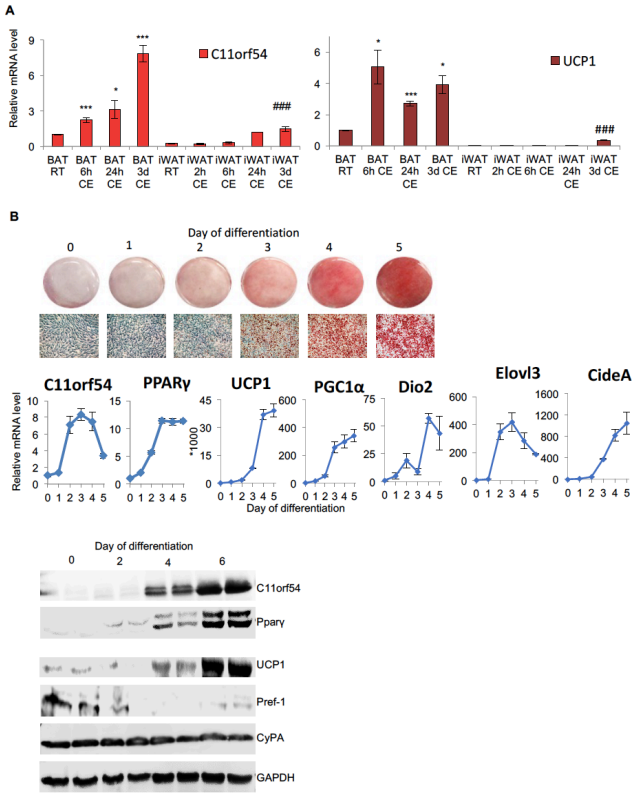

Figure 28. C11 expression is induced upon cold exposure and during BAT CL differentiation.
(A). RT-qPCR in BAT and ingWAT upon CE. (B) ORO pictures (top) and RT-qPCR for C11 and adipogenic markers (center) and immunoblotting (bottom) of BAT CL during differentiation.

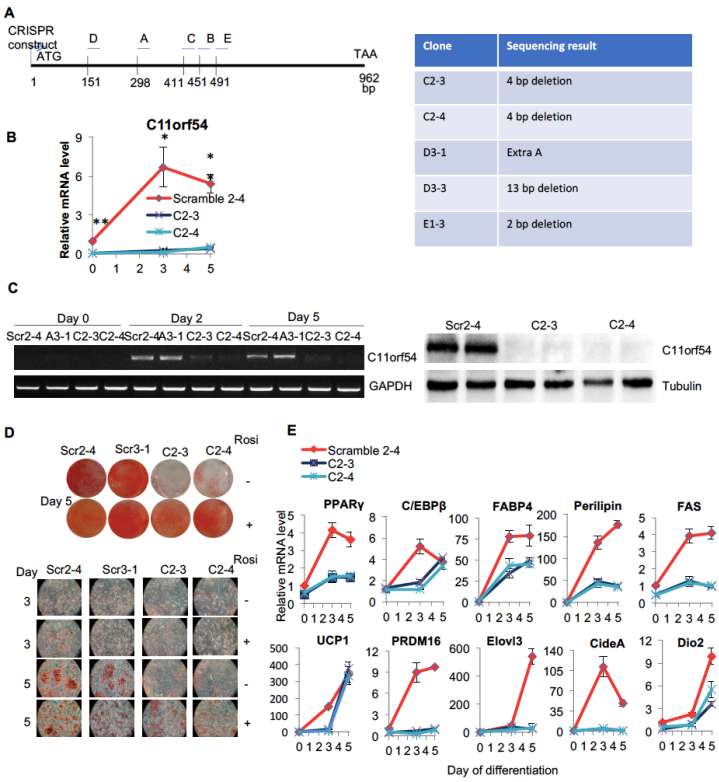

Clone	Sequencing result
C2-3	4 bp deletion
C2-4	4 bp deletion
D3-1	Extra A
D3-3	13 bp deletion
E1-3	2 bp deletion

Figure 29. CRISPR-mediated KO of C11 in BAT CL impairs BAT differentiation.
(A) Scheme of C11 gene and sgRNA aligned, used for CRISPR-mediated KO (left) and a table for resulting mutations (right). (B) RT-qPCR for C11 in control and KO BAT cell lines. (C). Endpoint PCR for C11 cDNA in various lines during BAT CL differentiation (left) and immunoblotting for C11 in differentiated cells (right). (D) ORO pictures of whole dish (top) and zoomed in view (bottom). (E) RT-qPCR for various markers during differentiation in control and KO lines.

Since published crystallographic data pointed that C11 may have potential enzymatic function and due to its high expression in BAT and in BAT CL during differentiation, I tested whether it may be involved in hydrolysis or formation of TAG- a major component and an energy storage form in adipocytes. I transfected Cos7 cells with EV or C11-HA, incubated with radioactively labeled fatty acid (C14-palmitate) for 2h, then changed the medium and collected cells and medium as time point “0” (T0) or incubated for longer and collected the samples at various indicated time points. Figure 30A demonstrated successful overexpression of C11 compared to EV sample on mRNA (left) and protein (right) levels. Interestingly, I found that C11 overexpression caused an increase in radioactivity in the medium, potentially indicating an enhanced metabolism in C11 overexpressing cells. Additionally, 2 independent TLC experiments allowed to resolve various radioactive lipid species in these cells and showed that C11 overexpression resulted in a dramatic increase in TAG levels in these cells compared to EV at T0 or 1, 2 or 4h post wash off of radioactive medium. No difference could be detected 16h post wash off, potentially due to a very low level of radioactivity in TAG of these samples indicating a fast turnover of fatty acids that are constantly being incorporated into TAG or being released from TAG. Surprisingly, no difference could be detected in other lipid species such as MAG, DAG, free FA or cholesterol.

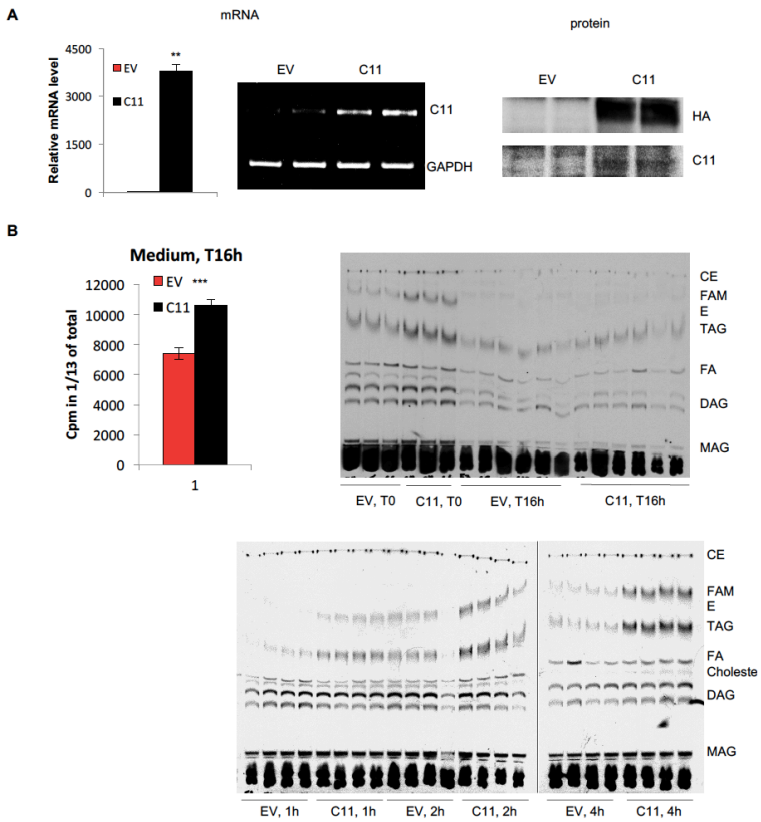

Figure 30. C11 may be involved in TAG synthesis. (A) RT-qPCR, end-point PCR and immunoblotting for C11-HA in Cos7 cells transfected with EV or C11-HA. (B)Radioactive C14 content in the medium collected from cells 16h post wash-off (left) and lipid separation by TLC of lipids extracted from control and C11 overexpressing cells incubated with C14-Palmitate for 2h and then collected 1,2,4 or 16h post wash off.

All together these results indicate that C11 is a BAT enriched gene, that has a fairly restrictive expression pattern. Subcellular fractionation followed by immunoblotting and immunostaining experiments suggested that C11 is localized in both cytoplasm and

nucleus. We have also shown that it is highly induced during BAT CL differentiation and upon cold exposure in BAT and iWAT, emphasizing its importance for BAT and its thermogenic function. TLC experiment with radioactively labelled palmitate indicates that C11 may facilitate TAG formation through yet to be identified mechanism. Further studies using metabolomics and overexpression and KO in mice will help to elucidate the exact role of C11 in BAT.

Chapter 5:
Conclusion

Obesity has reached epidemic proportions in the USA as well as globally, with the most updated statistics from 2013-2014 indicating that more than 1/3 of USA adults are obese and more than 2/3 are overweight (https://www.niddk.nih.gov/health-information/health-statistics/overweight-obesity). Thus, this disease and its potential treatment and management has drawn a lot of attention among the scientific community. Additionally, with the 2009 discovery that humans possess metabolically relevant BAT and BAT-like cells, the research in the BAT development and differentiation has exploded [1,2]. Since BAT and BAT-like cells found in WAT can burn substrates and produce heat though unique protein UCP1, it appears particularly useful to discover tissue specific regulators of UCP1 expression.

High-throughput screening of transcriptional activators of the UCP1 promoter enabled to identify a novel transcription factor, Zfp516 that is enriched in BAT and directly binds to the proximal UCP1 promoter. Tissue-specific pattern of Zfp516 expression helps to explain why UCP1 is only expressed in BAT and BAT-like cells in WAT and not in other tissues. Detailed analysis of Zfp516 KO mice revealed a nearly complete absence of BAT in embryos and these mice formed a muscle-like tissue in place of BAT with myogenic gene expression profile. This phenotype indicates a requirement of Zfp516 in embryogenesis for BAT formation. However, due to perinatal lethality of Zfp516 KO mice, the temporal aspect of Zfp516 induction in embryogenesis for BAT development remains unclear. Additionally, transgenic mice with Zf516 overexpression in adipose tissue show enhanced browning in iWAT and drastically reduced weight gain upon HFD accompanied by improved metabolic parameters. We have also shown that Zfp516 interacts with Prdm16, a brown-fat enriched co-activator important for BAT differentiation [3–6], but unlike Prdm16, Zfp516 is induced upon cold exposure. Thus, in order to identify other binding partners of Zfp516 involved in thermogenic response rather than BAT differentiation or development, our lab performed TAP assay followed by mass-spectrometry and found lysine specific demethylase 1, Lsd1 as a binding partner of Zfp516. Detailed experiments demonstrated a direct interaction between Zfp516 and Lsd1 and a cold-inducible nature of Lsd1. Myf5-Cre mediated Lsd1 KO exhibited severe lack of BAT and perinatal lethality in mice, resembling Zfp516 total body KO. Zfp516 interaction with Lsd1 appeared to be critical for Lsd1 function in BAT and implicated an important epigenetic mechanism for regulating thermogenic gene expression in BAT.

Since BAT-like cells named “beige”, “brite” or UCP1^{+} adipocytes were identified in WAT following cold exposure or β3-adrenergic treatment, development and differentiation process of WAT adipocytes also represent a critical research avenue for combating obesity. Unlike classical BAT that in rodents is located in interscapular region, WAT is dispersed in various depot among the body and can be generally classified in subcutaneous (under the skin) and visceral (surrounding internal organs under the abdominal cavity) [7,8]. Recent research indicated that development of WAT may not be as straightforward as previously anticipated. Different depots may have different developmental origins and different mechanisms of postnatal expansion and even adipocytes within the same tissue may be heterogeneous in origin. Additionally, the molecular identity of true adipose precursors remains controversial. Given that SVF contains multiple type of cells, it remains unclear whether cells that can give rise to adipocyte represent one population or multiple cell types with various degrees of

adipogenic commitment and differentiation. Generation of adipose precursor-specific deletion of Sox9 in an inducible manner and fluorescent labeling of these cells, allowed us to reveal the hierarchy in adipose progenitors within WAT. My data indicates that Pref-1^+:$Sox9^+$ early adipose precursors represent stem-cell like cells that are earlier than cells expressing PDGFRα in adipogenic pathway, the gene that is commonly used as preadipocyte/adipose progenitor marker [9,10]. Additionally, I showed that Sox9 downregulation is required for adipocyte differentiation in cultured primary SVF cells form WAT and in 3T3-L1 cell line and that enhanced differentiation in Sox9 KO lines can be rescued by adding Sox9 back to these cells, indicating specific and direct effect of Sox9. Furthermore, mice with Sox9 ablation from Pref-1^+ early adipogenic precursors exhibit adiposity resulting in insulin resistance.

All together, these data provide valuable insight in developmental and differentiation process of brown, white and "beige" adipocytes. These studies revealed novel BAT targets for potential obesity therapeutics and demonstrated the presence of hierarchy of adipose progenitors within WAT. Further research is needed to identify and establish other markers for early adipose precursors of brown and white adipocytes and their role in human physiology.

References

1. Cypess, A. M. *et al.* Identification and importance of brown adipose tissue in adult humans. *N. Engl. J. Med.* **360,** 1509–1517 (2009).
2. Cypess, A. M. *et al.* Anatomical localization, gene expression profiling and functional characterization of adult human neck brown fat. *Nat. Med.* **19,** 635–639 (2013).
3. Harms, M. J. *et al.* Prdm16 Is Required for the Maintenance of Brown Adipocyte Identity and Function in Adult Mice. *Cell Metab.* **19,** 593–604 (2014).
4. Kajimura, S. *et al.* Regulation of the brown and white fat gene programs through a PRDM16/CtBP transcriptional complex. *Genes Dev.* **22,** 1397–1409 (2008).
5. Kajimura, S. *et al.* Initiation of myoblast to brown fat switch by a PRDM16-C/EBP-beta transcriptional complex. *Nature* **460,** 1154–1158 (2009).
6. Ohno, H., Shinoda, K., Spiegelman, B. M. & Kajimura, S. PPARγ agonists induce a white-to-brown fat conversion through stabilization of PRDM16 protein. *Cell Metab.* **15,** 395–404 (2012).
7. Sanchez-Gurmaches, J. & Guertin, D. A. Adipocytes arise from multiple lineages that are heterogeneously and dynamically distributed. *Nat. Commun.* **5,** 4099 (2014).
8. Sanchez-Gurmaches, J., Hung, C.-M. & Guertin, D. A. Emerging Complexities in Adipocyte Origins and Identity. *Trends Cell Biol.* **26,** 313–326 (2016).
9. Berry, R. & Rodeheffer, M. S. Characterization of the adipocyte cellular lineage in vivo. *Nat. Cell Biol.* **15,** 302–308 (2013).
10. Lee, Y.-H., Petkova, A. P., Mottillo, E. P. & Granneman, J. G. In Vivo Identification of Bipotential Adipocyte Progenitors Recruited by β3-Adrenoceptor Activation and High-Fat Feeding. *Cell Metab.* **15,** 480–491 (2012).